

Photoswitchable peptidomimetics with diarylethene building blocks

Zur Erlangung des akademischen Grades eines
DOKTORS DER NATURWISSENSCHAFTEN

(Dr. rer. nat.)

Fakultät für Chemie und Biowissenschaften

Karlsruher Institut für Technologie (KIT) – Universitätsbereich
genehmigte

DISSERTATION

von

M.Sc. Oleg Babii

aus

Tlumach

Dekan: Prof. Dr. Peter Roesky

Referent: Prof. Dr. Anne S. Ulrich

Korreferent: Prof. Dr. Hans-Achim Wagenknecht

Tag der mündlichen Prüfung:

19 Dezember 2014

Table of contents

Table of contents	2
Acknowledgements	5
Abbreviations	6
1. Introduction	8
1.1. Operational photocontrol of biological processes.....	8
1.2. Molecular photoswitches.....	10
1.3. DAETs as promising photoswitches.....	11
1.3.1. Synthesis of DAETs.....	12
1.3.2. Physical and chemical properties of DAETs.....	13
1.3.3. DAET-based fluorescent probes.....	21
1.3.4. Applications of DAETs in biological systems.....	23
1.4. Membrane-active peptides.....	24
1.4.1. Peptides employed in this study.....	25
1.5. Photocontrol of peptide conformation and function.....	27
1.5.1. Peptides with photoresponsive amino acid residues.....	28
1.5.2. Peptides with photoresponsive backbone.....	28
1.5.3. Peptides with photoresponsive cross-linked side chains.....	30
2. Aims of the present study	32
3. Results and Discussion	33
3.1. Development of novel DAET building blocks for incorporation into peptides.....	33
3.1.1. The building block containing hydrazide group as an amino group surrogate (Sw ^I).....	33
3.1.2. Building blocks containing proline as an amino function (Sw ^{II}).....	36
3.2. Photoresponsive linear model peptides with the Sw ^I building block.....	38
3.2.1. Peptide synthesis.....	39
3.2.2. Conformational changes upon photoswitching in solution.....	41
3.2.3. Conformational changes upon photoswitching in membranes.....	43
3.3. Photoswitchable analogues of the antimicrobial peptide GS with the Sw ^I building block.....	49
3.3.1. Synthesis of GS analogues.....	51

3.3.2. Photochromic properties of the GS analogues.....	52
3.3.3. Hydrophobicity of the GS analogues.....	54
3.3.4. Circular dichroism analysis of GS analogues.....	55
3.3.5. Antimicrobial activity of GS analogues.....	58
3.3.6. Visualization of the antimicrobial activity of GS analogues.....	60
3.3.7. Hemolytic activity of GS analogues.....	62
3.4. Photoswitchable analogues of the antimicrobial peptide GS with the Sw ^{II} building block.....	64
3.4.1. Synthesis of GS analogues.....	65
3.4.2. Anticancer activity of GS analogues.....	67
3.5. Photocontrolled fluorescent cell imaging with DAET containing peptides.....	68
3.6. Photoswitchable analogues of the anticancer peptide SVS-1 with the Sw ^{II} building block.....	70
3.6.1. Synthesis and purification of SVS-1 analogues.....	72
3.6.2. Structural analysis of SVS-1 analogues.....	73
3.6.3. Antimicrobial activity of SVS-1 analogues.....	77
3.6.4. Anticancer activity of SVS-1 analogues.....	79
4. Summary.....	82
5. Zusammenfassung.....	83
6. Experimental part.....	84
6.1. General organic synthesis.....	85
6.2. Synthesis of peptides containing Sw ^I and Sw ^{II}	89
6.2.1. Synthesis of β/α -model peptide and its ¹⁹ F-labeled analogues.....	89
6.2.2. Synthesis of α/α -model peptide and its ¹⁹ F-labeled analogues.....	89
6.2.3. Syntheses of GS analogues containing Sw ^I	90
6.2.4. Syntheses of GS analogues containing Sw ^{II}	91
6.2.5. Syntheses of SVS-1 analogues containing Sw ^{II}	91
6.3. Solid-state ¹⁹ F-NMR measurements.....	92
6.4. Circular dichroism measurements.....	93
6.5. Antimicrobial activity assays.....	93
6.6. Visualization of antimicrobial activity.....	94
6.7. Hemolytic activity assays.....	95
6.8. Anticancer assays.....	95

7. References	97
List of publications	103
Conference contributions	103

Acknowledgements

I would like to thank my supervisor Prof. Dr. Anne S. Ulrich for the patient guidance and providing me with an excellent atmosphere for doing research.

I am grateful to Dr. Sergii Afonin for his support and encouragement during my work.

I would like to thank Prof. Dr. Igor V. Komarov for help with the planning of my research project and organizing biological studies in Kyiv.

Special thanks to:

Dr. Pavel K. Mykhailuk for useful advices in organic chemistry,

Dr. Stephan L. Grage for introducing into NMR spectroscopy,

Dr. Marina Berditsch for helping me to develop my background in microbiology,

Dr. Parvesh Wadhvani, Andrea Eisele, Kerstin Scheubeck for their help with peptide syntheses,

Sabine Reisser and Dr. Thomas Steinbrecher for productive joint work on the Gramicidin S project,

Dr. Volodymyr Kubyskin for his help with the study of Gramicidin S,

Dr. Liudmyla Garmanchuk for the help with cytotoxicity tests,

Dr. Joachim Bürck, Siegmund Roth and Bianca Posselt for their help with CD measurements,

Dr. Johannes Reichert for the help with fluorescence spectroscopy measurements,

Patricia Kammerer for helping in the study of SVS-1 peptide,

Christian Schwechheimer for his help in synthesis of the photoswitchable building blocks,

Dr. Tamta Turtzeladze, Dr. Birgid Lange, Gabriele Buth and Anni Barwig for their help with formalities,

Special thanks to the referees for their impartial judgment.

Abbreviations

AMPs	Antimicrobial peptides
AMPB	4-[(4-aminomethyl)phenylazo]benzoic acid
AMPP	[3-(3-aminomethyl)phenylazo]phenylacetic acid
Boc	<i>tert</i> -Butoxycarbonyl
CD	Circular dichroism spectroscopy
DAETs	Diarylethenes
DIPEA	<i>N-N</i> -Di-iso-propylethylamine
DMEM	Dulbecco's modified Eagle's medium
DMF	Dimethylformamide
DMPC	1,2-dimyristoyl- <i>sn</i> -glycero-3-phosphocholine
DMPG	1,2-dimyristoyl- <i>sn</i> -glycero-3-phospho- <i>rac</i> -(1-glycerol)
DMSO	Dimethylsulfoxide
FBS	Fetal bovine serum
Fmoc	9-Fluorenylmethyloxycarbonyl
GS	Gramicidin S
HBTU	<i>N</i> -[(1 <i>H</i> -Benzotriazol-1-yl)(dimethylamino) methylene]- <i>N</i> -methylmethanaminium hexafluorophosphate <i>N</i> -oxide
HOBt	1-Hydroxybenzotriazole
MALDI-TOF	Matrix-assisted laser desorption/ionization mass-spectrometry (time-of-flight detection)
MBHA	4-methylbenzhydramine
MIC	Minimum inhibitory concentration
MTT	Microculture tetrazolium assay
NMR	Nuclear magnetic resonance spectroscopy
PB	Phosphate buffer
PDT	Photodynamic therapy
POPC	1-palmitoyl-2-oleoyl- <i>sn</i> -glycero-3-phosphocholine
POPS	1-palmitoyl-2-oleoyl- <i>sn</i> -glycero-3-phospho-L-serine
PTT	Photothermal therapy
PyBOP	(Benzotriazol-1-yloxy)tripyrrolidinophosphonium hexafluorophosphate
P/L	Peptide to lipid ratio (mol/mol)
RBC	Red blood cells

RP-HPLC	Reverse-phase high-performance liquid chromatography
RT	Retention time
SDS	Sodium dodecyl sulfate
SPPS	Solid-phase peptide synthesis
TFA	Trifluoroacetic acid
TLC	Thin layer chromatography
Tris-HCl	2-Amino-2-(hydroxymethyl)-1,3-propanediol hydrochloride
UV	Ultraviolet light
Vis	Visible light

1. Introduction

1.1. Operational photocontrol of biological processes

Development of a new pharmacological agent is an extremely time- and effort-consuming process: on the way from a lead to a real drug plenty of complications are faced. Most often low bioavailability, reduced *in tissue* drug selectivity, presence of side effects, and poor overall biostability are the main “unforeseen” problems encountered in the early *in vivo* translational experiments^{1,2}. Often these problems are attributed to the insufficient pharmacokinetics of the pharmaceutical agent, e.g. due to non-specific tissue absorption, peculiarities of the distribution, metabolism and excretion pathways in a particular test organism³. For example, most anti-cancer drugs act through the interference with the process of cell division during mitosis⁴. As a result of low selectivity, besides tumor cells, they are affecting other fast-dividing pluripotent cells in a living organism⁵. Another problem of the practical drug application is the adaptation of the targeted cells which leads to resistance, like most widely discussed rapid development of acquired antibiotic resistance by bacteria⁶. Due to the narrow therapeutic index, antibiotics are often used at the suboptimal concentrations allowing and even stimulating bacteria to evolve into resistant variants. Luckily, many of the abovementioned problems could be coped with already on the agent design stage if additional controllers are built-in as obligatory design elements.

One of the most attractive ways to achieve such an extra handle is using the concept of dynamic photocontrol^{7,8,9,10,11}. This is because light is non-invasive, easily to manipulate and orthogonal to most biological stimuli, which potentially allows precise spatial and temporal control. Using light for dynamic control of a therapeutic agent is a subject of photopharmacology that is actively developing in recent years¹². The main applied areas of photopharmacology are photodynamic and photothermal therapies, controlled drug and gene delivery.

The photodynamic therapy (PDT) utilizes special molecules, photosensitizers, which under irradiation with light generate active species of oxygen ($^1\text{O}_2$)¹³ or nitric oxide (NO)¹⁴. The presence of these at illuminated locations causes immediate local cytotoxic effect of high temporal efficiency. In the photothermal therapy (PTT) the light is used to heat the tissues in the range of 41-47°C for several minutes¹⁵. The heating causes irreversible damage of the tissues in the light-exposed areas. Addition of exogenous dyes and nanoparticles is used to

increase the absorption of light and promote the destructive effect. The PDT and PTT are widely used, in particular for the treatment of cancer and infectious diseases.

In the photocontrolled drug delivery approaches the biologically active agent is either deactivated by protecting the pharmacophore with a photocleavable group or encapsulated into a photoresponsive entrapping material. In the former, the “photocaging” strategy, the light stimulus is used to activate systemically administered caged molecules, which can be small drugs, proteins, or nucleic acids^{16,17}. Not only time, but also dosage and location can be precisely controlled by the intensity and duration of the activating light signal. Though typical biological tissues are insufficiently transparent to visual light, the use of the two-photon excitation, e.g. employing the near-infrared light allows overcoming the problem. The photochemical internalization strategy, the “phototrapping”, most often employs nanostructures loaded with the biologically active agents, which could change their loading capacity such that entrapped material could be released upon triggering signal of light. Different surface-modified metal nanoparticles¹⁸, dendritic and polymeric nanomaterials¹⁹, vesicles²⁰ and mesoporous silica-based nanoparticles²¹ have been validated as promising photo-traps for *in vivo* applications. These nanostructures besides carrying the cargo usually have better (at least different) pharmacokinetic properties than the carried active agent itself. For example, they can co-deliver inside the cell molecules which normally cannot cross the cell membrane.

Another large area within current medicinal photopharmacology is the exploitation of molecular photoswitches – small organic molecules capable of undergoing reversible photoisomerization reactions¹². Typically within related structure-function paradigm, specific biological effect of a therapeutic agent is manifested through its interaction with a particular (mostly proteinous in chemical nature) target, which could be functionally a receptor, an enzyme or an ion channel²². The modification of the drug molecule with a photoswitch permits easy structure manipulation allowing indirect regulation of its macroscopic characteristics such as shape and hydrophobicity and as a result to control its interaction with the target.

The incorporation of molecular photoswitches into peptides or proteins shifts the control handle of their structures and functions to the process of switch photoisomerization. Here the relative strength of the photoinduced impact (the conformational transition of the photoswitch) to the overall size of the modified object (the polypeptide) starts playing important role. The switch isomerization could be too weak to propagate structural changes to the whole polypeptide (if the polypeptide is large) or the switch could be itself too large as an

add-on moiety and completely destroy the original peptide function (if the polypeptide is too small). Therefore it is crucially important to understand general principles and to investigate structural effects of the isomerization process for any novel molecular photoswitch, or a new way of the switch installation. In particular, for creating a photoswitchable peptide-modifying unit, on the structure and function of model polypeptides, including small peptides¹². Such studies are not only of a fundamental interest, they also generate new drug leads as various bioactive peptides are present in living systems. The chosen objects of the studies can themselves become promising targets for modification with molecular switches.

1.2. Molecular photoswitches

In recent years chemically engineered photoswitchable compounds have become more and more popular tools for addressing different biological questions and a variety of synthetic photoswitches have been designed. Most of the known photochromic systems undergo either *cis/trans* isomerization of a double bond or unimolecular pericyclic reaction (Figure 1.1.). Molecular photoswitches are logically classified according to changes that are occurring upon photoisomerization. The changes may involve alteration of the geometrical structure, polarity, oxidation/reduction potential, fluorescence and other physical properties. In cases of azobenzene, stilbene, spiropyran, and hemithioindigo photoswitches the *cis/trans* isomerization occurs during the interaction with light. This results in significant geometric and steric alterations as the consequence of the switching process. The azobenzenes and spiropyrans are especially useful for reversibly creating the steric bulk¹¹. Essentially different situation is observed in diarylethene and fulgide systems where changes in conformational flexibility can be generated through switching process, while geometrical changes are usually not so large.

For advantageous biological applications the photoswitches are required to additionally possess other physical properties, such as: (i) being able to undergo sufficiently fast photoisomerization, (ii) demonstrating high quantum yields especially at the wavelengths nondestructive for living cells, and (iii) exhibiting high fatigue resistance in aqueous environments¹². Besides, one of the particularly important requirements is a high thermal stability of both photoforms. Usually, the photogenerated colored isomers are thermally unstable and convert to the initial state without irradiation. Thermally reversible compounds (classified as T-type molecular switches, Figure 1.1.a, 1.1.b, 1.1.c) are the majority of known photochromic compounds, including azobenzenes and spiropyrans. In contrast, stilbenes,

furylfulgides, and diarylethenes (DAETs) with heterocyclic aryl groups belong to the thermally irreversible (P-type) photochromic compounds (Figure 1.1.a, 1.1.d, 1.1.e). Obviously, last three structures are the most prospective candidates for the development of technically applicable photoswitches.

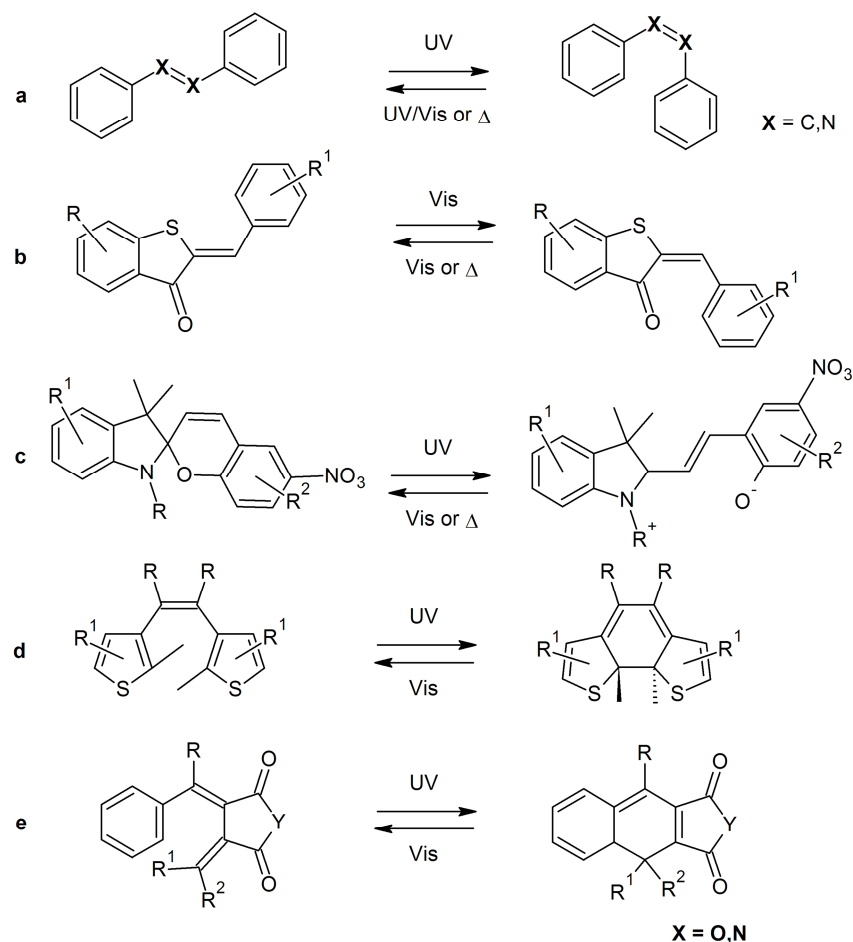


Figure 1.1. Overview of the photoinduced forms for the most studied molecular photoswitches: (a) azobenzenes ($X=\text{N}$), stilbenes ($X=\text{C}$); (b) hemithioindigos; (c) spiropyrans; (d) diarylethenes; (e) fulgides ($Y=\text{O}$), and fulgimides ($Y=\text{N}$).

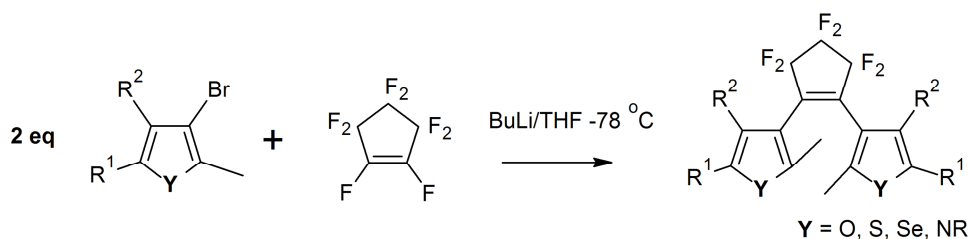
1.3. DAETs as promising photoswitches

From the practical perspective of photoswitches application in biological systems DAETs are the most promising candidates among P-type photoswitches for several reasons. A major drawback of stilbenes is their tendency to undergo irreversible oxidation in the *cis* form²³. Furylfulgides and related compounds also possess poor chemical stability²⁴. On the contrast, DAETs advantageously differ from stilbenes and furylfulgides in their remarkably high fatigue resistance. The cycle of switching between two forms by the alternate irradiation

with UV or visible light could be repeated more than 10 000 times without apparent chromophore degradation²⁵. Both ring-cyclisation and ring-opening processes occur rapidly in the picosecond time scale. These features suggest DAETs as preferable scaffold of the all known DAE-based structures for applications in the engineered photocontrolled biological processes.

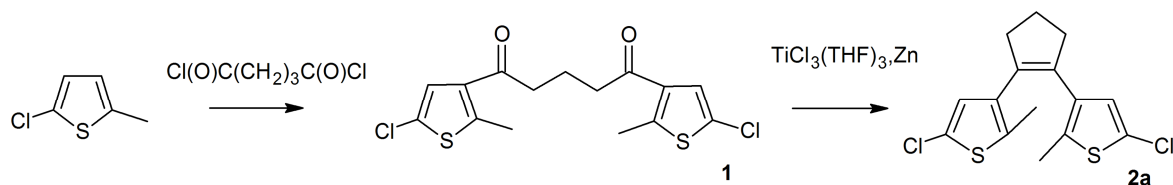
1.3.1. Synthesis of DAETs

Among large number of synthesized and studied DAETs the most commonly used are diarylperfluorocyclopentenes²⁵. These compounds can be prepared in a very simple and reliable way shown in the Scheme 1.1. Both symmetric and non-symmetric DAETs with various heterocyclic aryl groups could be obtained by the reaction of perfluorocyclopentenes with aryllithium. The use of the equimolar amounts of the perfluorocyclopentene and aryllithium leads to mono-substituted perfluorocyclopentenes which can subsequently be applied for the synthesis of non-symmetric DAETs²⁶.



Scheme 1.1. Synthesis of diarylperfluorocyclopentenes through the reaction of perfluorocyclopentene with aryllithium.

In 2003, Feringa and coworkers proposed an alternative way for synthesis of the DAETs possessing a non-fluorinated aliphatic ring²⁷. The synthetic approach is based on the acylation of heterocyclic derivatives, followed by a McMurry intramolecular ring-closing reaction²⁸. The original example is shown in the Scheme 1.2. The key step is the formation of a new ethylene group during cyclisation of the corresponding 1,5-diaryl-1,5-diketone **1** into diarylethene **2a**. Based on the McMurry coupling, the DAETs with different aryl groups and four- to six-membered aliphatic rings were synthesized^{25,26}.



Scheme 1.2. McMurry pathway to dithienylcyclopentenes.

1.3.2. Physical and chemical properties of DAETs

The first example of the thermally irreversible photochromic DAET was reported in 1988 by Irie et al.²⁹. Since then various types of DAETs having thiophene, indole, furan, thiazole, and selenophene aryl groups have been prepared. Major synthetic developments were directed towards increase in the thermal stability of DAETs and their fatigue resistance during photochromic reactions.

Theoretical³⁰ and experimental¹² investigations of the DAETs revealed that the thermal stability of the closed-ring isomers depends on three main factors: (i) stabilization energy of the aromatic groups, (ii) electronic properties of the substituents at the aryl groups, and (iii) steric repulsion of the substituents at the reactive carbons.

It was shown (factor i), that when aryl groups have low aromatic stabilization energies like in the cases of thiophene, furyl, or benzothiophene groups, the closed-ring isomers become thermally stable. At the same time, when aryl groups have high aromatic stabilization energies like in the cases of phenyl, indolyl, or pyrrolyl groups, the closed forms appear thermally reversible. Direct correlation between the aromatic stabilization energies of the aryl aromatic systems (Table 1.1.) and the thermal stability could be therefore drawn^{12,30}.

Table 1.1. Aromatic stabilization energies for different aromatic systems³⁰

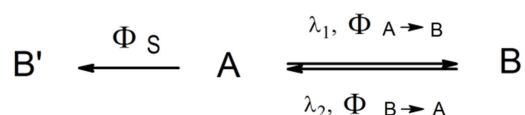
Group	Energy [kcal/mol]
phenyl	27.7
pyrrolyl	13.8
furyl	9.1
thienyl	4.7

Introduction of the electron-withdrawing substituents at the aryl group (factor ii) leads to decrease the thermal stability of the closed-ring forms. The effect is explained by the weakening of the reactive carbon-carbon bonds in the photogenerated closed-ring isomers¹¹.

On the other hand, introduction the electron-donating groups stabilizes the formed carbon-carbon bond in the closed-ring isomers. However, such substitution decreases at the same time the oxidation/reduction potential of the DAETs and makes them more sensitive to oxidation³¹.

Bulky substituents at the reacting positions (factor iii) also have been demonstrated to enhance thermal reversibility of the closed-ring isomers^{23,32}. These studies established inverse proportional relationship between the thermal stability and theoretically calculated bond length linking the reactive carbon atoms²⁴.

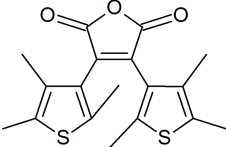
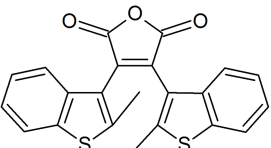
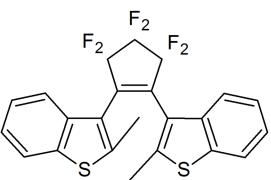
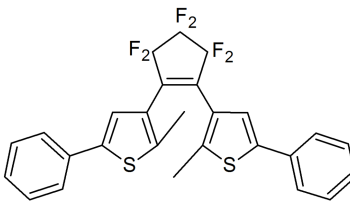
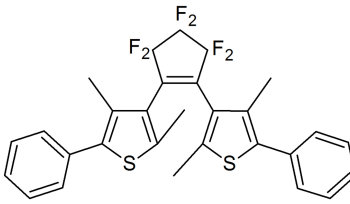
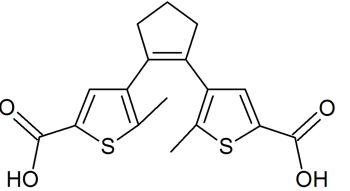
Another important property of the molecular photoswitches is their fatigue resistance – the ability to undergo photochromic transformations without destruction. In the photoswitching process, interaction of a photochromic compound with light leads to particular rearrangement of chemical bonds. However, undesirable side reactions can take place during this process. The equation below illustrates the photochromic conversion between compounds **A** and **B** (quantum yields $\Phi_{A \rightarrow B}$ and $\Phi_{B \rightarrow A}$) accompanied by a non-reversible side reaction leading to the compound **B'** with the quantum yield Φ_S . Formation of the side products limits the number of possible photochromic cycles. Even if the side reaction quantum yield Φ_S is as small as, for example, 0.01, 40% of the initial amount of **A** will be decomposed after 50 cycles of coloration/decoloration.



The fatigue resistance of several DAET derivatives has been quantitatively measured^{11,33}. Selective examples are shown in the Table 1.2.

From these and similar studies two factors – oxidative stability and nature of rearrangements were concluded to determine the photochromic stability of DAETs. For example, compound **3a** showed low durability in the presence of oxygen due to endoperoxide formation by reaction with the photogenerated singlet oxygen^{12,38}. The stability of this DAET increased remarkably when benzothiophenes were substituted for the thiophene rings (compound **6a**)³⁹. The benzothiophene derivatives were found to have better oxidation stability, suggesting therefore that the oxidative stability might be a reason for the enhanced photostability.

Table 1.2. Fatigue resistance of DAETs.

Compound	Number of repeatable cycles*		Reference	
	presence of oxygen	absence of oxygen		
	3a	70	480	34
	4a	3.7×10^3	1.0×10^4	35
	5a	$>1.3 \times 10^4$ (in methylcyclohexene)	-	25
	6a	80 (in hexane)	200 (in hexane) > 10^4 (in crystal)	36
	7a	200 (in hexane)	$> 2 \times 10^3$ (in hexane)	36
	8a	> 10	-	37

*The number of photochromic cycles at which the absorption of the open-ring isomer has decreased to 80% compared to initial cycle.

In another study, the difference in fatigue resistance of compounds **6a** and **7a** provided the clue for understanding the nature of molecular rearrangements underlying the photodestruction³⁰. Compound **7a** differ from **6a** by additional methyl groups at the 4- and 4'-positions of the thiophene rings. The absorbance of the colorless form of compound **7a** remained almost constant during coloration/decouration, while the absorbance of **6a**

significantly decreased already after 200 cycles. A photostable violet-colored by-product was isolated from the fatigued solution of **6a**. The molecular structure of the by-product was determined by X-ray crystallographic analysis as a six-membered fused-ring structure **9** (Figure 1.2.). It appears that in the oxygen-free environment the rearrangement leading to the by-products of this type is the main fatigue degradation process of the dithienylethenes lacking substituents at the 4- and 4'-positions of the thiophene ring.

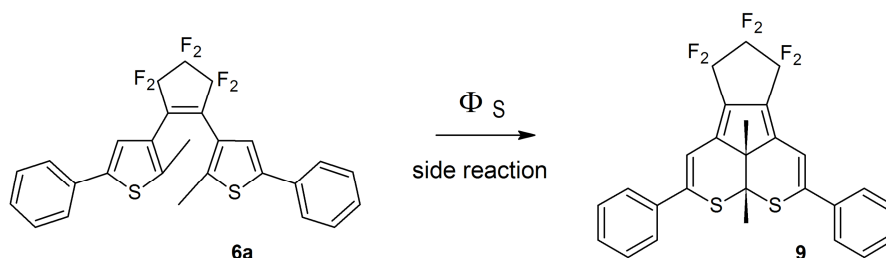


Figure 1.2. The by-product formation during fatigue degradation of the DAET molecule with free 4-,4'-positions of the thiophene rings.

The overwhelming majority of studied DAETs are diarylperfluorocyclopentenenes, presumably due to convenience of the synthetic approaches to them³⁰. Besides, the perfluorinated five-membered ring, as was demonstrated in the above example, provides the DAET molecules with additional oxidative stability during photochromic cycles. Corresponding dithienylcyclopentenenes generally demonstrated lower fatigue stability comparing to the fluorinated counterparts (e.g. compound **8a**)^{27,37}. Therefore, dithienylcyclopentene-containing DAETs are inappropriate to be used in photoelectronic devices, but they have found broad application in others technologies where the large number of switching cycles is not required⁸. For example, fatigue resistance is not a limitation for photoactivated one-step drug releasing systems because their functions are accomplished after a single transformation to the active form. Besides, the non-fluorinated DAETs are less hydrophobic and their molecules are less bulky comparing to the fluorinated analogues.

Optical properties of the photoswitches are obviously most critical for any light-controlled application. Typical changes in the absorption spectrum of a DAET derivative upon photoisomerization are shown in the Figure 1.3. Typically, the open-ring isomers of DAETs have absorption bands at shorter wavelengths than the closed-ring isomers. Most DAETs show very large spectral shifts upon photoisomerization. The π -electrons delocalize throughout the two fused thiophene rings in the closed-ring isomers and the delocalization path extends further to the substituents at the aryl rings. Notably, the maxima in the

absorption spectra of the closed-ring isomers strongly depend on the type of substituents at the aryl rings⁴¹.

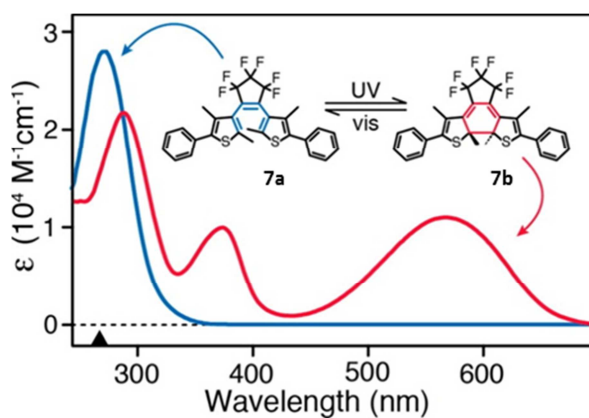


Figure 1.3. Absorption spectra of DAETs exemplified by the compound **7**. Blue line corresponds to open-ring form **7a**; red line – to the closed-ring form **7b**. Adapted from ref. ⁴⁰.

Photochromic compounds that have the absorbance bands shifted to the “red” region (600–830 nm) have been considered more advantageous for the application in optical memory media. The use of the long-wavelength light for the photoisomerization is also more preferable for bio-applications, mostly due to better tissue penetrating ability of the long-wave light. In an attempt to develop a near-infrared light-sensitive photochromic DAET compounds, the effects of substituents on their absorption maxima was examined. Figure 1.4. summarizes typical absorption maxima of the closed-ring isomers^{25,34,35,42,43,44,45}. Most important factors that determine the absorption profile for DAETs were found in these studies. The absorption spectra of the open-ring isomers were shown to depend on the nature of the cycloalkene moiety. The closed-ring isomer of the maleic anhydride derivative **10b** had the absorption bands shifted to the longer wavelengths when compared with the perfluorocyclopentene derivative **3b**. Expansion of the π -conjugated chain by introduction of phenyl groups at the 5- and 5'-positions of the thiophene rings (compound **7b**) resulted in a bathochromic shift. Compound **7b** had the long-wave maximum shifted to 562 nm, comparing to 534 for **10b**.

The absorption maximum can be shifted even further (to 597 nm) by incorporation electron-donating diethyl amino groups at the 4- and 4'-positions of the phenyl substituents, compound **12b**⁴². Useful insights were documented in studies of asymmetrical DAETs possessing an indole at one side and a thiophene at the other side of the molecules. The maleic anhydride derivative **11b** gave an absorption maximum at 578 nm⁴⁴.

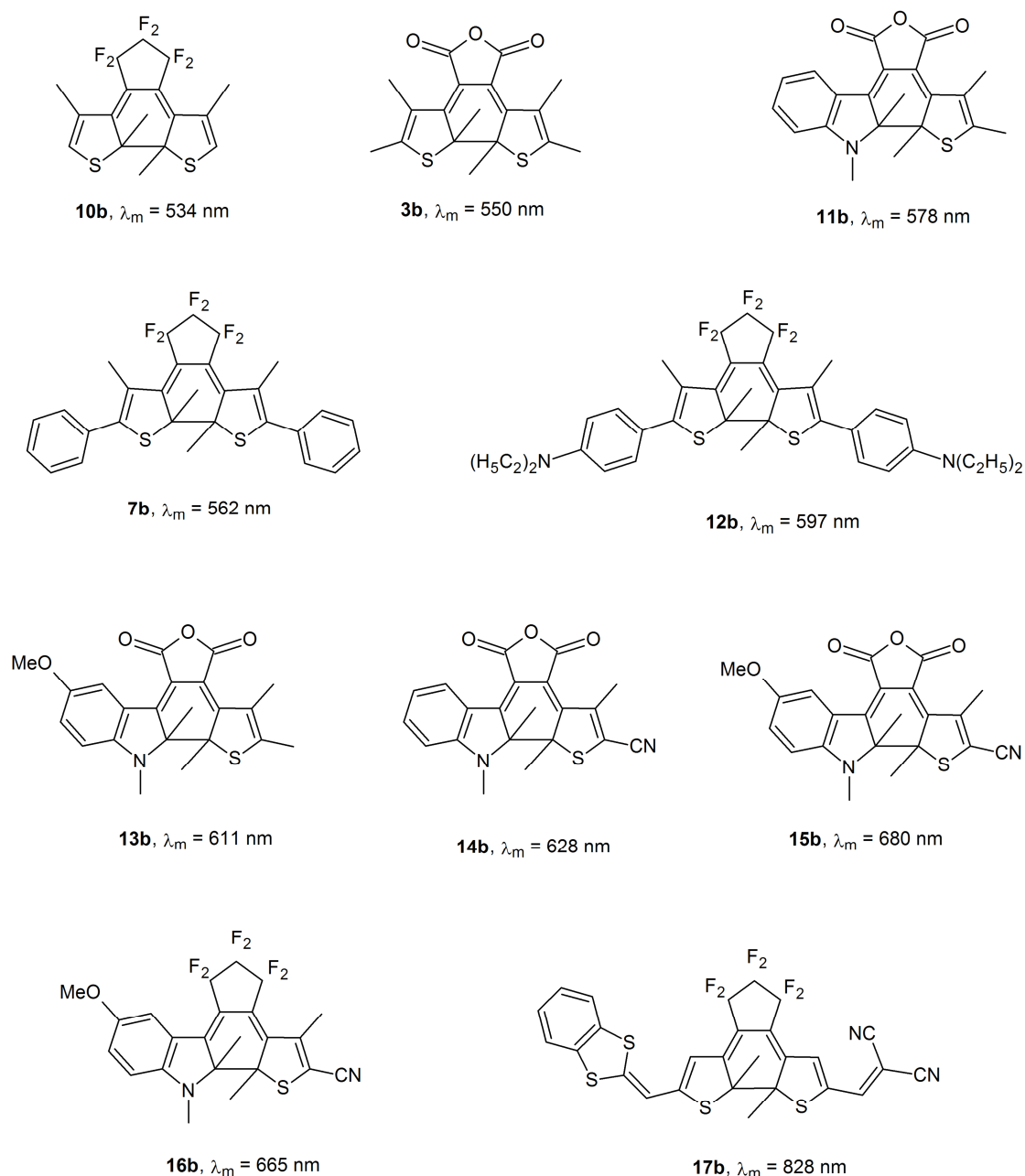


Figure 1.4. Absorption maxima of the selected closed-ring isomers of DAETs^{34,36,42,45,46,47}

Introductions of an electron-donating group into indole ring (**13b**) or an electron-withdrawing group into the thiophene ring (**14b**) were both shown to shift the absorption maxima to longer wavelengths. Simultaneous presence of both electron-donating and electron-withdrawing substituents was shown to cause even larger shifts: to 680 nm in **15b** and to 665 nm for the perfluorocyclopentene analogue **16b**. Moreover, introduction of a strong electron-donating benzodithiole substituent and a strong electron-withdrawing dicyanoethylene substituent at the 5- and 5'-positions of the thiophene rings caused significant shift of the absorption maximum of the closed-ring isomer **17b** to 828 nm⁴⁵.

Another practically important absorption characteristic is the molar absorption coefficient. High sensitivity requires high molar absorption coefficients and high quantum yields. In general, introduction of electron-rich substituents or large- π -conjugated systems in DAETs was shown to effectively increase both the parameters^{48,49}.

It has been shown that DAETs with five-membered heterocyclic rings populate two conformations in solution: parallel (C_s symmetry) and antiparallel (C_2 symmetry)^{34,35,42}. The ratio of the two conformations is normally around 1:1. As shown in the Fig.1.5, the photocyclization reaction can proceed only with the DAET molecules in the antiparallel conformation. Therefore, the cyclization quantum yields cannot exceed the molar fraction of the antiparallel conformation.

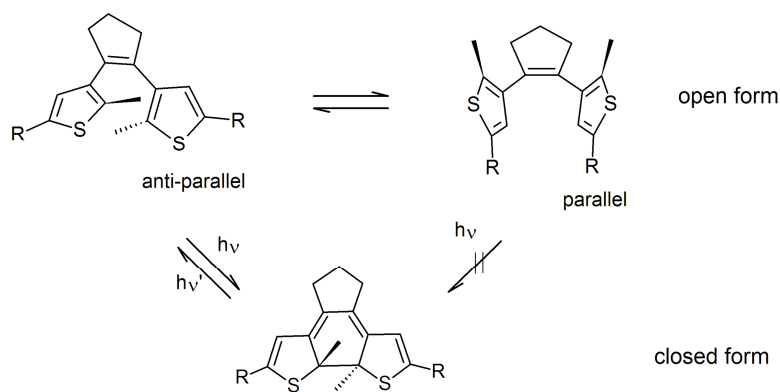


Figure 1.5. Parallel and anti-parallel conformations of DAETs in the photoisomerization process.

Literature quantum yields of several DAETs with ~1:1 ratios are summarized in the Table 1.3. The parallel/antiparallel ratio of the conformers could be shifted by steric constraints in the molecules causing one of the conformations to be energetically more favorable. To enhance the quantum yield it is therefore necessary to increase the abundance of the antiparallel conformation. One way to do this was suggested to be through introduction of bulky substituents to the thiophene rings. Such effect was illustrated on DAETs with benzothiophene rings substituted by isopropyl groups at the 2- and 2'-positions⁵⁰. In line with this observation, for compounds **7a** and **12a** almost all photoexcited molecules were present in the antiparallel conformation. The actual quantum yields were therefore close to 1.

Table 1.3. Quantum yields of cyclisation and cycloreversion reactions for selected DAETs.

Compound	Quantum yields		Reference
	cyclization	cycloreversion	
10	0.21	0.13	46
6	0.68	0.013	36
7	0.46	0.015	36
12	0.37	0.0025	42
8*	0.9	0.025	37

*ratio of conformers is shifted to anti-parallel.

Another approach to increase the antiparallel conformation population was shown for DAET molecules confined in a hollow host. Since the DAET molecules in the antiparallel conformation have extended rod-like structures and should be more compact in the parallel conformation, the shape difference can be used to stabilize one of the conformations. Cyclodextrins were suggested as the host molecules for this purpose^{51,52,53}.

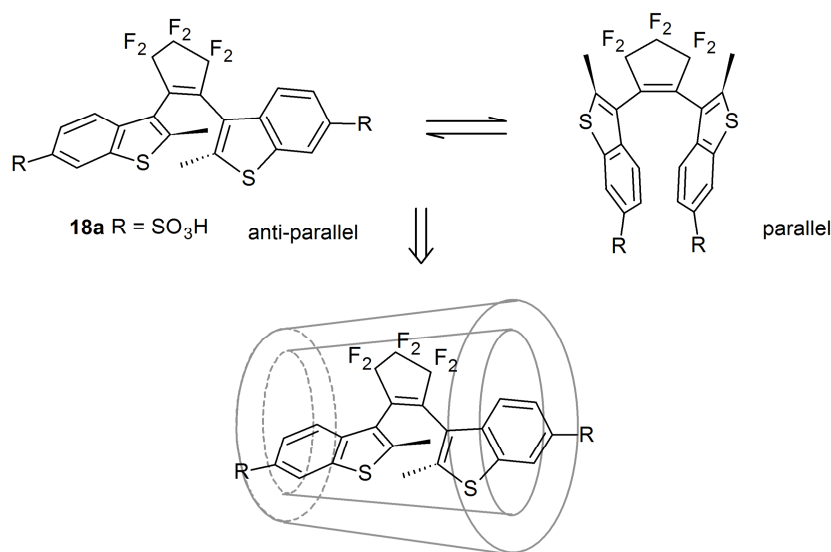


Figure 1.6. Schematic illustration of the DAET **18a** in anti-parallel conformation included into cyclodextrin cavity.

If the cyclodextrin cavity fits more to the rodlike structure than the compact structure, the latter is rejected from the cavity (Figure 1.6.). Indeed, compound **18a** demonstrated increased ratio of the antiparallel conformation and higher quantum yield of the cycloconversion in the presence of β - or γ -cyclodextrins. Such “external” modulation of

photochromic properties of DAETs was called “gated photochromism”⁵⁴. Gated photochromism have been extensively studied for different applications including photosensors and probes for controlling various chemical and physical properties with light^{37,55,56}.

1.3.3. DAET-based fluorescent probes

Since the photoisomerization of DAETs can modulate their fluorescence characteristics, several attempts were done to employ DAETs for fluorescent bioimaging^{57,58}. Notably, DAETs have been known to exhibit the fluorescence only in the open-ring forms.

Generally DAETs do not show strong intrinsic fluorescence. To improve the fluorescence quantum yield the DAETs could be modified by introduction of an additional fluorophore. Some examples of employing additional chromophores, such as anthracene, 4-amino-N-methylphthalimide, 2,4,5-triphenylimidazole, p-phenylene are shown in the Figure 1.7.^{59,60,61,62,63}

Another approach to optimize the DAETs fluorescent properties consists in oxidation of the sulfur atoms in the heteroaromatic rings^{64,65}. The changes of the sulphur oxidation level strongly influenced the fluorescent and photochromic properties in benzothiophene containing DAETs, as shown in Figure 1.8. The fluorescence of closed-ring form **23b** became stronger comparing to the open-ring form **23a**. Such a high fluorescence quantum yield of the closed-isomer like found for **23b** is unique to the oxidized DAETs.

These and similar fluorescent DAETs could be useful as labels for probing the DAET microenvironment, e.g. within intracellular objects, organelles, or in particular, be used as membrane fluorescent probes. For example compound **20a** showed a positive solvatochromic effect of the emission maxima, and its fluorescence quantum yield decreased in proportion to the solvent polarity increased⁶³.

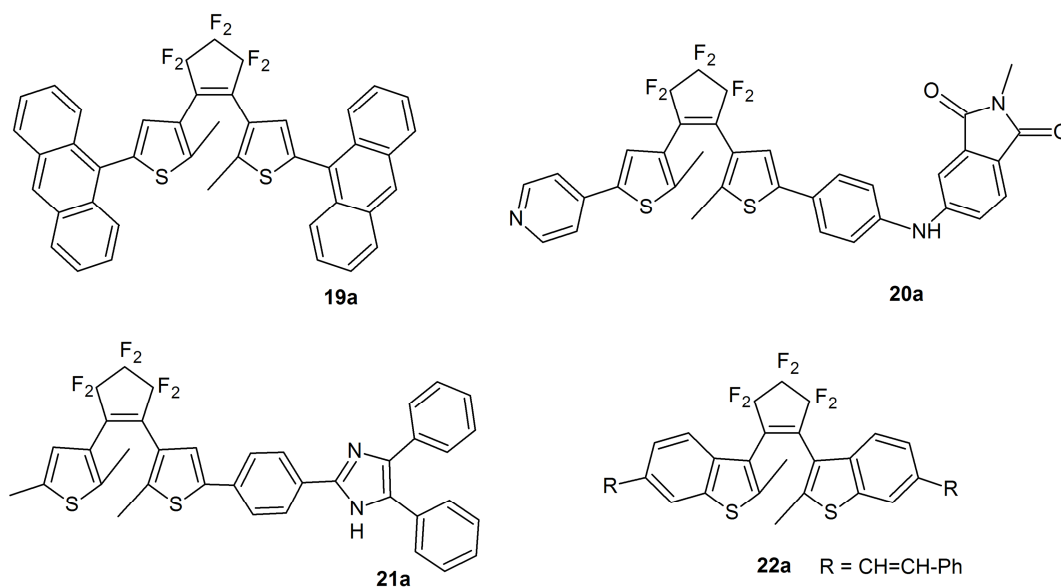


Figure 1.7. Different fluorophores conjugated with the diarylethene moiety in order to improve the DAET fluorescence properties (from ^{59,60,61,62,63}).

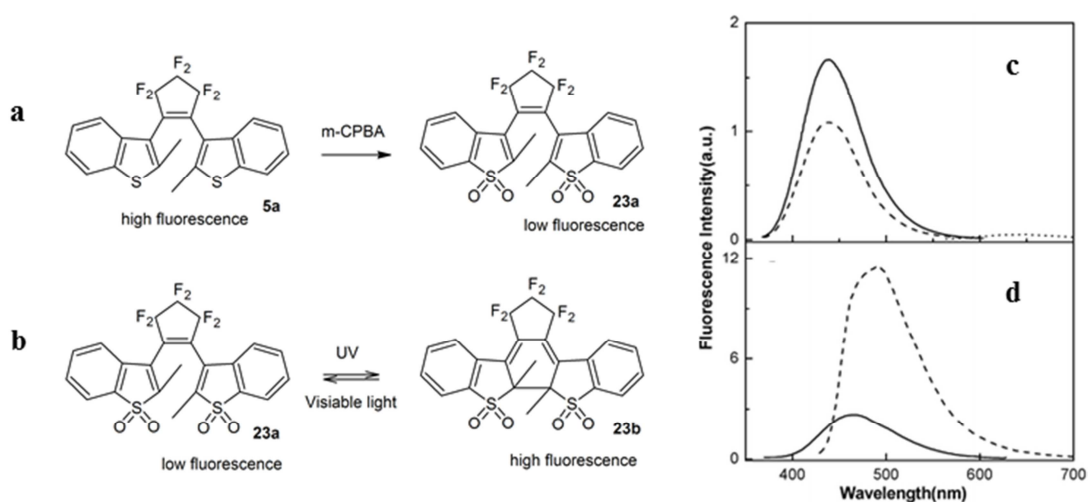


Figure 1.8. (a) Oxidation reaction by *m*-chloroperbenzoic acid of 5a into 23a; (b) photoisomerization of DAET 23; (c) and (d) are the fluorescence spectra of 5 and 23, respectively; solid line – open-ring isomers; dotted line – closed-ring isomers. Adapted from ref. ⁶⁵.

1.3.4. Applications of DAETs in biological systems

Besides a broad application in photonic devices DAETs have found important use in biochemistry, biotechnology and cell biology, in particular, for development of biosensors, analysis of biological dynamics, and in live cell imaging.

Namely, fluorescent DAET-derivatives have been used to develop probes for detection of metal ions. These probes are useful for investigation of environmental and biochemical processes in which metal ions such as Zn^{2+} are essential. The probe molecules combine the ion-sensing and DAET units. In one example, a photochromic thiophene-containing DAET was linked with terpyridine units via a phenylene linker (compound **26a**)⁶⁶. In another work, a DAET-derived Schiff base ligand was synthesized (compound **24a**)⁶⁷. Metal ion coordination to such compounds gave rise to a reversible changes in the emission band intensity and wavelength maximum.

A DAET-based compound was reported in an application for photocontrollable fluorescent labeling of biomolecules⁶⁸. The compound featured a photochromic DAET moiety, a fluorescein-derived fluorophore, and an amine-reactive succinimidyl ester fragment (Figure 1.9., compound **27a**). This DAET derivative displayed modulation of the intramolecular energy transfer from the fluorophore to the DAET moiety by light. The fluorescence of **27a** quenched upon photocyclization because of the spectral overlap of the absorption band of the closed-ring form (acceptor) with the emission band of the fluorophore unit (donor). Owing to the DAET moiety photoisomerization the fluorescence intensity of the compound decreased significantly upon irradiation with UV light but could be fully recovered after irradiation with visible light.

An amphiphilic DAET derivative composed of hydrophilic and hydrophobic chains attached to the aryl groups of DAET core has been developed as a photoswitchable probe for living cells imaging (Figure 1.9., compound **25a**)⁶⁹. It was used as a cell-permeable cellular biomarker with low cytotoxicity. The molecule formed stable (vesicle-like) nanostructures in aqueous solutions. Isomerization to the closed-ring form is accompanied by fluorescence self-quenching due to extension of the π -electron delocalization. This chromophore showed reversibility of the fluorescence switching inside the cell. It demonstrated descent biocompatibility and low toxicity that was confirmed with an MTT assay and trypan blue staining, used to measure the cell viability.

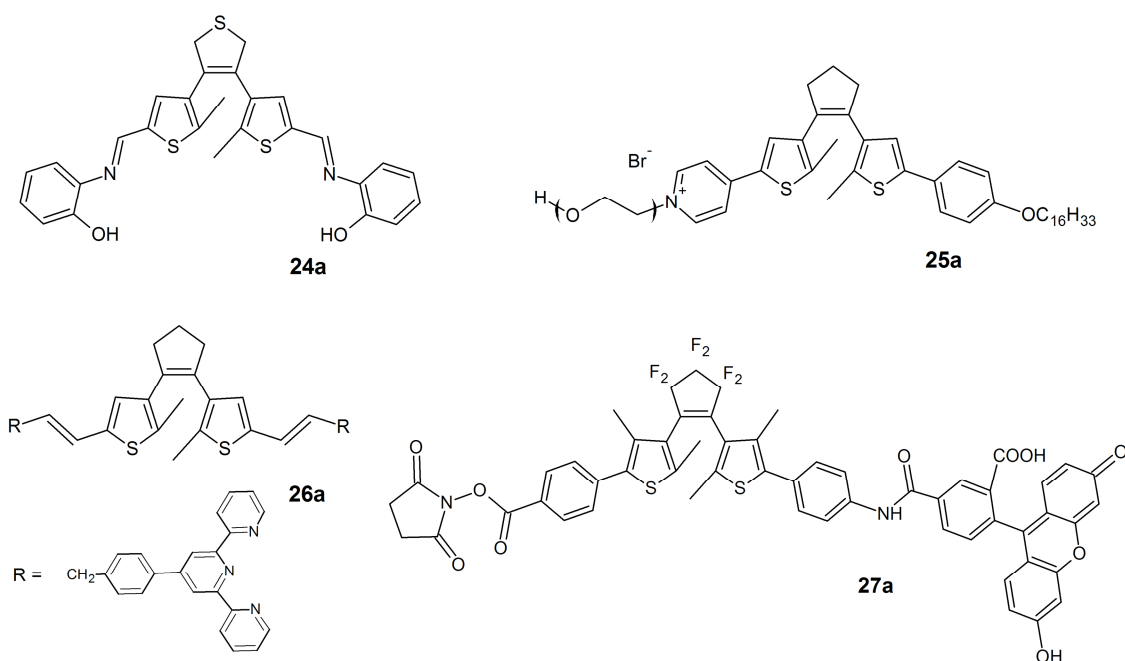


Figure 1.9. Selected fluorescent probes developed for biological applications constructed through conjugation of the DAET unit with an established fluorophore (from ^{66,67,68,69}).

In another study, reversibly photoswitchable dendritic nanoclusters for fluorescence imaging *in vivo* were developed⁷⁰. Dendrimers oligomerized with a DEAT derivative cross-linker to form a nanocluster, which was labeled with a standard fluorophore. The DAET unit was able to reversibly quench the fluorescence of the fluorophore inside the nanocluster through fluorescence resonance energy transfer (FRET). This effect was demonstrated using HeLa cell cultures and in *in vivo* experiments with zebrafish where these dendrimeric nanoclusters repeatedly switched “on” and “off” with contrast inside the cells without any apparent toxicity.

1.4. Membrane-active peptides

Membrane-active peptides are a class of peptides whose macroscopic biological activity is propagated through interaction with cell membranes. The major group of them is various membrane-damaging cytotoxic peptides. Perhaps the most well-established are the so-called antimicrobial peptides (AMPs) that are integral parts of innate immune systems of virtually all multicellular organisms and functionally serve as the first-line host defense tools against opportunistic microorganisms^{71,72}. The antimicrobial membrane-active peptides are frequently believed to share such common features as a small size (6-59 residues), high

positive net charge (abundant in Arg and Lys residues) and the ability to adopt simple amphipathic secondary structures (e.g. α -helical or β -sheet) in the presence of lipid membranes^{73,74}. Notably, some of the AMPs have pre-defined structures already in aqueous environments, i.e. even before binding to the membrane, for instance due to the cyclic overall structure or constraints imposed by disulfide bridges.

The mechanisms of action of AMPs were established to manifest through the unspecific binding to the lipid bilayers of cell membranes, followed by enhanced membrane permeabilization and collapse of the transmembrane electrochemical gradients. Different mechanistic models of particular AMP/membrane interactions have been proposed. The “barrel-stave” and “wormhole” models assume that AMPs, especially α -helix structured, collectively form transmembrane permanent or transient pores in membrane bilayers⁷⁵. These models are favored for the α -helically structured peptides and require peptides’ insertion into the membrane. Alternative, “carpet” or “detergent-like” mechanism of action was proposed for the AMPs that are not inserted deeply into the lipid bilayer, but rather bind peripherally to its surface and cause mechanic membrane disintegration at the threshold concentrations⁷⁶.

Despite abovementioned common features and modes of peptide-bilayer interactions, the spectra of species-specific activities for particular AMPs are known to vary significantly^{76,77,78}. The attempts to rationalize these across-kingdom selectivity observations centered around general differences in the lipid composition of the pro- and eukaryotic cell membranes. Explanations took into account protagonisation of the degree of lipid saturation, the presence of sterols, bilayer thickness and curvature, but most often the net charge of the plasmalemma and the across-membrane potential. The selectivity against bacteria in particular was explained by the higher affinity of the highly cationic AMPs to the negatively charged bacterial cell membranes. Noted by similar connotations with respect to the overall negative cell-surface charge of the transformed cancer cells, some AMPs have been studied as non-specific membranolytic anticancer agents, showed indeed cytotoxic effects on the cancer cells and were therefore postulated as promising therapeutic agents for the cancer treatment⁷⁹.

1.4.1. Peptides employed in this study

Several structurally different membrane active peptides, namely: a cyclic Gramicidin S, a β -stranded fragment of the polycationic β -sheet [KIGAKI]₃, a short α -helical BP100, and a β -hairpin-folded SVS-1 have been used in this study.

Gramicidin S (GS) is a cyclic decapeptide antibiotic with a sequence of *cyclo*(Val-Orn-Leu-^DPhe-Pro)₂ that was isolated from the soil bacterium *Aneurinibacillus migulanus* (formerly *Brevibacillus brevis*) in 1942⁸⁰. It has antiparallel β -sheet conformation stabilized with two type II' β -turns formed around the ^DPhe-Pro fragments. The GS molecule is amphipathic: two polar positively charged ornithine side-chains are directed to one side of the β -sheet while four hydrophobic side-chains are pointing to the opposite direction⁸¹. GS shows activity against broad spectrum of Gram-positive and Gram-negative bacteria, pathogenic fungi⁸². However, due to the high hemolytic activity it is used only for topical applications.

The cationic peptide [KIGAKI]₃ is a model peptide that was designed as an ideal amphipathic β -strand with antimicrobial activity⁸³. This peptide was used for the study of the β -aggregation in membranes, where it was shown to adopt a highly amphipathic β -sheet structure when bound to the lipid bilayer at elevated concentrations. Comparing to the α -helical peptides from which it was originated, the [KIGAKI]₃ has shown higher antimicrobial activities and was less hemolytic, therefore it is potentiated as a promising antimicrobial agent.

BP100 (KKLFKKILKYL-NH₂) is a short cecropin A-melittin hybrid peptide obtained through a combinatorial chemistry approach⁸⁴. It is active against Gram-negative bacteria and was shown to be effective in *in vivo* tests for growth inhibition of the plant pathogenic bacteria. In the case of eukaryotic cells it was shown to act as a cell-penetrating peptide⁸⁵ and recently also its fusogenic activity in the model membranes was shown⁹⁸.

SVS-1 [KVKVKVKV^DPPTKVKVKVK-NH₂] is an 18-residue peptide that was designed to adopt an amphipathic β -hairpin when bound to negatively charged cell membranes⁸⁶. It is constructed of two strands of alternated valine and lysine residues being connected by a type II' β -turn fragment (-V^DPPT-). The peptide was shown to possess toxicity against cancer cells and at the same time reduced hemolytic potential. This selectivity of the peptide was attributed to the ability of a β -sheet to self-assemble in the presence of negatively charged cancer cell membrane. The all-D isomer of the peptide was shown to have the same cytolytic properties, thus SVS-1 was concluded to act through direct membrane lysis and not to involve any receptor-mediated process. Also as a control peptide an analogue (SVS-2) was studied. SVS-2 contains only single residue substitution: here L-proline is used instead of original D-proline. Such minimal modification destroys β -turn and disables therefore formation of the β -hairpin. Consequently, SVS-2 appeared not to have cytolytic activity against cancer cells⁸⁶.

1.5. Photocontrol of the peptide conformation and function

Three principally different methods that were used to incorporate photoresponsive switches in peptides were described in the literature (Figure 1.10.).

It should be noted that in all studies except a few reports the molecular switches other than DAETs were used until now^{87,88}. Most often, the azobenzene fragments were incorporated into peptides as the photoswitching units. This imposed some restrictions on application of the photoswitchable peptides due to limitations known for the azobenzenes. The main problems were thermoreversibility of azobenzenes, their low chemical stability and non-complete conversion efficiency between the two forms. Therefore, the use of DAET-based fragments that are free of these disadvantages is highly promising (see Chapter 1.3.).

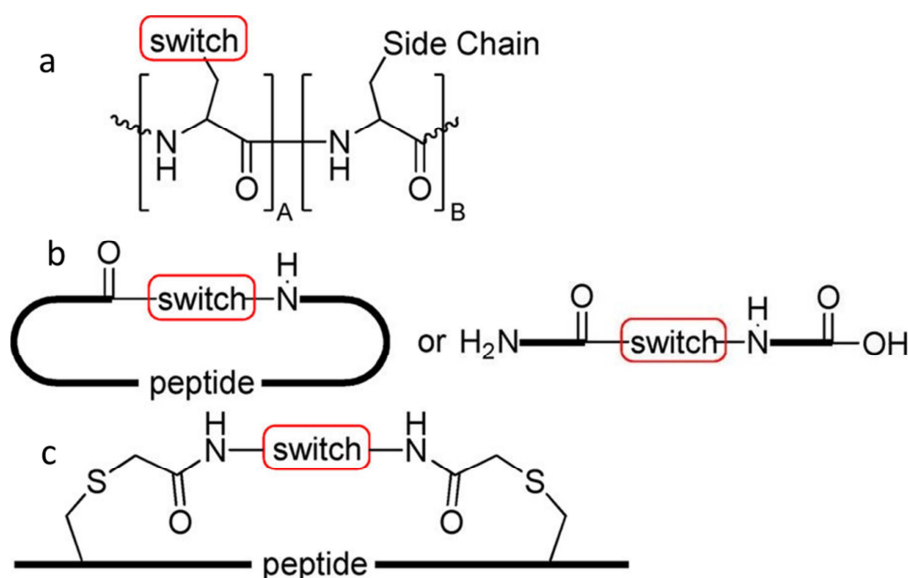


Figure 1.10. Main approaches used to modify peptides with molecular switches. (a) Incorporation of the amino acid derivatives with photoresponsive side-chains into peptides. (b) Introduction of molecular switches directly into the backbone of cyclic or linear peptides. (c) Cross-linking the amino acid side chains in peptides with molecular switches. Adapted from ref. ¹².

1.5.1. Peptides with photoresponsive amino acid residues

Photoresponsive peptides were investigated for the first time by Goodman already in 1960th, structural changes of photoswitch-modified peptide derivatives induced by light exposure was demonstrated⁸⁹. Copolymers of phenylazophenylalanine and γ -benzyl-glutamic acid were prepared. Changes in Cotton effect were observed upon irradiation, indicating light-induced structural changes of the polypeptide backbone as was confirmed by circular dichroism. Further extensive studies of such systems showed that photoisomerization of photochromic residues can induce major conformational changes in peptide structure^{90,91,92,93}. However, to achieve significant influence the number of the incorporated photoswitchable amino acids had to be high; up to 40% of all amino acid residues should be present in the modified peptide. This drawback is a limiting factor for broad applications of such systems. Later on, other methods for peptide modification with molecular photoswitches were developed and they showed much more promising results.

1.5.2. Peptides with the photoresponsive backbone

Perhaps the most prominent example of the peptides bearing the photoresponsive backbone is the illustrated in Fig. 1.11. photosensitive azobenzene-modified cyclic hepta- and hexapeptides which allowed photocontrol of cell adhesion⁹⁴. The designed peptidomimetics have the Arg-Gly-Asp (RGD) sequence as active functioning moiety. This is the ubiquitous motif which is recognized by integrin cell-surface receptors of a large number of adhesive extracellular matrices, blood cells, and cell-surface proteins. Photocontrol of the RGD-containing peptides was proposed as a tool for investigating or modifying the intermolecular adhesion⁹⁵. In this particular example, the photosensitive peptides contained photoswitching 4-[(4-aminomethyl)phenylazo]benzoic acid (AMPB) residue as a part of the peptide backbone, along with the RGD motif. It was found that the conformationally more constrained *trans*-azobenzene-modified cyclic peptide **28** showed a higher binding affinity for $\alpha\beta$ 3 integrin than the *cis* form. Shift of the lysine position (peptide **29**) caused significant reduction in the affinity to the immobilized integrin. However, the difference in affinities between the *cis*- and *trans*-peptides increased by more than a factor of 2 and therefore photomodulation of integrin affinity was concluded to be more efficient for peptide **29**⁹⁶.

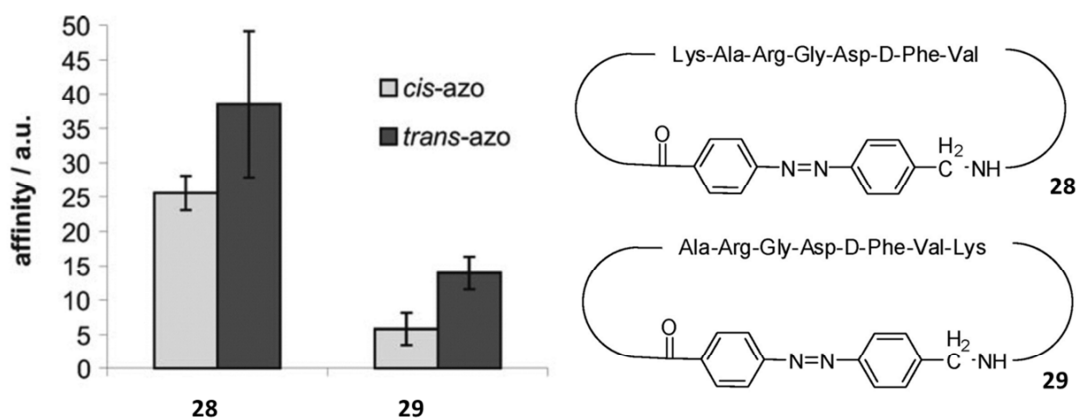


Figure 1.11. Affinities of the azobenzene-modified cyclic peptides **28** and **29** to surface-immobilized $\alpha_5\beta_3$ integrin⁹⁶. “cis” relates to the photostationary state with 80% cis-azo isomer, and “trans” relates to the thermally relaxed molecule with 100% trans-azo isomer. Adapted from ref. ¹².

Many other photoresponsible cyclic peptides have been reported in last two decades^{97,99}. For example, the photosensitive peptide hormone somatostatin that regulates a range of biological functions, including cell growth¹⁰⁰ and cyclic, AMPB-modified peptide derived from the binding site of the PDZ domain of neuronal nitric oxide synthase that is participate in muscle contraction¹⁰¹.

The modification of β -hairpin structured peptides with photoswitchable units shares the structural principle with cyclic peptides and is based on the replacing the β -turn region with the molecular switch. The stability of the secondary structure of the β -hairpin peptides is somehow weaker than that of the cyclic peptides and depends stronger on the interaction between the linked antiparallel peptide strands (i.e., hydrogen bonding and side chain–side chain interactions)¹⁰².

The photoswitchable β -hairpin peptide **30** (a modification of the 12-residue peptide sequence derived from the protein GB1) that has a ^DPro-Gly motif in the β -turn replaced with an azobenzene switch was studied (Fig. 1.12.)^{103,104}. NMR spectroscopy revealed that *cis*-**30** adopted a well-defined β -hairpin structure resembling the parent peptide. However, the *trans* configuration was shown to be less structured; higher order of aggregation was documented for this configuration. The *trans*-**30** reversibly switched on/off several times until the aggregation process led to complete precipitation of the peptide from solution.

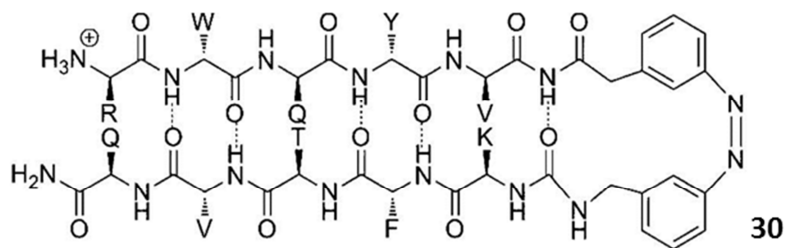


Figure 1.12. Model hairpin peptidomimetic **30** containing a *cis*-azobenzene (3-(3-aminomethylphenylazo)phenylacetic acid, AMPP) as a turn element, shown with the hydrogen bonding pattern of the β -hairpin (from ref. ^{12,103}).

Other examples of photoresponsive β -hairpin peptides have been reported¹⁰⁵. The β -hairpin folding and unfolding process was photocontrolled in tryptophan-rich model peptides, the secondary structure of which is stabilized by the effect called “tryptophan zipper”^{106,107}. In other works successful incorporation of the stilbene chromophore in the peptide backbone was demonstrated^{108,109}.

1.5.3. Peptides with photoresponsive cross-linked side chains

α -helix is one of the most abundant secondary structure elements in natural peptides and proteins. Thus, photocontrol of the α -helical peptide structure could help in developing powerful instruments for medicinal applications of peptides as well as for understanding the mechanisms of their biological action in biological systems.

The control over the α -helix folding could be achieved by introducing two cysteine residues into peptides and cross-linking these with a photoresponsive bridging unit of the length, matching in one of the photoforms the distance expected for an α -helix^{110,111}. For example, the cysteine residues were introduced at i and $i+7$ positions in a model peptide JRK (Figure 1.13.)¹¹². The positions were selected to match the linker length in the azobenzene *cis* configuration. As indicated by CD measurements, the isomerization of the azobenzene switch from *trans* to *cis* configuration increased the helical content from 12% to 48%.

The role of the linker length, its flexibility, position of the cross-linked amino acids and type of molecular switch were addressed in the above cited and similar studies^{12,113}. These studies not only successfully demonstrated the possibility to control the α -helical folding by photostimulation, but also suggested general principles useful for developing photoswitchable peptides based on other molecular switches^{87,88}.

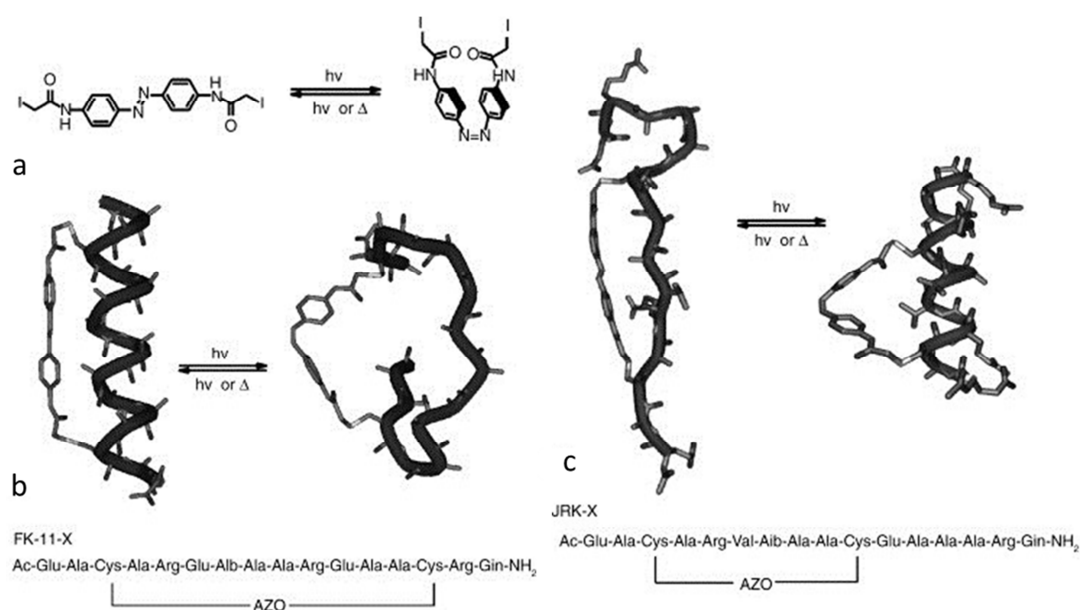


Figure 1.13. Direct photocontrol over the α -helix folding. (a) Chemical structure of the azobenzene containing cross-linker “Azo”, (b) models showing the decreased helicity induced in the FK-11-X peptide upon trans-to-cis isomerization of the attached azobenzene cross-linker. (c) Models showing the increased helicity in the JRK-X peptide induced upon trans-to-cis isomerization of the attached azobenzene cross-linker. The peptide sequences are shown below the models. Adapted from ref.¹¹².

2. Aims of the present study

The incorporation of molecular photoswitches into peptides or proteins should allow reversible control of their structure and functions by means of photoisomerization. The aim of this study was to explore the practical possibilities of polypeptide modification using photoswitchable diarylethene-based building blocks, and to investigate the effects of the photoinduced isomerization on the structure and function of several biologically active peptides.

Specific goals of this work were:

- Design and synthesis of molecular photoswitches based on diarylethene derivatives as building blocks to make them suitable for direct incorporation into peptides via routine peptide synthesis protocols.
- Synthesis of diarylethene modified photoresponsive peptidomimetics based on two biologically active molecules (antimicrobial gramicidin S, anticancer peptide SVS).
- Fundamental characterization of the peptidomimetics in terms of their physico-chemical properties, and establishment of protocols for their photoisomerization.
- Characterization of the core diarylethene chromophore with respect to its influence on the secondary structure of peptide models (α -helices, β -strands).
- Characterization of the photoresponsive peptides in cellular assays in terms of their biological functions (antimicrobial, hemolytic, cancer proliferation).

Peptidomimetics that were designed and studied in this work can find practical applications: in the development of novel medical approaches, in particular for photodynamic pharmacotherapy, and as photoswitchable fluorescent probes for bioimaging and diagnostics.

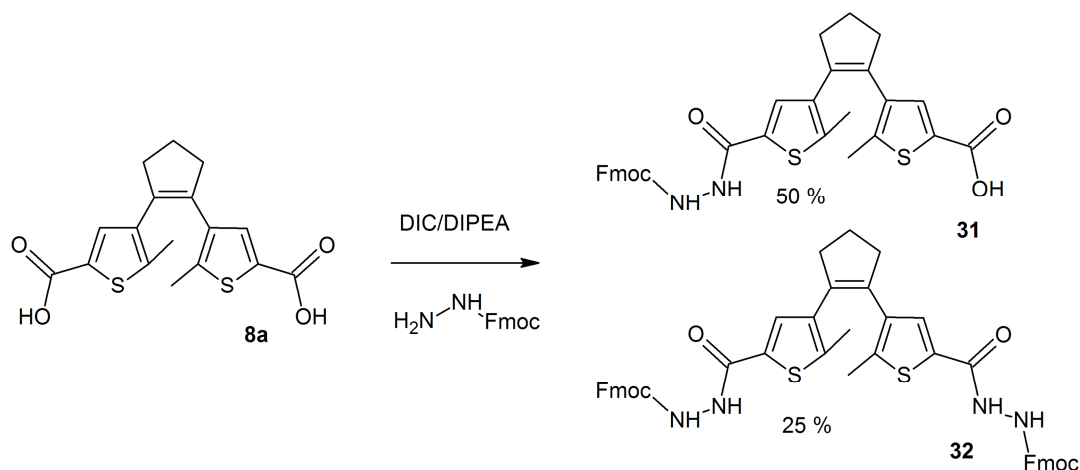
3. Results and Discussion

3.1. Development of novel DAET building blocks for incorporation into peptides

The diarylethene unit requires specific modifications in order to be incorporated into peptides. In particular, carboxylic and *N*-Fmoc protected amino groups have to be introduced into the molecule. Besides, to be applicable in the Fmoc strategy of solid-phase peptide synthesis (SPPS) the building block has to be resistant to aggressive reagents including piperidine and trifluoroacetic acid.

3.1.1. The building block containing hydrazide group as an amino group surrogate (Sw^{I})

To satisfy the above described requirements a building block **31** ($\text{Fmoc-Sw}^{\text{I}}$) - an amino acid mimic - was designed. It has a carboxylic group directly attached to one of the thiophene ring and a hydrazide group attached to the second ring (Scheme 3.1.). It should be noticed that direct attachment of the amino group to the thiophene ring is avoided in the design. This is important, because the aminothiophene-derived diarylethene systems are known to be sensitive to oxidation¹¹⁴. In the following, for the notion of the building block **31** and the residue of **31**, respectively $\text{Fmoc-Sw}^{\text{I}}$ and Sw^{I} , will be used. The peptides employing Sw^{I} are discussed in more details in the Chapters 3.2., 3.3., 3.5., while Chapters 3.4., 3.6. are describing the Sw^{II} -based peptides.



Scheme 3.1. Synthesis of the photoswitchable building block **31** ($\text{Fmoc-Sw}^{\text{I}}$) containing a hydrazide group as an amino function surrogate.

In order to synthesize Fmoc-Sw^I, the diarylethene derivative **8a** functionalized with two carboxylic groups was selected as the direct precursor (Scheme 3.1.). Synthesis of this diacid was described in the literature and can be up-scaled to tens of grams²⁷. In order to introduce the Fmoc protected amino group surrogate, compound **8a** reacted with one equivalent of Fmoc-hydrazide in the presence of coupling reagents (DIC/DIPEA). Since **8a** has two carboxylic groups which can compete in the reaction with Fmoc-hydrazide, the final product contained 25% of the non-reacted diacid **8a**, 50% of the mono-substituted target product Fmoc-Sw^I and 25% of the double-modified by-product **32**. The crude material was washed with 0.5 M solution of aqueous sodium bicarbonate in order to get rid of the non-reacted diacid **8a**. The sodium salt of Fmoc-Sw^I remained in organic solvent due to its high hydrophobicity, while the sodium salt of **8a** transferred to the aqueous solution and discarded. The by-product **32** did not interfere with the following peptide synthesis, therefore, **31** was used as obtained containing the by-product. Pure Fmoc-Sw^I and **32** were obtained for the identification using preparative RP-HPLC.

As was tested (see discussion below) the building block is fully compatible with SPPS. It can be used as a normal Fmoc-protected amino acid in the automated peptide synthesis allowing to prepare peptides in a routine way. The backbone of a peptide with introduced building block Fmoc-Sw^I is shown in Figure 3.1. Major conformational changes of the peptide backbone are expected to be occurring during photoisomerization of the DAET unit.

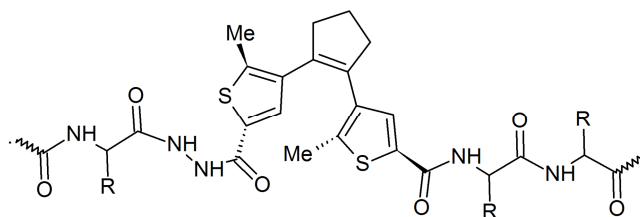


Figure 3.1. Peptide backbone modified using photoswitchable building block Fmoc-Sw^I.

In order to evaluate the Sw^I photochromic and fluorescent properties, a small water-soluble peptidomimetic (KI-Sw^I, sequence: KIGAKI-Sw^I-KIGAKI) was constructed (see protocol in Chapter 6.2). The peptidomimetic was designed to have no natural amino acids that can interfere with the absorption and fluorescence of the photoswitchable unit. RP-HPLC-elution profiles of the purified peptide were recorded before and after the irradiation with UV light (Figure 3.2.). As can be seen, complete conversion from open-ring form (black

line) to colored closed-ring form (red line) can be achieved after irradiation with UV light. Furthermore, the obtained colored closed-ring form converted back to the open-ring form after irradiation with visible light. The peptidomimetic in closed-ring form was found to possess shorter retention time contrary to the open-ring form. The effect is most probably due to changes in the hydrophobicity of the photoswitchable unit Sw^I (open-ring vs. closed-ring), because the glycine-containing small peptidic part is unlikely to be folded under the RP-HPLC conditions.

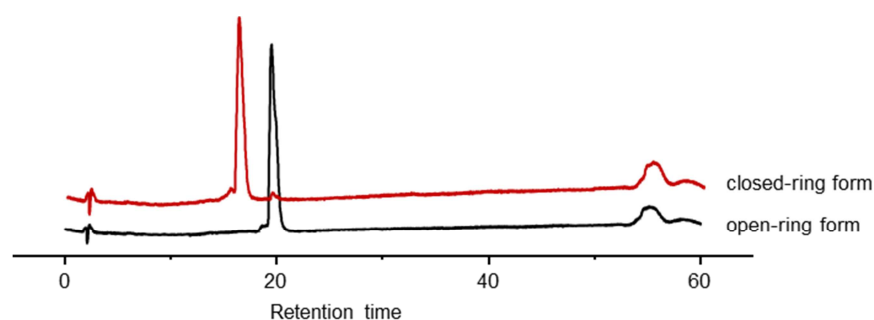


Figure 3.2. Analytical RP-HPLC of the peptide KI-Sw^I before irradiation with UV light (black line) and after it (red line) (chromatographic conditions see in Chapter 6.).

The absorption and fluorescent spectra of the KI-Sw^I were recorded in water solution for both photoforms (Figure 3.3a). The open-ring form absorbed in the UV region, and the closed-ring form revealed two bands in the visible region, at 349 and 536 nm.

The fluorescent properties of the Sw^I unit were also studied. In Figure 3.3b a spectrum of the KI-Sw^I fluorescence (excitation at 295 nm) in the open-ring form is shown. The peptide gave green fluorescence with a maximum at 430 nm. Interestingly, the highest fluorescence quantum yield was observed with the excitation at 295 nm, while the corresponding absorption maximum was at 265 nm. Perhaps, during the excitation of the open-ring form two competing processes occurred: conversion to the closed-ring form and the fluorescence emission. As was expected for this type of DAETs, the closed-ring form showed no fluorescence.

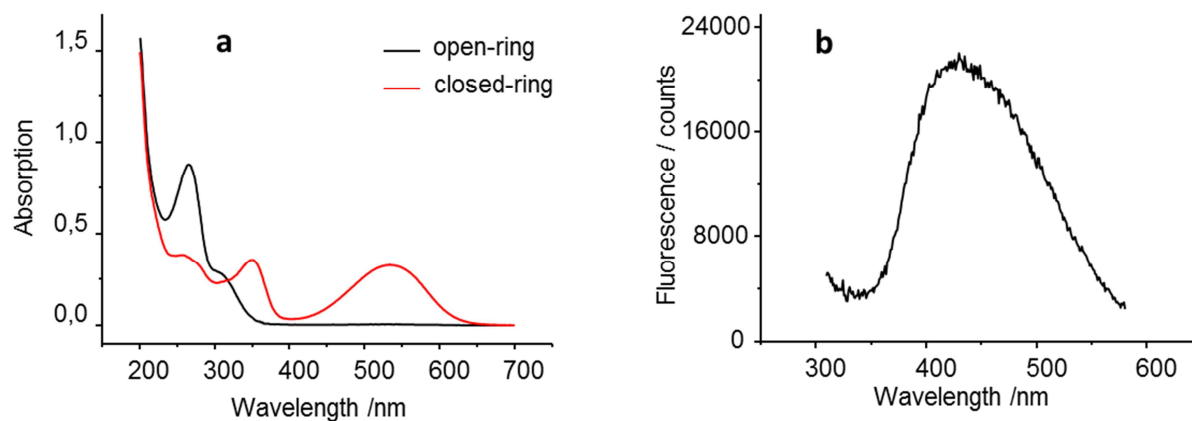


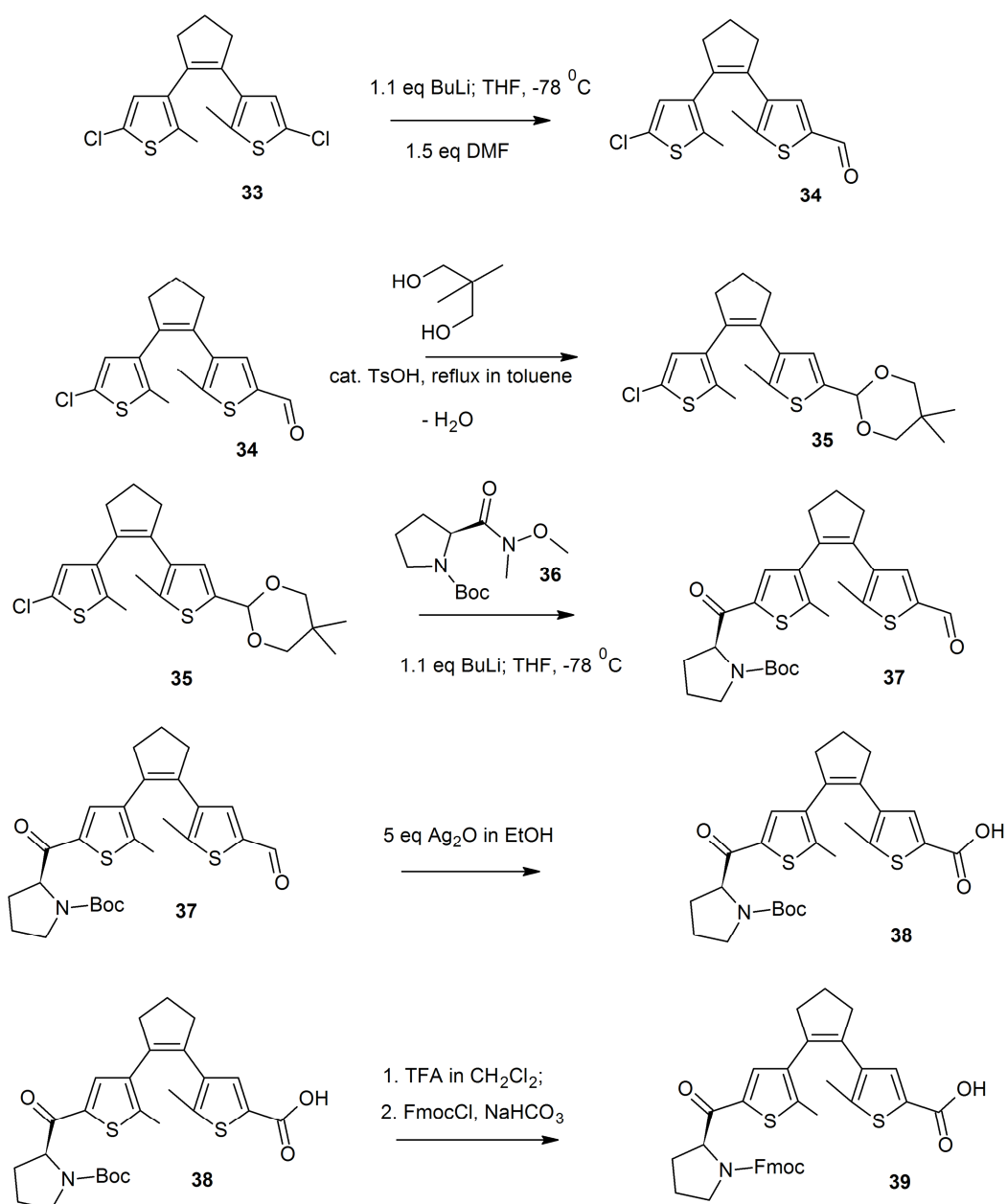
Figure 3.3. (a) Absorption spectra of the open-ring and closed-ring forms of the peptidomimetic $KI-Sw^I$ recorded at $30 \mu M$ concentration in 10 mM phosphate buffer ($\text{pH } 7.4$) at ambient temperature. (b) Fluorescence spectrum of the peptidomimetic $KI-Sw^I$ in open-ring form; $21 \mu M$ in 10 mM phosphate buffer ($\text{pH } 7.4$); excitation at 295 nm , ambient temperature.

3.1.2. Building blocks containing proline as an amino function (Sw^{II})

Due to expected chemical instability of the hydrazide fragment, the building block Fmoc- Sw^I was redesigned to avoid this drawback. Different type of building blocks (Sw^{II}) was developed, where a residue of an amino acid was used instead of the hydrazide group.

On the contrary to the rotationally flexible hydrazide group the backbone of an α -amino acid has more defined conformation. Therefore in this type of building blocks it should be possible to fine adjust geometrical position of the amino function with respect to the DAET core by simply varying the amino acid residue. In this work two DAET building blocks of the Sw^{II} type were synthesized: one with the residue of L-proline (Fmoc- Sw^{LPro}) and another with the residue of D-proline (Fmoc- Sw^{DPro}).

The synthesis of new building blocks was performed starting from compound **33** (Scheme 3.2.). Compound **33** was synthesized according to the published protocol²⁷. It has chloride substitutions at the 2- and 2'-positions of dithienylcyclopentene molecule that can be lithiated in order to functionalize the thiophene rings. Importantly, selective monolithiation was also possible for **33**. Treatment of **33** with one equivalent of *n*-butyllithium in an inert atmosphere at $-78 \text{ }^\circ\text{C}$ led to the monolithiation. Followed addition of the dimethylformamide gave the mono-formylated derivative **34** with almost quantitative yield of 90%. The formyl group was then temporally protected with 2,2-dimethyl-1,3-propanediol to give the acetal **35**.



Scheme 3.2. Synthetic route for the preparation of the photoswitchable building block *Fmoc-Sw^{LPro}*.

The second functional chloride group in **35** was then lithiated and reacted with *N*-Boc protected L-proline-derived Weinreb amide (**36**). Compound **36** was synthesized according to the published protocol¹¹⁵. The formyl group in the resulting product **37** was oxidized with silver oxide to yield the carboxylic group (compound **38**). The final building block **39** (*Fmoc-Sw^{LPro}*) was obtained after exchanging the *Fmoc*-protection for the *Boc*-protection at the proline residue. The same synthetic approach was also used for the preparation of D-proline containing building block (*Fmoc-Sw^{DPro}*).

As described above, the method was illustrated on the example of a proline residue incorporation into the photoswitchable building blocks. However, other protected amino acid Weinreb amides can be used in order to obtain other DAET building blocks suitable for SPPS.

3.2. Photoresponsive linear model peptides with the Sw^I building block

First, the photoswitchable DAET building block Fmoc-Sw^I was incorporated in linear peptidomimetics. This allowed (i) verification of the building block compatibility with the standard SPPS procedures; (ii) assessment of the extent of the conformational perturbation imposed by the DAET switch onto different secondary structure elements as well as (iii) evaluation of efficiency of the photoswitching process in membrane environments.

Two model peptidomimetics were designed: an asymmetric “ β/α -model peptide” and a symmetric “ α/α -model peptide”. The first comprised a β -strand connected successively to the Sw^I unit and a short amphipathic α -helix; the second has two identical α -helices connected by their *N*-termini to the DAET fragment (Figure 3.4.). The choice of the polypeptide units was made considering their small size and amphipathic nature, to interact with lipid membranes and to allow obtaining structural information in form of ¹⁹F-NMR constrains.

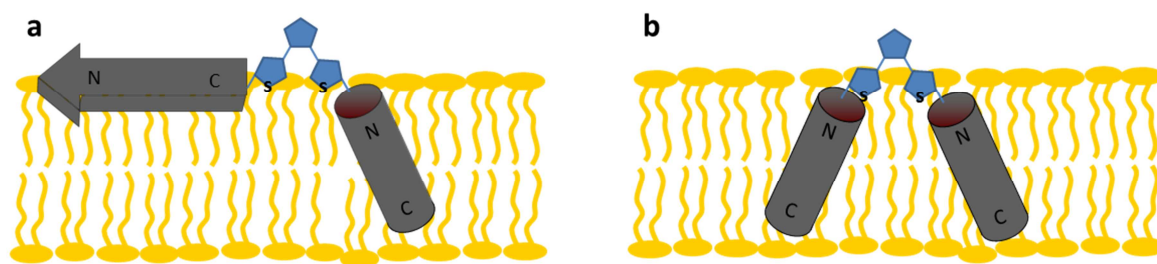


Figure 3.4. Modular build-up and expected orientations of the linear model peptidomimetic with the DAET unit in the middle of the polypeptide backbone: (a) “ β/α -model peptide”; (b) “ α/α -model peptide”. The non-perturbed “ideal” conformational states are illustrated as a flat arrow (β -part) and as solid cylinders (α -part). *N*- and *C*-termini of the peptidic units are indicated. Photoswitchable DAET unit is colored in blue. Lipid bilayers are drawn not to the scale and illustrate only overall expected peptide topologies.

Thus, the β -stranded unit of the final constructs was an octapeptide derivative of the antimicrobial peptide [KIGAKI]₃, while the α -helix unit was derived from the complete

sequence of the membrane-active peptide BP100. Both parent peptides were extensively studied previously by solid-state ^{19}F -NMR^{116,117}, and were known to possess very stable amphipathic secondary structures over broad range of membrane compositions and concentrations. ^{19}F -NMR data (^{19}F dipolar couplings at different locations along the sequence) were known for both units.

3.2.1. Peptide synthesis

The designed peptidomimetics were prepared with peptide units constructed using canonical amino acids (the “wild type”) for the CD investigation in solution. In addition, a series of singly or doubly amino acid-substituted ^{19}F -labelled analogues of all the peptidomimetics were obtained for the ^{19}F -NMR measurements. The analogues contained an artificial amino acid CF_3 -Bpg (L-3-(trifluoromethyl)bicyclopent-[1.1.1]-1-yl glycine, ^{19}F -label)¹¹⁸ in place of a non-polar residue. CF_3 -Bpg was designed as an ideal ^{19}F -label for substituting hydrophobic residues as it resembles closely Val, Leu, Ile, Met in terms of hydrophobicity and size. Moreover, the CF_3 -Bpg side chain hydrophobicity allows the substitution of this ^{19}F -label for Ala and aromatic amino acid residues, since such exchanges were demonstrated to influence neither structure nor function of antimicrobial peptides over many examples¹¹⁹. The CF_3 -Bpg was applied here in the same fashion as was routinely used in the solid-state ^{19}F -NMR structural studies of membrane-active peptides before^{120,121}.

Overall, ten ^{19}F -labeled analogues of the “ β/α -model peptide” were synthesized, four with the ^{19}F -labels in the β -strand region and six with the labels in the α -helical fragment. The amino acid sequences of the synthesized peptidomimetics are shown in the Table 3.1. For this group of peptides the synthesis was carried out with manual SPPS (Fmoc strategy) in conventional way where the Fmoc-protected DAET unit was introduced just like any other amino acid (details are described in the Chapter 6.2.1.).

The α/α -model peptide was also prepared “wild type” for CD study and labeled for ^{19}F -NMR measurements. Five CF_3 -Bpg-containing analogues were produced, each possessing two fluorine labels, one in every copy of the α -helix (Table 3.2.). Since the model consisted of two identical α -helical fragments the *N*-termini of which were connected by the building block **8a** (DAET diacid), the following procedure was used. Complete helical sequences were built first on the solid support using automated SPPS. The Fmoc-deprotected polypeptide chains were cross-linked in one step with the DAET building block **8a** while

remaining bound to the resin. The detailed synthetic procedure is described in the Chapter 6.2.2.

Table 3.1. List of the synthesized ^{19}F -labelled analogues of the β/α -model peptide.

Peptide	Sequence*
β/α -model peptide (wild type)	KIKIGAKI-Sw ¹ -KKLFFKKILKYL-NH ₂
$\beta 2\text{I}/\alpha$	K-CF ₃ -Bpg-KIGAKI-Sw ¹ -KKLFFKKILKYL-NH ₂
$\beta 4\text{I}/\alpha$	KIK-CF ₃ -Bpg-GAKI-Sw ¹ -KKLFFKKILKYL-NH ₂
$\beta 6\text{A}/\alpha$	KIKIG-CF ₃ -Bpg-KI-Sw ¹ -KKLFFKKILKYL-NH ₂
$\beta 8\text{I}/\alpha$	KIKIGAK-CF ₃ -Bpg-Sw ¹ -KKLFFKKILKYL-NH ₂
$\beta/\alpha 3\text{L}$	KIKIGAKI-Sw ¹ -KK-CF ₃ -Bpg-FKKILKYL-NH ₂
$\beta/\alpha 4\text{F}$	KIKIGAKI-Sw ¹ -KKL-CF ₃ -Bpg-KKILKYL-NH ₂
$\beta/\alpha 7\text{I}$	KIKIGAKI-Sw ¹ -KKLFFKK-CF ₃ -Bpg-LKYL-NH ₂
$\beta/\alpha 8\text{L}$	KIKIGAKI-Sw ¹ -KKLFFKKI-CF ₃ -Bpg-KYL-NH ₂
$\beta/\alpha 10\text{Y}$	KIKIGAKI-Sw ¹ -KKLFFKKILK-CF ₃ -Bpg-L-NH ₂
$\beta/\alpha 11\text{L}$	KIKIGAKI-Sw ¹ -KKLFFKKILKY-CF ₃ -Bpg-NH ₂

* Sw¹ denotes the residue of the building block **31**.

Table 3.2. List of the synthesized ^{19}F -labelled analogues of the α/α -model peptide.

Peptide	Sequence*
α/α -model peptide (wild type)	Sw ^A (KKLFFKKILKYL-NH ₂) ₂
α/α -3L	Sw ^A (KK-CF ₃ -Bpg-FKKILKYL-NH ₂) ₂
α/α -4F	Sw ^A (KKL-CF ₃ -Bpg-KKILKYL-NH ₂) ₂
α/α -7I	Sw ^A (KKLFFKK-CF ₃ -Bpg-LKYL-NH ₂) ₂
α/α -8L	Sw ^A (KKLFFKKI-CF ₃ -Bpg-KYL-NH ₂) ₂
α/α -10Y	Sw ^A (KKLFFKKILK-CF ₃ -Bpg-L-NH ₂) ₂

* Sw^A denotes the residue of the diacid **8a**.

Gratifyingly, no side-reactions were observed during the synthesis of the β/α -models. The crude peptidomimetics were standardly purified on the preparative RP-HPLC column and 100% purity was confirmed by analytical HPLC after lyophilization. On the contrary, crude materials of the cross-linking syntheses (α/α -model peptide) revealed completely non-coupled peptide chains alongside with the target products, as well as mono-reacted CO₂H-

Sw^A-peptide derivatives. The target peptidomimetics were identified with the MALDI analysis and separated as described in Chapter 6.2.2.

The elution profiles of the purified peptides of both “wild type” models were recorded before and after the irradiation with UV light (Figure 3.4.). It was possible to quantitatively convert the open-ring forms into the closed-ring forms by the irradiation with UV light. The reverse reactions (decoloration) under the exposure to the visible light were found to proceed completely as well. In both model peptides moderate changes in the retention times (<5 min) were observed during the photoisomerization. The shift was in the same direction and value as was observed earlier in a similar study on another linear peptide derivative (see Chapter 3.1.1.). Presumably, the RP-HPLC retention time difference reflected intrinsic differences in the hydrophobicities of the two DAETs photoforms, with the constrained closed-ring compounds being slightly more polar.

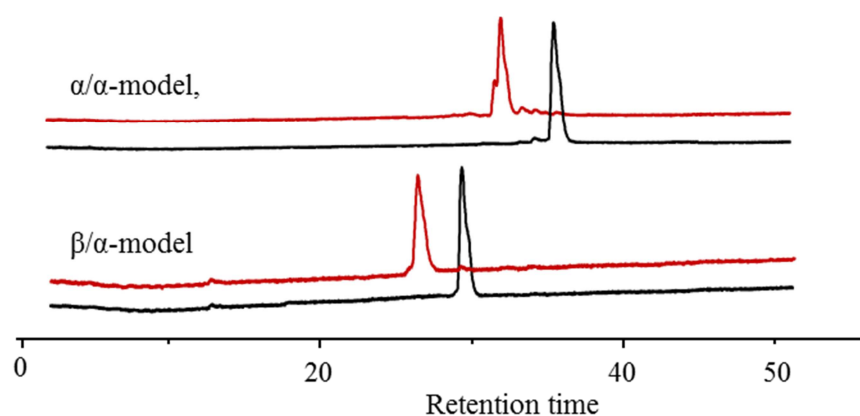


Figure 3.4. Analytical RP-HPLC of the α/α -model peptide and β/α -model peptide before irradiation with UV light (open-ring form, black line) and after it (closed-ring form, red line). (Conditions see in Chapter 6.).

3.2.2. Conformational changes upon photoswitching in solution

CD spectra (Figure 3.5.) of both model peptides were recorded in order to observe changes in their secondary structure and evaluate potential conformational and spectral impact of Sw^I in different isotropic environments. No significant changes were observed during the photoisomerization for both models – the CD spectra were identical in the closed-ring and the open-ring forms. One might conclude that conformational perturbation (at least in the selected models under tested conditions) caused by the photoswitching process seemed to be small if not completely absent. These measurements also demonstrated that the CD

spectral range useful for peptide structural analysis was free of any contribution from the Sw^I chromophore.

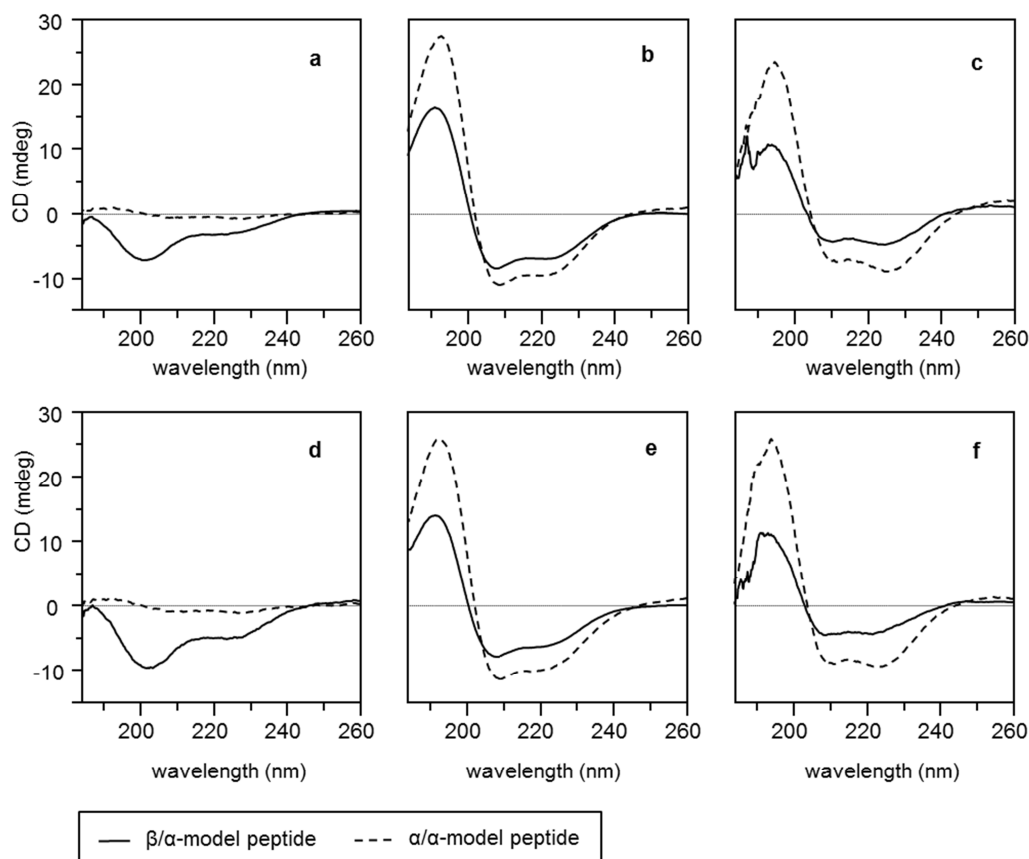


Figure 3.5. CD spectra from linear model peptides in different environments at a concentration of 100 $\mu\text{g/ml}$. β/α -model peptide (solid line) and α/α -model peptide (dashed line) in solution (a, d, 10 mM PB, pH 7.4); in detergent micelles (b, e, 25 mM SDS); in DMPC vesicles (c, f, P/L = 1/50). The peptides were in the open-ring forms (a, b, c) and in the closed-ring forms (d, e, f).

In addition, the CD data allowed obtaining useful insights into conformational properties of the peptidic units of the model peptides. According to previous studies, the parent peptides [KIGAKI]₃ and BP100 should be unstructured in aqueous buffers. In the presence of lipid membranes, both peptides were known to bind the bilayers and undergo structural transition to the amphipathic β -strand and α -helix, respectively^{116,117}. In full accordance to this, the β/α -model peptides were unstructured in buffer solution, as their CD curves resembled that for a random coil (no positive bands and a pronounced negative band at ca 200 nm). The α/α -model peptide gave no signal in aqueous buffer at all, independently of the photoswitching process, that may be due to aggregation of the peptide, never observed for the stand-alone BP100 (the α -helical unit). As expected, both model peptides gave the CD

lineshapes with the dominating α -helical signal in SDS and DMPC vesicles, indicating the binding of peptides to the micelles/membranes. Notably, the α/α -model peptide gave the CD spectra characterized by stronger α -helical contribution, while for the β/α -model peptide the β -part in the membranes appeared to structurize independently.

3.2.3. Conformational changes upon photoswitching in membranes

Solid-state ^{19}F -NMR measurements were performed for the model peptides labeled by CF_3 -Bpg in macroscopically oriented lipid bilayers. The studied peptidomimetics were reconstructed into a model lipid membrane (DMPC) at low peptide to lipid molar ratio (1:100) to avoid aggregation. The measurements were done below and above the main lipid phase transition temperature (at 15° and 40°C respectively; DMPC phase transition occurred at ca. 23°C) for each prepared oriented sample. In all the NMR experiments the oriented samples were aligned parallel to the magnetic field. The peptides were measured in both open-ring and closed-ring forms. Further details of the sample preparation and NMR spectroscopy are given in the Chapters 6.3. To check if oriented samples were prepared ^{31}P -NMR measurements were performed prior to ^{19}F -NMR. Observation of the ^{31}P -NMR signals from the phospholipids (headgroups of DMPC molecules), allows quantitative assessment of the degree of the peptidomimetic orientation in the lipid bilayers. More than 70% lipids were found to be oriented in all the prepared samples, (data not shown), therefore, an assumption was made that the peptides should possess similar degree of alignment.

It was noticed above that the parent antimicrobial peptide [KIGAKI]₃ was originally designed as an amphipathic β -strand. It was demonstrated to exist in a concentration-dependent equilibrium between single-stranded monomeric form and the aggregated β -sheets in the membrane-bound state. Both forms can be distinguished by solid-state ^{19}F -NMR. In the case of the single-stranded monomeric form a dipolar coupling of ca. +8 kHz should be observed, while the aggregated β -sheets are characterized by ca. +15 kHz splitting. Figure 3.6. illustrates the solid-state ^{19}F -NMR spectra for the β/α -model labeled in the β -stranded fragment at high temperature.

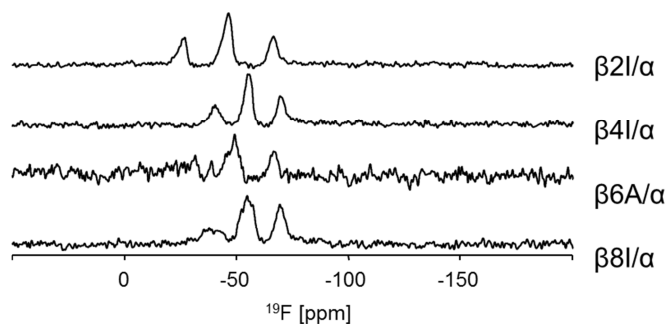


Figure 3.6. Representative solid-state ^{19}F -NMR spectra of the β/α -model peptide CF_3 -Bpg-labeled analogues. The peptides are measured with their Sw^{I} units being in the closed-ring state. The peptides were reconstituted in DMPC ($P/L = 1:100$) and measured at 40°C .

As can be seen, all the measured peptides showed a single triplet with the positive coupling constants within 6.8-9.3 kHz range if their DAET fragments Sw^{I} were in the closed-ring rigid state (see Table 3.3. for the coupling values). Such appearance is compatible with the highly dynamic β -strand bound to membrane such as the hydrophobic side-chains point towards the membrane interior, with the cationic side-chains of lysines pointing to the opposite direction, namely, to the aqueous phase. Slightly lower coupling constant values obtained for the peptidomimetics labeled at positions 4 and 8 could be explained by their proximity to the two strand-perturbing sites in the molecule (glycine and Sw^{I} residues, respectively), assuming that the Sw^{I} behaves as a β -strand breaker. In general, the spectra resembled closely the low-concentration ($P/L < 1:400$) state of the parent 18-mer peptide. Interestingly, the characteristic coupling constant value of ca. +8.0 kHz for monomers was observed for the β/α -model peptide at a significantly higher P/L of 1:100 despite the similarity of the molecular size of the two peptides. Aggregation behavior of the β/α -peptide was not studied further but this discrepancy may be simply explained by the steric congestions imposed by Sw^{I} moiety which might prevent the β -sheet self-assembly¹²².

Table 3.3. ^{19}F - ^{19}F dipolar couplings of the β/α -model peptide analogues labeled in the β -strand unit, as determined in the oriented DMPC bilayers at 40°C .

State of the Sw^{I}	Dipolar coupling (J, [kHz]) in:			
	$\beta 2\text{I}/\alpha$	$\beta 4\text{I}/\alpha$	$\beta 6\text{A}/\alpha$	$\beta 8\text{I}/\alpha$
open-ring form	9.3	7.0	8.3	3.0 and 6.8
closed-ring form	9.3	6.8	8.3	6.8

When the Sw^I unit was converted to the open-ring flexible state, the spectra of the peptidomimetics did not change, with a single exception observed for the peptidomimetic labeled at position 8, where the label is directly attached to the photoswitch. As can be seen in the Figure 3.7., 6.8 kHz splitting persisted, but additional signal with ca. 3 kHz splitting emerged. Conversion back to the closed-ring form led to disappearance of this new signal, confirming that it was caused by the Sw^I photoswitching. The signal could be assigned to one of the two conformations of the open-ring Sw^I (i.e. parallel and antiparallel, see Chapter 1.3.2.), that is in line with the above suggested β -breaking ability of the Sw^I unit.

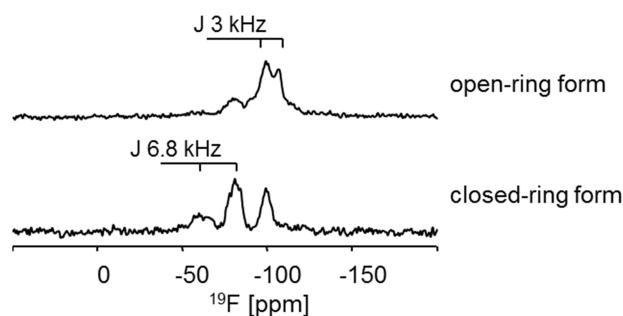


Figure 3.7. Solid-state ^{19}F -NMR spectra of the $\beta 8\text{I}/\alpha$ -peptide in DMPC ($P/L = 1:100$) at 40°C . Upper line: the Sw^I in the open-ring form; bottom line: corresponding closed-ring form.

Measurements at the temperature below the lipid phase transition did not reveal any difference comparing to the above described observations, except that the ^{19}F -NMR signals were broadened as expected for peptides in less mobile gel-phase lipids.

Next, the α -helical part of the β/α - and α/α -model peptides was closely investigated by the analysis of ^{19}F -NMR spectra of the peptidomimetics labeled in the α -helix units. The measurements were performed under the same conditions as describe above. The resulting spectra are shown in Figures 3.8 (β/α -model) and 3.9, 3.10 (α/α -model), the splitting values are summarized in Table 3.4. and 3.5. Like in the case of β/α model peptides, the spectra measured in liquid-phase bilayers featured relatively narrow signals while broad signals were observed at low temperatures, in some cases precise measurements of the dipolar coupling constants was impossible.

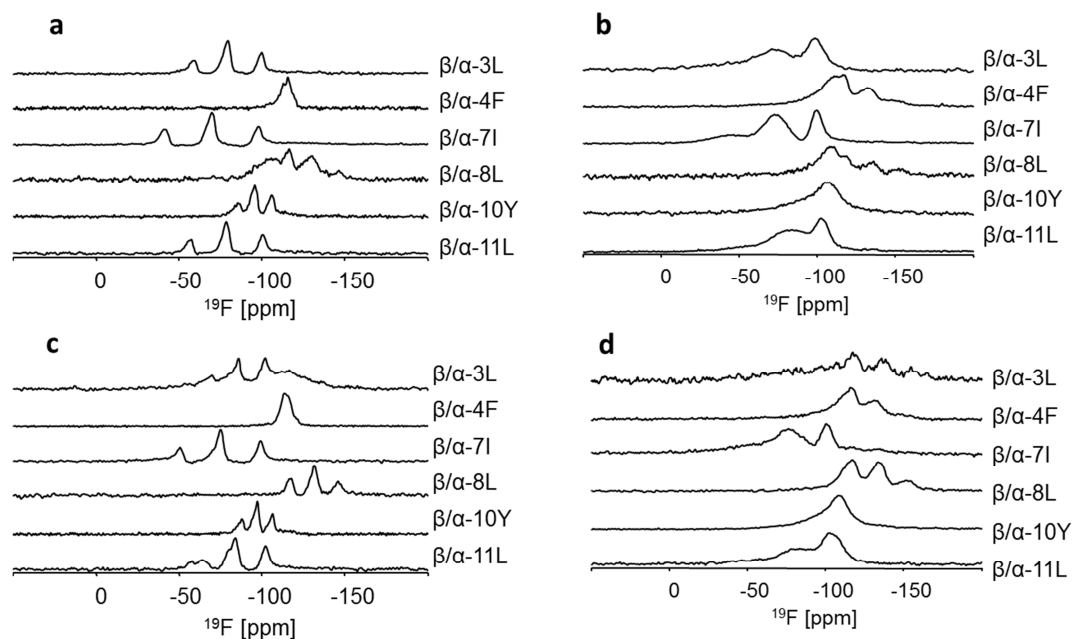


Figure 3.8. Series of solid-state ^{19}F -NMR spectra of the β/α -model peptides labeled by $\text{CF}_3\text{-Bpg}$ in the α -helical fragments in the oriented DMPC bilayers; (a), (c) at 40°C , (b), (d) at 15°C ; (a) and (b) correspond to the DAET unit being in open-ring form, while (c) and (d) - in the closed-ring form.

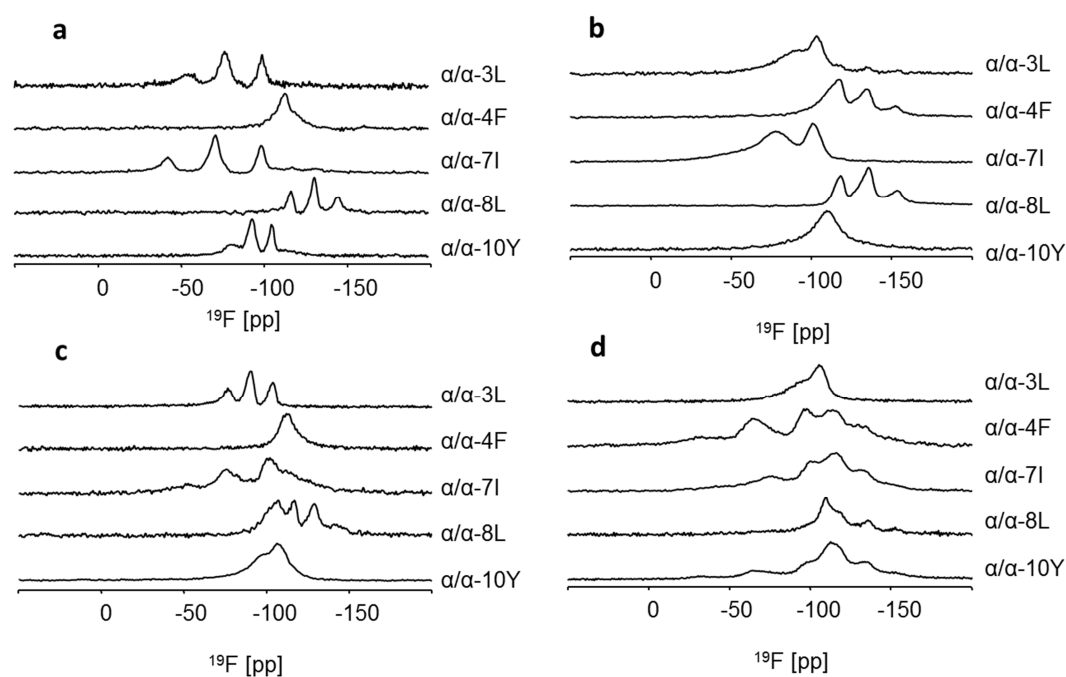
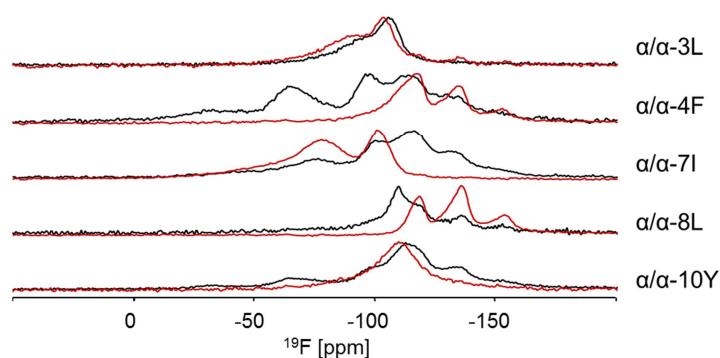


Figure 3.9. Series of solid-state ^{19}F -NMR spectra of the α/α -model peptide analogues labeled by $\text{CF}_3\text{-Bpg}$ in the α -helical fragments in the oriented DMPC bilayers; (a), (c) at 40°C , (b), (d) at 15°C ; (a) and (b) correspond to the DAET unit in open-ring form, while (c) and (d) - in the closed-ring form.



Scheme 3.10. Solid-state ^{19}F -NMR spectra of α/α -model peptide in the oriented DMPC bilayers at 15°C (below lipid phase transition). Spectra of the closed-ring forms (red lines) aligned with corresponding spectra of the open-ring forms (black lines).

Table 3.4. Fluorine dipolar coupling constants of the α -helical part of β/α -model peptide analogues as determined in oriented DMPC bilayers at 40°C and 15°C .

State of the Sw^{I}	Dipolar coupling (J, [kHz]) in:					
	β/α -3L	β/α -4F	β/α -7I	β/α -8L	β/α -10Y	β/α -11L
open-ring form, 40°C	7.6	0	10.5	-5.4	3.8	8.3
closed-ring form, 40°C	6.0	0	9.1	-5.4	3.6	7.4
open-ring form, 15°C	9.9	-6	10	-6.6	0	7.7
closed-ring form, 15°C	-7.5	-5.6	9.2	-6.6	0	7.7
reference*, 35°C	5.4	0	7.7	-4.6	2.6	6.1
reference*, -20°C	4.5	-7.1	9.8	7.4	0	12.1

*J values from the parent peptide as reported for the same labeling positions in the conditions of fluid or gel-state bilayer of DLPC/DLPG¹²³

Table 3.5. CF_3 -group dipolar coupling constants of the α -helical part of α/α -model peptide analogues as determined in the oriented DMPC bilayers at 40°C and 15°C .

State of the Sw^{I}	Dipolar coupling (J, [kHz]) in:				
	α/α -3L	α/α -4F	α/α -7I	α/α -8L	α/α -10Y
open-ring form, 40°C	8.6	0	10.6	-5.3	4.5
closed-ring form, 40°C	5.1	0	9.6	-4.7	3.4
open-ring form, 15°C	5	-6.6	9.3	-6.8	0
closed-ring form, 15°C	4.6	-6.6/12*	9.3/-6.4*	-6.8/0*	0/12*

* Coupling value observed in the satellite signal

Remarkably, these spectra closely resembled the set of splitting pattern in the spectra of the parent BP100 peptide measured under similar conditions¹²⁴. Even changes happened upon the liquid and gel-state bilayer phase transition (in particular, for the corresponding peptides labeled at positions Phe4 and Tyr10) are essentially similar, at least for the peptidomimetics with the Sw^I unit in the open-ring state.

Comparison of the NMR data measured for the liquid-phase bilayer for both peptidomimetics labeled at the same positions revealed no difference in the spectra between and upon photoswitching. The spectra of the doubly-labeled α/α -model peptides contained one pair of the ¹⁹F-NMR signals confirming that the two identical α -helical parts are structured and aligned in the bilayer similarly. This is what could be expected assuming that the open-ring conformationally flexible DAET residue in these peptidomimetics allows virtually autonomous interaction of the BP100 units with the lipid membrane. Even in the gel-phase lipids the open-ring DAET fragment should permit independent alignment of the BP100 helices in both cases. Notably, the parent BP100 peptide which was shown to be aligned in the S-state in the bilayer (with the helix axis parallel to the membrane plane), was found extremely mobile. The fact that the model peptides studied here are approximately double the size of the BP100 and nevertheless revealed similar ¹⁹F-NMR signal patterns challenged the suggestion that only the small size is the reason of the high BP100 mobility. It should also be noted that BP100 units in both peptidomimetics studied here, on the contrary to the parent peptide, do not have the *N*-terminal amino group, protonated under the conditions used. Still, all the spectra are very similar, suggesting that similar helix alignments for BP100 with a reduced net charge. The fact could not be attributed to any special membrane-attraction to the aromatic DAET moiety, since more hydrophobic open-ring DAET fragment brings no difference to the membrane-bound orientation of the BP100 unit. Contrasting the influence of the latter DAET state to the first adjacent residue of a β -strand (Figure 3.7.) and apparent β -breaking potential, for α -helix edges open-ring DAET photoswitches appeared to be almost non-perturbing.

The closed-ring photoswitches seemed to be more structurally perturbing for the helical fragments in the studied peptidomimetics. As highlighted in the Figure 3.10., the doubly-labeled α/α -model peptides gave very complex ¹⁹F-NMR spectra in the gel-phase bilayers. In each case about a half of the spectral intensity corresponds to the gel-state spectra of the β/α -model peptides and of the wild type BP100. This could be due to symmetric structure of the α/α -model, where one BP100 unit will align as expected for BP100. The second unit in the α/α -model is influenced by perturbation from the rigid planar closed-ring

DAET moiety in the low viscous environment of the gel-state lipids and has no chance to adapt to the same orientation. Since no similar observation was made with the β/α -model, such constraint should apply only to helical fragments, or restricted position is compatible to the native orientation of the β -strand.

In line with the above observation, the only observed difference to the dipolar splitting pattern in the β/α -model spectra was recorded for the Leu3 position in the gel-state bilayers, i.e., for the β/α -3L analogue. The value of -7.5 kHz splitting, however, is very close to the signal expected for the powder, i.e. for the non-oriented immobilized CF_3 -labelled peptide. It might mean that the perturbation sphere of the backbone-incorporated Sw^{I} unit does not exceed three adjacent residues.

Since significant conformational changes of the peptidomimetic molecules were observed only in the gel-phase lipids and not in the liquid-phase bilayers or in the CD spectra, one might conclude that the Sw^{I} unit photoswitching induces only minor conformational perturbation of the peptides under study. This means that the unit could be easily accommodated in the peptides and its impact on the linear peptide structure and function is minimal. In other words, photoswitching of DAET fragment may be too weak to induce strong structural effects in the middle of a linear peptide. From the other hand, this conclusion might not be true for cyclic peptides or hairpin-like folds, which could be structurally perturbed by Sw -like photoswitching to much higher extent.

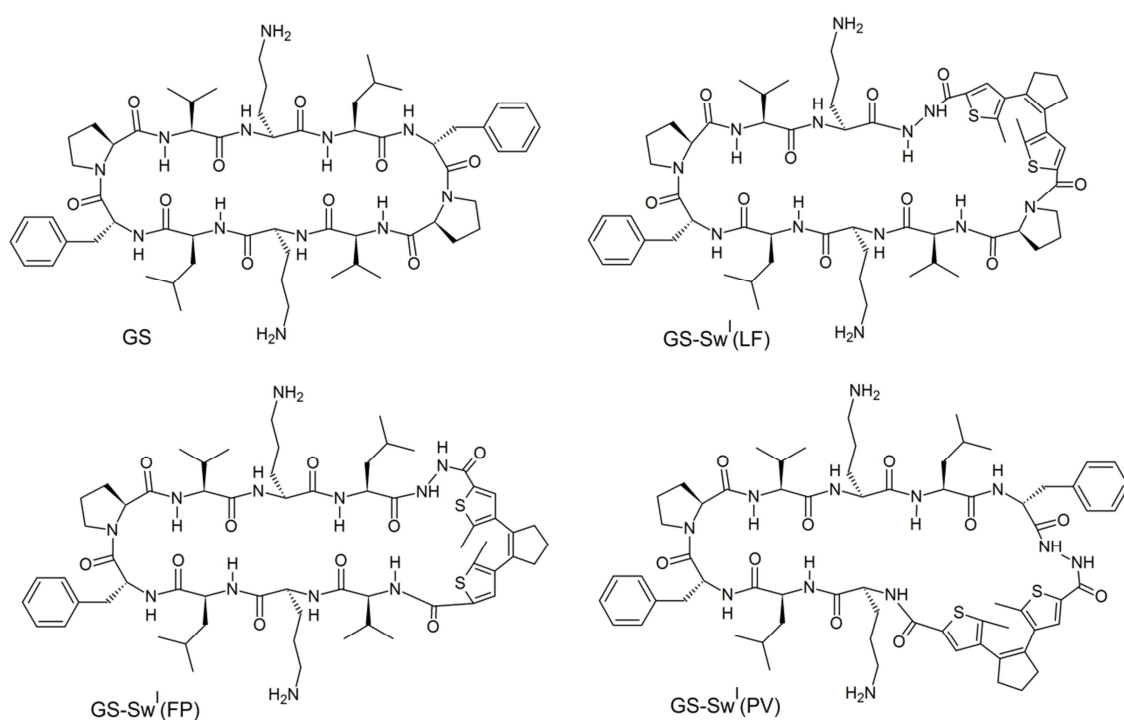
3.3. Photoswitchable analogues of the antimicrobial peptide GS with the Sw^{I} building block

Gramicidin S (GS) photoswitchable analogues were prepared to explore the DAET building block Sw^{I} in a cyclic peptide context, and to investigate the possibility of controlling a peptide functional activity with light. First, GS modification with the Sw^{I} fragment was performed.

GS is a small natural peptide with a range of biological activities, including antimicrobial, hemolytic and antifungal. It has a peculiar symmetric structure: two identical peptidyl fragments are conjugated with each other to form the *cyclo*(PVOL^DF-PVOL^DF) sequence. The secondary structure of GS is characterized by two parallel short β -strands (-Val-Orn-Leu-) that are constrained from both sides with two type II' β -turns (-Leu-^DPhe-Pro-Val). GS is well characterized; relationship of its structural features and observed biological

activities is well-established¹²⁵. This knowledge gives a basis for rational design of DAET-containing GS derivatives.

Two main features are known to be of particular importance for the GS antibacterial activity: the presence of positively charged ornithine residues and the overall amphiphilic character of the peptide (its “sidedness”)¹²⁶. Obviously, the design of the photoswitchable analogues must leave this feature intact. Therefore, modifications of both β -turns fragments (-Leu-^DPhe-Pro-Val-) seems logical^{127,128}, and in order to obey the amphiphilicity requirement, substitutions with a non-polar moiety (like the residue of Sw^I) could be done in any of the two segments. As follows from simple molecular modeling¹²⁹, the size of the Sw^I fragment approximately corresponds to two amino acid residues. In order to empirically find the optimal site for the GS β -turn modification with the Sw^I, different dipeptidyl substitutions were done. The Sw^I residue was exchanged for three different pairs of the amino acid residues in the β -turn as shown in Figure 3.11, giving three possible DAET-modified GS peptidomimetics.



Scheme 3.11. Cyclic gramicidin S (GS) and its designed photoswitchable analogues. GS-Sw^I(LF) denotes peptidomimetic with substituted leucine and phenylalanine residues by the Sw^I fragment, GS-Sw^I(FP) represents the replacement of phenylalanine and proline residues, and GS-Sw^I(PV) of proline and valine residues, respectively.

3.3.1. Synthesis of GS analogues

The synthesis of GS analogues was based on the previously published protocol which included construction of linear precursors by SPPS, followed by an intramolecular cyclization in solution¹³⁰. However the method was substantially modified during the implementation, as described in Chapter 6.2.3. The amino acid sequences of the synthesized peptidomimetics are shown in Table 3.6.

As in the case of synthesis of linear peptidomimetics (Chapter 3.2.1.), construction of linear sequences proceeded without problems, the Fmoc-Sw^I building block was compatible to the Fmoc-SPPS. A major problematic step was found to be the head-to-tail cyclization of the linear precursors. The prevailing process which led to low yields of final GS analogues was intermolecular polycondensation as confirmed by MALDI. This side reaction is known to obscure cyclization when the linear fragments are structurally not well preorganized in solution¹³⁰. Indeed, the non-modified GS (the wild type) can be synthesized with almost quantitative yield at the cyclization step when the preorganization is ensured¹³⁰. Performed under the same conditions, the cyclization of the GS analogues proceeded with markedly lower efficiency (20-30%, as analyzed by RP-HPLC). This result points to potential perturbation of the GS backbone by the building block Sw^I, so the linear peptides apparently have different conformation, unfavorable for the cyclization process and are less well preorganized compared to the wild type sequence.

Table 3.6. Amino acid sequences of gramicidin S and its photoswitchable analogues.

Peptide	Sequence*
GS	<i>cyclo</i> (^D FPVOL ^D FPVOL)
GS-Sw ^I (LF)	<i>cyclo</i> (^D FPVO-Sw ^I -PVOL)
GS-Sw ^I (FP)	<i>cyclo</i> (^D FPVOL-Sw ^I -VOL)
GS-Sw ^I (PV)	<i>cyclo</i> (^D FPVOL ^D F-Sw ^I -OL)

* Sw^I denotes the residue of the building block **31**.

Nevertheless, pure GS analogues were obtained after two-step RP-HPLC purification (Chapter 6.2.3.). First, a preparative column was used to separate the products from the main impurities. Next, on a semi-preparative HPLC column, the purity of the peptides was increased to >95%. As will be discussed below, the photoconversion of the GS open-ring analogues to the closed-ring forms proceeded with 20-80% efficiency, mostly depending on

the solvent. Therefore, chromatographic separation was used to obtain pure closed-ring forms for all three GS analogues.

3.3.2. Photochromic properties of the GS analogues

After completion of the synthesis and successful purification of the Sw^I -modified GS analogues, their basic photochromic properties were studied. The solutions containing the peptidomimetics in 100 $\mu\text{g/ml}$ concentration were exposed to either UV or visible light for different intervals of time. The process of converting from one form to the other was monitored by an analytical RP-HPLC (Figure 3.12.). It turned out that the photoconversion of peptides from the open-ring to the closed-ring form did not proceed completely even after prolonged exposure to UV light. Addition of a denaturizing (chaotropic) agent to the peptide solutions significantly increased the yield of the photogenerated closed-ring forms. This observation can be explained assuming structural features of GS. The structure of the parent peptide is additionally stabilized by four intramolecular hydrogen bonds. Presumably, similar hydrogen bonds prevent the GS analogues from adopting conformations suitable for the conversion into the closed-ring form, but they could be broken by denaturizing agents.

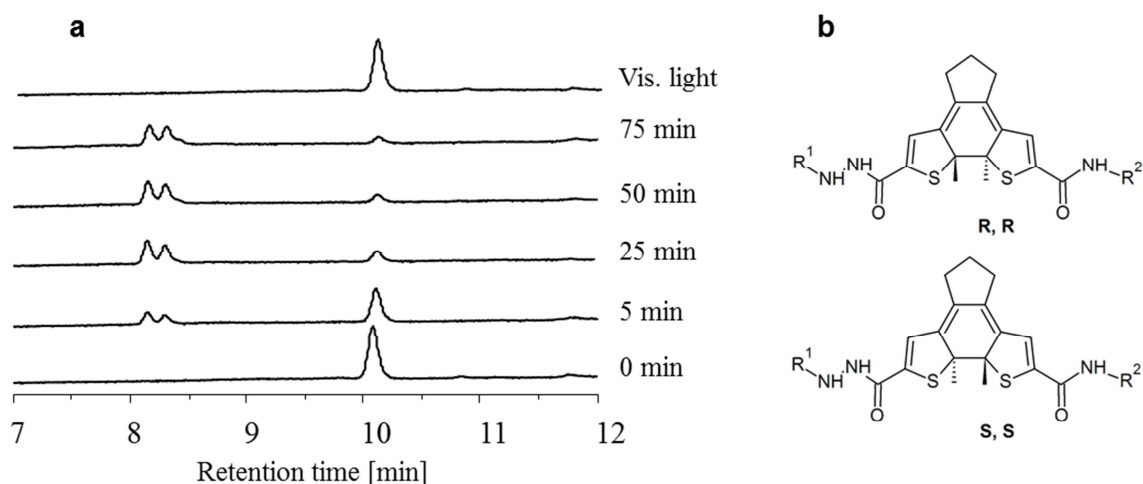


Figure 3.12. (a) Analytical RP-HPLC chromatograms of $GS-Sw^I(FP)$ at 100 $\mu\text{g/ml}$ in water, recorded during the course of illumination with UV light, and with visible light. The peak at 10 min retention time corresponds to the open-ring form; two peaks at around 8 min are two diastereomeric isomers of closed-ring form. (b) Two diastereomers (R,R and S,S configurations) of the closed-ring form of the studied Sw^I derivatives.

It is known (Chapter 1.2.5.) that the photocyclization reaction of DAETs can proceed only from the antiparallel conformation. If the molecule is artificially fixed in the parallel conformation, for instance through structuring of the peptidic unit in the GS analogues, the yield of the photoconversion declines (Figure 3.13.). The closed-ring forms of the GS analogues were found to be thermally stable and could be stored for a long time without any detectable conversion to the open-ring photoforms, unless the visible light is applied.

It should be noted that the closed-ring forms of DAETs exist as two diastereomeric isomers¹³¹ with R,R- or S,S-configurations at the two chiral carbon atoms. The two isomers of the closed-ring form were possible to distinguish in some cases by analytical RP-HPLC (Figure 3.12a.). Although the diastereomers might have different physical and chemical properties, they were not separated in this study and were used for functional tests as mixtures.

The reverse photoisomerization of GS analogues from colored closed-ring forms to the initial colorless forms was also evaluated. In this case, 100% conversion could be achieved under the exposure to visible light without addition of denaturing agent (Figure 3.13c.).

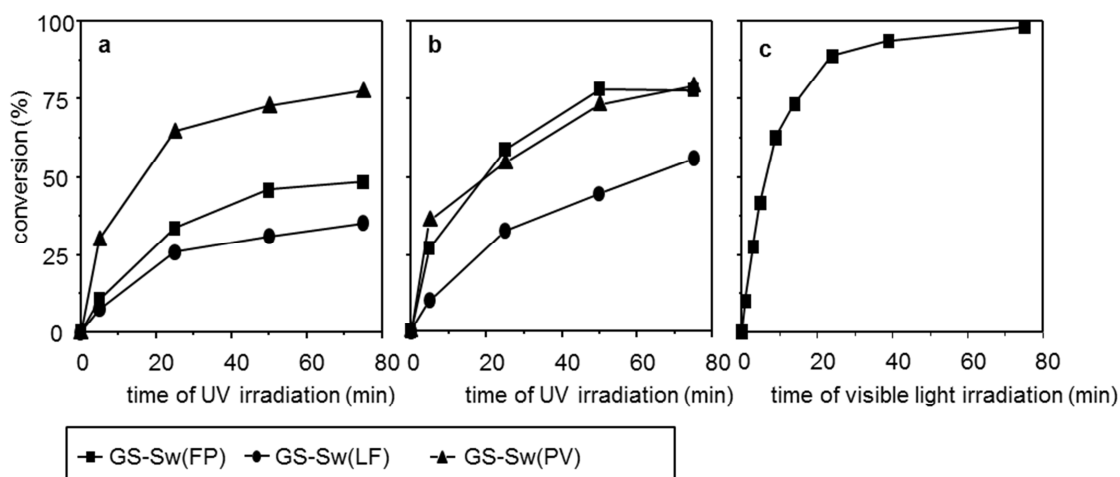


Figure 3.13. Kinetics of the photoconversion of GS analogues under different conditions: (a, b) from the open-ring forms to the closed-ring forms by irradiation with UV light at 25°C, 100 µg/ml solution in a water-acetonitrile mixture, 3:1 v/v (a); in 1 M aqueous urea (b); For GS-Sw^I(FP) from the closed-ring to the open-ring form by irradiation with visible light in a water-acetonitrile mixture, 3:1 v/v, at 25°C 100 µg/ml (c).

3.3.3. Hydrophobicity of the GS analogues

Hydrophobic and amphiphilic characteristics are critical parameters for many membrane-active peptides including GS. The changes in the hydrophobicity of small peptides could be monitored with the RP-HPLC as it correlates with their retention times (RT)¹³². For example, substitution of an L-amino with a D-amino acid in the GS and its derivatives caused significant decrease of the amphiphilicity which manifested as pronounced reduction of the RT values¹³³.

To characterize hydrophobic properties of the GS analogues, the elution profiles of the peptidomimetics (see Chapter 3.3.1) were studied in both photoforms and were compared to the wild type GS (Figure 3.14.). The longest RT, which corresponds to the highest hydrophobicity, was found for the GS wild type. All three GS analogues in their open-ring forms eluted with RTs of about 10 minutes. The RT values increased in the following sequence: GS-Sw^I(LF) < GS-Sw^I(FP) \approx GS-Sw^I(PV) < GS.

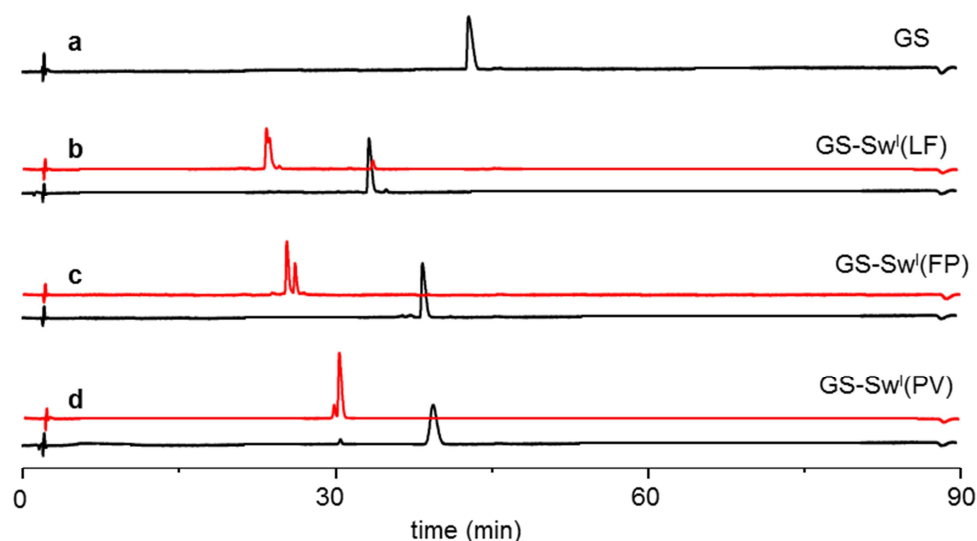


Figure 3.14. Analytical RP-HPLC elution profile (a) of the GS wild type, and its photoswitchable analogues (b) GS-Sw^I(LF), (c) GS-Sw^I(FP), and (d) GS-Sw^I(PV), each in the open-ring (black) and closed-ring form (red). (Conditions see in Chapter 6.).

Photoconversion of the peptides to their closed-ring forms led to decrease of the RTs with the order being maintained. The pairs of diastereomers (discussed in the previous chapter) of closed-ring forms were found to have almost equal RTs, as expected. This result suggests that

the open-ring forms are similar to the wild type GS in terms of the hydrophobicity, and the corresponding closed-ring analogues are more polar. Interestingly, of photoswitchable peptides (Chapters 3.1 and 3.2) similar but much less pronounced effect was observed in the linear models, that was presumably a result of different intrinsic polarity of the two photoforms of the DAET unit.

3.3.4. Circular dichroism analysis of GS analogues

CD spectra of the peptidomimetics were measured in order to estimate the changes in secondary structures upon the photoisomerization of the DAET unit. The CD spectra in phosphate buffer were of low quality due to poor water solubility of the wild type GS and the analogues. Successful measurements were done in membrane-mimicking environments, namely, in 50% trifluoroethanol (TFE) and in detergent micelles (SDS, 25 mM). The peptidomimetics were studied in their both photoforms using the following procedure. The CD spectra of the closed-ring forms were measured first. Next, the samples were exposed to visible light for time periods needed to convert 100% of the peptidomimetics into the colorless open-ring forms (visual control), and the second set of the CD spectra was recorded. The control experiments performed with wild type GS showed no effect of light on the sample quality or any radiation damage. The obtained CD spectra are collected in Figure 3.15.

Cyclic structure and the presence of D-amino acids in GS prevented precise secondary structure assessment by deconvolution of the CD signals¹³⁴. Furthermore, extraction of the structural information from the CD lineshapes was also complicated by the presence of the DAET moiety. The diarylethene unit is itself a chromophore and gives photoform-dependent CD signal, which extends to the long-wavelength range useful for peptide secondary structure estimation¹³⁵. Due to these reasons, the CD spectra of the GS analogues were only compared with the GS wild type spectra for some qualitative assessments.

The CD spectra of the open-ring forms of GS-Sw^I(LF) and GS-Sw^I(FP) in TFE were similar to the wild-type GS spectra, with non-resolved negative bands at ca. 210 and 220 nm. The peptidomimetic GS-Sw^I(PV) spectra also had the same negative bands, resolved better, at ca. 220 and 200 nm. This peptidomimetic showed essentially the same spectrum in the 180-260 nm spectral window after the photoconversion, only the intensity of the signals increased. On the contrary, the GS-Sw^I(LF) and GS-Sw^I(FP) converted to the closed-ring form gave the essentially different CD spectra, with the lineshapes similar to that of the GS-

Sw^I(PV) analogue, suggesting structural similarity for all the three closed-ring peptidomimetics.

The presence of detergent micelles did not affect the wild type GS CD spectra, as could be expected from the stability of the hydrogen bond-stabilized fold of the peptide. The CD spectra of the GS analogues in the open-ring form did change as a consequence of conformational changes upon micelle binding. The band at ca. 220 nm pronounced most strongly and the low wavelength signal (ca. 210 nm) converted into a shoulder. Interestingly, in the closed-ring states all three peptidomimetics revealed very similar signal shapes below 260 nm, resembling signals observed for them in TFE.

Irrespective of the conditions, the main negative CD bands in the spectra of the closed-ring form peptidomimetics appeared systematically shifted towards lower wavelengths, i.e. towards more “random coil”-like lineshape with a pronounced minimum at ~200 nm. Such spectra resembling that of the unfolded polypeptides may indicate less order for the peptidomimetic backbones. This interpretation of the CD spectra of the closed-ring peptidomimetics will explain also their similarity which was noted above. Under both membrane-mimicking conditions measured, the spectra thus reflected stiffer and much less structured conformations as compared with GS wild type. The spectra of the open-ring forms, on the other hand, differed between the two membrane-mimicking environments, which supports higher flexibility of the molecular backbones expected for these photoforms. Under both conditions, the open-ring molecules clearly exhibit “non-random” CD signals. For one of the conformations (in 50% TFE) the CD lineshape resembled that of GS (with a pronounced minimum at ~210 nm, and a lower minimum at ~220 nm). As was discussed above, RP-HPLC analysis (Chapter 3.3.3.) had shown that the perturbation of the backbone conformation by the photoswitch in the open-ring forms most likely lead to a lesser perturbation in the amphiphilicity of the molecules than in the closed-ring form. Notably, TFE solution is the only condition when open-ring forms of the GS analogues appeared to have the structure close to that of the wild type peptide. TFE is a special solvent with regard to its interaction with membrane-active peptides. On the one hand, it has the same dielectric constant as the bilayer interface ($\epsilon \sim 20$) and is therefore a good mimic of the membrane surface. On the other hand, TFE is known for its structuring effects on the polypeptides – it is often nodded as a solvent which “artificially” promotes α -helical fold. The latter observation provides ambiguity to the interpretations of peptide structures in TFE – the conformations may be artificially driven. In the case of GS analogues this α -helix promoting action of TFE could be excluded, because these small peptides due to their cyclic structure simply cannot

fold as an α -helix. Therefore observed similarity between GS structure and the structures of the open-ring forms of the photoswitchable analogues in TFE rather suggest the flexible analogues to be able to fold as GS at conditions of membrane interface. The SDS data reveals much less structural similarity to the wild type GS, even for the open-ring forms. Perhaps in this case SDS membrane model is less representative of the biomembranes, e.g. in that the negatively charged detergent headgroups are sulfates. Sulfate headgroups may interact strongly with the aromatic system of the DAET cores, and this impact may be stronger than the fold-promoting influence onto peptidyl parts of the molecules.

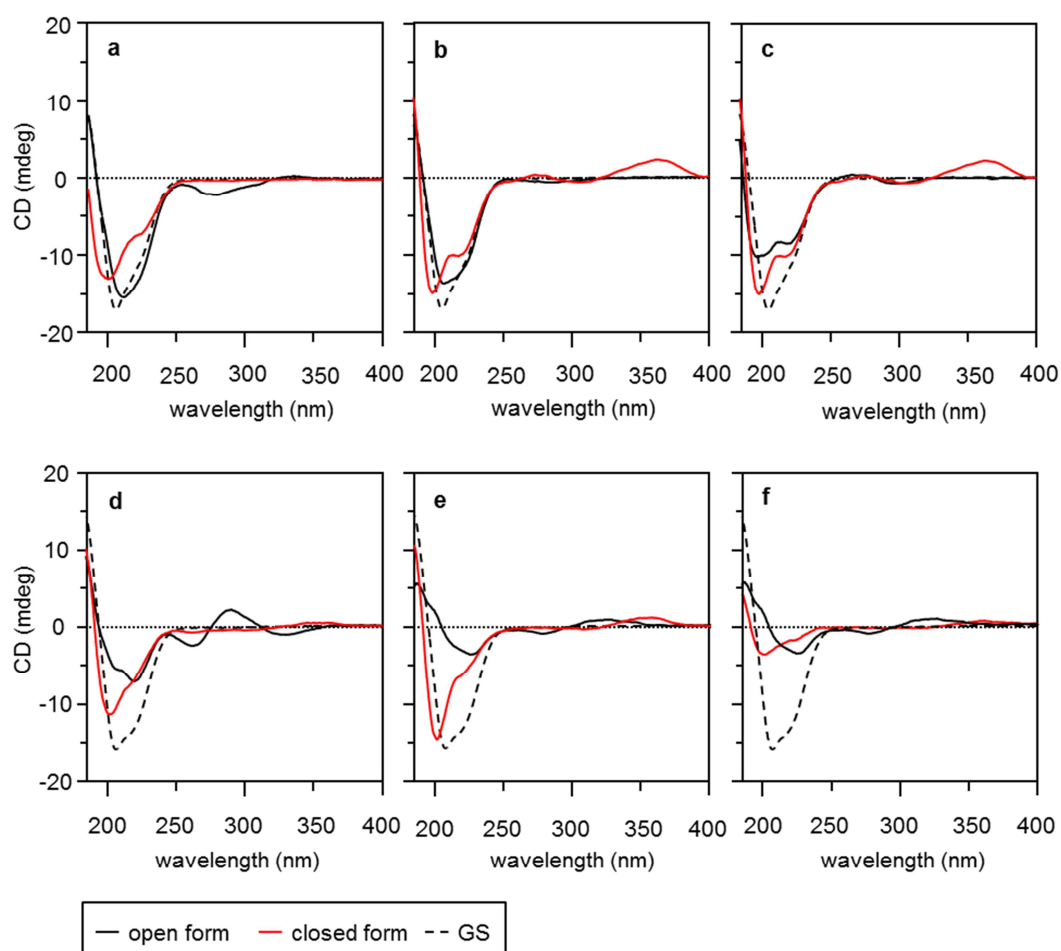


Figure 3.15. Circular dichroism spectra of GS (black dashed line) and each of the three analogues in the open-ring (black line) and closed-ring (red line) forms measured at (a, b, c) a concentration $75 \mu\text{g/ml}$, at 25°C , in 50 vol% TFE; (d, e, f) in SDS micelles, with a peptide:detergent molar ratio of 1:25. (a, d) GS-Sw¹(LF); (b, e) GS-Sw¹(FP); and (c, f) GS-Sw¹(PV).

For one of the peptidomimetics more detailed investigation was undertaken. Two diastereomers of the closed-ring form of GS-Sw¹(FP) were isolated with RP-HPLC and each

diastereomer was studied individually by the CD spectroscopy (Figure 3.16.). This study should get better insight into the CD signature of the DAET unit. Since no steric assignment was done, the isomers were named isomer 1 (shorter RT) and isomer 2 (longer RT). The obtained CD spectra (Figure 3.16.) of the both isomers gave similar negative bands at short wavelength (~200 nm), however there was significant difference at longer wavelengths. In particular, strong positive band for the isomer 1 and a mirrored negative signal for the isomer 2 were observed at 360 nm. This wavelength corresponds to the absorption band of closed-ring form of DAET (Chapter 3.1.1.). However, there was no signal in the CD spectra at the second absorption region around 560 nm. The value of CD signal at this wavelength could be used to identify the diastereomer configuration of any DAET modified peptidomimetics if the positive and negative values are assigned to particular diastereomers.

Preparative separation of isomers of the closed-ring form was possible only for the peptide GS-Sw^I(FP). Other GS analogues had too close RTs to be separated by RP-HPLC.

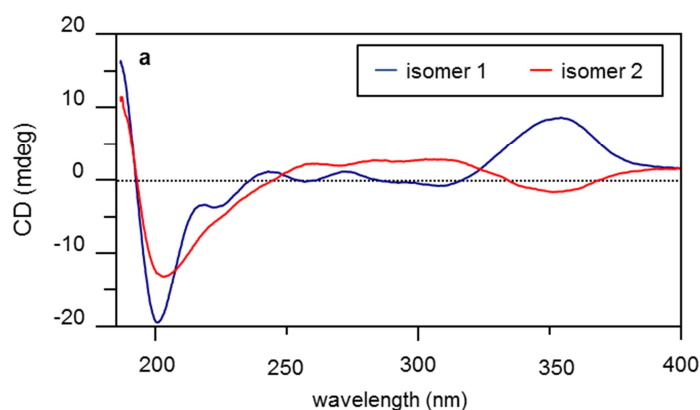


Figure 3.16. Circular dichroism spectra of the peptides GS-Sw^I(FP) closed-ring form diastereomers measured at a concentration 125 $\mu\text{g/ml}$, at 25°C, in SDS micelles, with a peptide:detergent molar ratio of 1:25. Blue line corresponds to isomer 1, red to isomer 2.

3.3.5. Antimicrobial activity of GS analogues

Since GS is a well characterized peptide antibacterial agent, the studies performed here were focused on answering three main questions. First, it was important to check if the diarylethene-modified GS analogues had any antimicrobial activity. If so, it was interesting to learn whether bacterial selectivity (action against Gram-negative vs. Gram-positive strains) for the new GS analogues was preserved. Finally, the most interesting question was if there were any differences in antibacterial activities between the open- and the closed-ring forms.

The antimicrobial activities of the photoswitchable GS analogues in both photoforms were tested by means of broth dilution assays. These assays were performed against planktonic forms of bacteria and are expressed as minimum inhibitory concentrations (MICs) needed to prevent growth of bacterial culture (see details in Chapter 6.5.).

The stock solutions of the peptidomimetics in the open- and closed-ring forms were prepared in advance and all the precautions were made to maintain the photophorms of the peptidomimetics intact during all the experiments. The MIC values obtained for GS-Sw^I(LF) GS-Sw^I(FP) are summarized in Table 3.7. As can be seen, the GS analogues possess the antibacterial activity similar to that of the parent antibiotic GS. Like the GS wild type, the photoswitchable analogues showed low activity against Gram-negative bacteria, but remained active against Gram-positive strains. There was no significant difference in performance of the two tested peptidomimetics, and the closed-ring forms showed lower activity against tested bacteria.

Table 3.7. Antimicrobial activity of GS and its photoswitchable analogues tested against Gram-positive and Gram-negative bacteria strains.

Bacterium	MIC ($\mu\text{g/ml}$)				
	GS	GS-Sw ^I (LF)		GS-Sw ^I (FP)	
		open-ring	closed-ring	open-ring	closed-ring
<i>E. coli</i>	32	128	256	64	>256
<i>S. aureus</i>	2	8	16	8	64
<i>B. subtilis</i>	1	4	8	4	32
<i>S. typhimurium</i>	128	>256	>256	128	>256

The antimicrobial activity assays were repeated for all three peptidomimetics with focusing on the precise evaluation of the differences between the open-ring and closed-ring forms. For this study three Gram-positive strains: *S. aureus*, *S. epidermidis* and *S. xylosus* were selected. The initial concentrations of the open- and closed-ring forms were 128 and 256 $\mu\text{g/ml}$, respectively. In order to decrease the systematic error in setting the concentrations, the initial stock solutions (prepared gravimetrically) were corrected. For this purpose, accurate RP-HPLC calibration curve was established and the concentration in the initial stock solutions was determined. The second set of solutions was prepared by dilution. Antimicrobial activity determinations were performed under dim light to prevent the visible

light-induced DAET ring-opening of the peptides in their closed-ring photoforms. The results (Table 3.8.) clearly showed that the antimicrobial activity of the GS analogues persisted and indeed can be controlled by light. All three peptides in the open-ring forms exhibited high antimicrobial activity, being almost as active as GS itself. The analogues in the closed-ring form were distinctly less active than in the open-ring forms on all bacterial strains tested. The biggest differences were observed for the peptide GS-Sw^I(LF). In the more active open-ring form against *S. aureus* the peptide showed MIC of 8 µg/ml while in the lesser active closed-ring form the activity was four dilutions smaller (MIC equal 128 µg/ml).

Table 3.8. Antimicrobial activities of GS and of its photoswitchable analogues tested on Gram-positive bacteria strains.

Bacterium	MIC (µg/ml)						
	GS	GS-Sw ^I (LF)		GS-Sw ^I (FP)		GS-Sw ^I (PV)	
		open [*]	closed ^{**}	open [*]	closed ^{**}	open [*]	closed ^{**}
<i>S. aureus</i>	2	8	128	4	32	4	16
<i>S. epidermidis</i>	2	16	128	8	64	4	32
<i>S. xyloso</i>	1	8	128	8	32	4	32

^{*} refer to open-ring form; ^{**} refer to closed-ring form.

3.3.6. Visualization of the antimicrobial activity of GS analogues

As was shown in the above antimicrobial studies (Chapter 3.3.5.) for all three GS analogues it was possible to define a therapeutically important concentration range in which the photoswitchable peptides in the open-ring forms suppressed bacterial growth, while being inactive in the closed-ring forms.

The ability to control antimicrobial activity with light could find an application in medicine, e.g. in photodynamic therapy⁸. The above experiments were performed using isolated GS analogues in either open-ring or closed-ring forms. As a proof-of-principle study, demonstration of the functional *in situ* photocontrol was performed. The peptide GS-Sw^I(FP) was selected for the validation. The experiments were performed with bacteria growing on solid media. To the growth medium of the agar inoculated with *S. xyloso* the peptidomimetic was added in the least active closed-ring form. Then selected areas on the Petri dish were irradiated with the visible light through a mask. This allowed activating the peptidomimetic

through photoconversion to the open-ring form in a spatially-controlled fashion. Finally, the plates were incubated and inspected for the presence of bacterial colonies as usually done in agar-diffusion antimicrobial tests (see Chapter 6.6. for details).

In order to determine the optimal conditions different concentrations of the deactivated peptidomimetic and different times of illumination were tested (Figure 3.17.). Experimental details are described in Chapter 6.6.

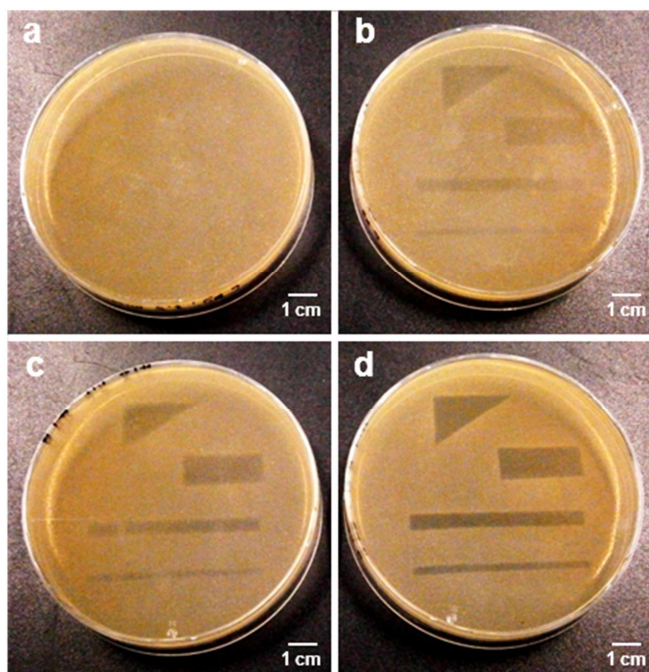


Figure 3.17. Antimicrobial effect of the photoswitchable peptidomimetic $GS-Sw^I(FP)$ on *S. xylosus*. The GS analogue in the closed-ring form was applied to agar medium together with bacterial cells and irradiated with visible light through a mask. Applied (a) at $6 \mu\text{g/ml}$ in the closed-ring form followed by 9 min exposure to visible light that corresponds to 60% conversion to active open-ring form (as calculated from the curve in Figure 3.13c.); (b) at $6 \mu\text{g/ml}$, conversion 80% in 16 min; (c) $8 \mu\text{g/ml}$, conversion 60% in 9 min; (d) $8 \mu\text{g/ml}$, conversion 80% in 16 min.

The optimal conditions were found to be the following: application of the peptidomimetic at the concentration $8 \mu\text{g/ml}$ followed by illumination with visible light for 16 min (estimated to reach 80% conversion, see Chapter 3.3.2.) which should correspond to generation of $6.4 \mu\text{g/ml}$ of the more active closed-ring form. It has to be noted that in neither experiment intermediate levels of activity were observed rendering *in situ* photocontrol as discrete switching-on/switching-off process.

Results of the demonstration experiment are shown in Figure 3.18., where an image of Mona Lisa was used as the mask.

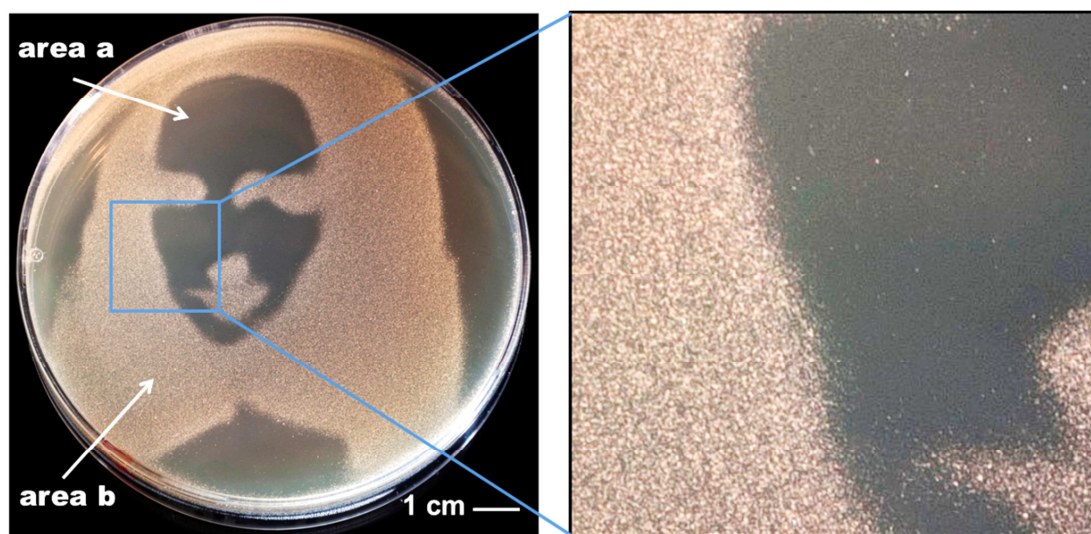


Figure 3.18. Demonstration of the photoswitchable properties of the peptidomimetic GS-Sw^I(FP) on the agar-grown *S. xylosum*. (a) Corresponds to the open-ring form generated during the course of irradiation with visible light. (b) Corresponds to the peptidomimetic in less active closed-ring from below MIC.

3.3.7. Hemolytic activity of GS analogues

Besides antimicrobial activity, hemolysis is another important characteristic that has to be considered during practical applications of antimicrobial peptides¹³⁶. To be useful as antimicrobial agent for treatment different infections in humans, an antibiotic must demonstrate selective toxicity between mammalian and microbial cells. It has to be noted that for GS the hemolytic side effect is a major problem associated with its clinical application¹³⁷.

Hemolytic activity of the GS analogues was characterized by determination of their HC₅₀ values (the concentrations required for 50% hemolysis of erythrocytes) according to the protocol described in Chapter 6.7. The obtained dependences of the hemolysis on the peptidomimetic concentrations are shown in Figure 3.19. The HC₅₀ values determined from these graphs are listed in Table 3.9. Smaller HC₅₀ values indicate higher hemolytic activity, and *vice versa*. The results showed that in the open-ring forms the photoswitchable analogues retained high hemolytic activities similar to GS wild type. While in the rigidified closed-ring forms they were much less hemolytic, just as it was seen for their antimicrobial activities.

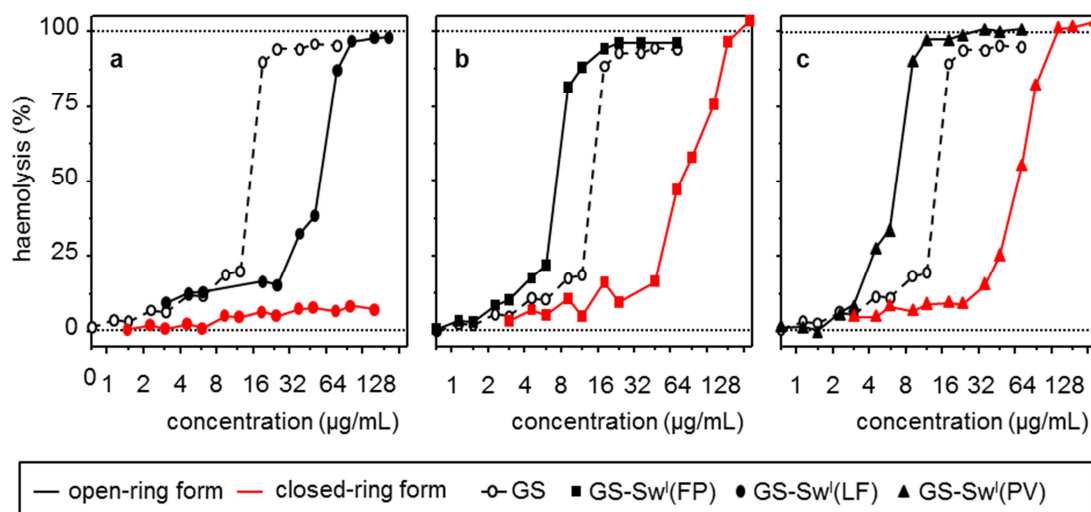


Figure 3.19. Concentration-dependent lysis of the red blood cells. GS (black dashed line) is compared to its analogues in the open-ring (black line) and closed-ring (red line) forms. (a) GS-Sw^I(LF), (b) GS-Sw^I(FP), and (c) GS-Sw^I(PV).

The ratio between HC₅₀ and MIC values defines a therapeutic window at which the agent can be applied without harmful effect to an organism. Thus the photocontrol of the hemolytic activity of antimicrobial agents, as was demonstrated above, is opening a way for their applying in areas where it was not possible before due to the toxic side-effects.

Table 3.9. HC₅₀ values for GS and for its photoswitchable analogues observed as 50% lysis of human erythrocytes compared to the action of 0.1% Triton X-100.

	Peptides						
	GS	GS-Sw ^I (LF)		GS-Sw ^I (FP)		GS-Sw ^I (PV)	
		open [*]	closed ^{**}	open	closed	open	closed
HC ₅₀ (µg/ml)	12	47	>>128	6.5	72	6	58

^{*} refer to open-ring form; ^{**} refer to closed-ring form

3.4. Photoswitchable analogues of the antimicrobial peptide GS with the Sw^{II} building block

After successful demonstration of the photocontrol of the antimicrobial activity, a new more ambitious aim was set – to demonstrate photocontrol of an anticancer activity of the DAET-modified peptidomimetics. As for antibacterial activity, gramicidin S appeared as suitable template for such a purpose. GS was reported to possess high cytotoxic activity against both bacteria and eukaryotic cells^{138,139}. It was shown to have prospects for application in cancer therapy¹³⁸. In these *in vivo* experiments performed on a mouse model, daily intraperitoneal injections of 20-200 µg of GS per mice per day showed strong inhibitory effect on the growth of implanted tumors. However, GS simultaneously revealed high systemic toxicity and thus could not be applied for cancer therapy in unmodified form. The photoswitchable properties of GS analogues can help to eliminate the problem of high toxicity.

In the course of evaluation of the antimicrobial activity of the GS analogues containing DAET building block **31** (described in Chapter 3.3.) several drawbacks were identified. Major problem was found to be the overall low yields during peptidomimetic synthesis, particularly due to difficulties at the step of head-to-tail cyclization. Moreover, initially obtained amounts of GS analogues with the DAET switching unit Sw^I (dozens of milligrams) were enough to carry CD structural analyses and to measure antimicrobial and hemolytic activities in the *in vitro* assays. For anticancer activity tests, on the contrary, a broad study involving cell-based assays and tests on animal models was planned. These experiments required larger amounts of peptidomimetic material (in the range of 500 mg). Due to these reasons the approach for synthesis of photoswitchable peptidomimetics based on GS was modified through introduction of the new DAET-derivatives, the Sw^{II} (see Chapter 3.1.2). The new building blocks contained a canonical amino acid proline residue bearing the terminal amino group (L-enantiomer in **39** and of D-enantiomer in **40**).

As was mentioned above, synthesis of cyclic peptidomimetics with the hydrazide-containing building block Sw^I faced with several synthetic problems. Mass-spectroscopy analysis revealed that large amounts of linear peptides terminated at Sw^I position is forming during cyclisation step as the by-products (see the discussion in Chapter 3.3.1.). Therefore, several attempts were done to improve the yields of the cyclization step leading to cyclic Sw^I-modified GS analogues. In the original protocol of the GS-Sw^I(FP) synthesis the sequence [H-^DFPVOL-Sw^I-VOL-OH] was used as a linear peptide precursor. Here, the DAET unit was

placed in the middle of the peptide chain in analogy to the linear model peptides, which were produced in good yields (Chapter 3.2.1.). Assuming that the sequence of the linear peptide (e.g. the starting position) prior to cyclization determines its preorganization in solution¹³⁰ one might suggest, that the Sw^I unit may hinder achieving the conformation of the linear precursor favorable to the cyclization, and therefore limit its. To test this hypothesis, the position of Sw^I unit was shifted to the *N*-terminus. The shift, however, decreased the cyclisation yield due to the above mentioned chemical instability of the hydrazide connection and other multiple side-reactions occurred. Notably, the side-products were not the result of the polycondensation reaction, as was observed with the Sw^I in the middle of the sequence. Moreover, the undesired chemical transformations occurred exclusively at the macrocyclization step. Therefore, the DAET amino acid analogues were redesigned, providing the second-generation building blocks containing Sw^{II} fragments (see Chapter 3.1.2. for structures and synthesis).

The second-generation building blocks were used for further optimization of the GS photoswitchable peptides. Anticancer activity tests were performed on a GS analogue possessing the DAET unit in place of the of the phenylalanine and proline, residues in the wild-type molecule, as in GS-Sw^I(FP) (Chapter 3.3.). The peptidomimetic GS-Sw^I(FP) was selected as the lead because it demonstrated the largest change in retention times on analytical RP-HPLC between the two photoforms, among all the tested GS analogues. The only chemical modification to this lead was the use of the second-generation DAET building blocks. Since Sw^{II} exists in two enantiomeric forms, two peptidomimetics were obtained. The corresponding amino acid sequence of these peptidomimetics was *cyclo*(^DFPVOL-Sw^{XPro}-VOL) where Sw^{XPro} is either a residue of the building block **39** (Sw^{LPro}) or of **40** (Sw^{DPro}). The structure of these two peptidomimetic is shown in Figure 3.20.

3.4.1. Synthesis of GS analogues

In order to synthesize new photoswitchable GS analogues and upscale the synthesis the synthetic method described in Chapter 6.2.3 was further modified. In the new method for construction of the linear peptides the sequences [H-Sw^{XPro}-VOL^DFPVOL-OH] were used. The DAET unit was the last amino acid to be coupled in SPPS which reduced the exposure to the coupling-deprotection reagents and helped in maintaining the structural preorganization of the linear peptide favorable for the head-to-tail cyclization (see the discussion above).

Gratifyingly, the cyclisation reactions proceeded in excellent yields (>80%, as analyzed by RP-HPLC) and no side-product formation was detected. However, the building blocks **39** and **40** were available as racemic mixtures as proline residue partially enantiomerised during the synthesis (80:20 in one case and 60:40 in another). The target GS-analogues were nevertheless possible to separate using preparative RP-HPLC. The known enantiomeric excess was used to identify the final peptide products.

The RP-HPLC elution profiles of the new GS analogues are shown in the Figure 3.21. Two studied peptides showed very close RTs suggesting that they have similar physical and chemical properties. GS-Sw^{LPro}(FP) had slightly longer RTs (around 1 min on a chromatogram with a gradient slope of 1% solvent B/min). Interestingly, the RT values of both analogues in the open-ring forms were close to that of the wild type GS, while first-generation analogue GS-Sw^I(FP) eluted much earlier (Chapter 3.3.3). This difference can be explained by the increase of the peptide hydrophobicity after the introduction of the proline residue instead of the polar hydrazide group. It can also be a result of smaller perturbations of native amphipathic structure with the new building block Sw^{II}. The photoconversion to the closed-ring forms have resulted in significant decrease in RT (16 min using the gradient above), similar to all the GS analogues studied so far possessing the building block Sw^I.

Substantial amounts of peptidomimetics were synthesized and purified: 100 mg of peptidomimetic GS-Sw^{LPro}(FP) and 25 mg of GS-Sw^{DPro}(FP).

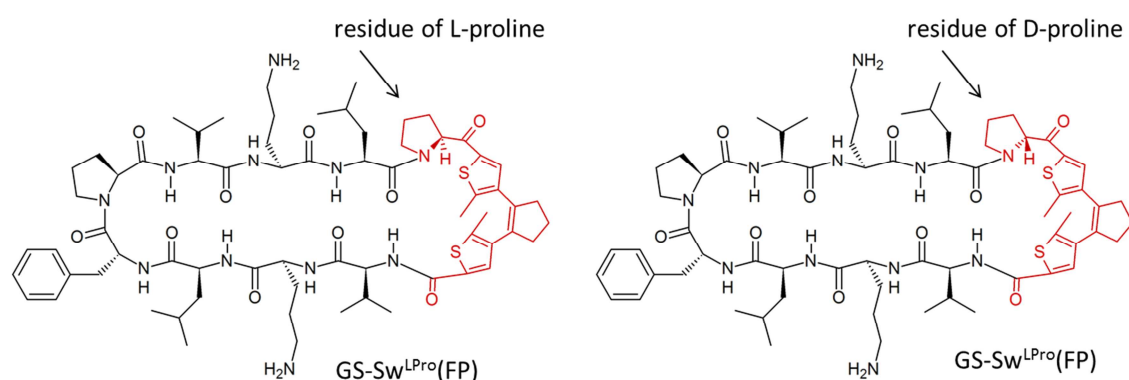


Figure 3.20. Structure of the GS analogues containing second-generation DAET building blocks Sw^{II} (shown in red). Two amino acids (Phe and Pro) substituted in the native GS sequence with the building block **39** or **40** gave the peptidomimetics GS-Sw^{LPro}(FP) or GS-Sw^{DPro}(FP), respectively.

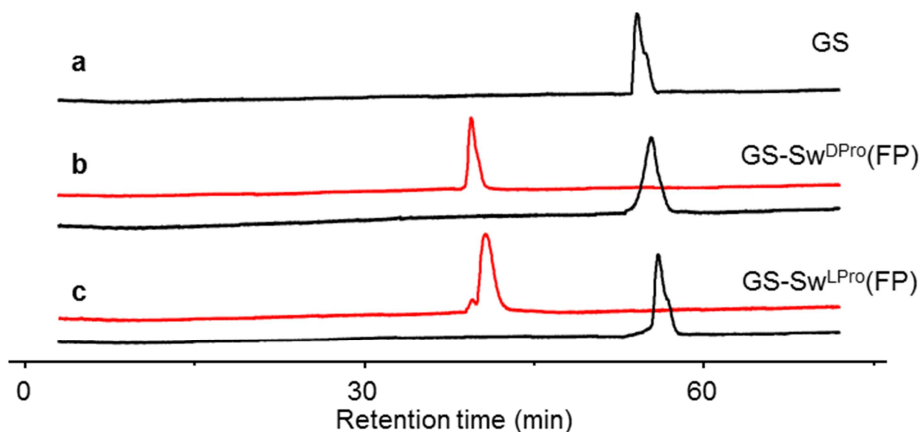


Figure 3.21. Analytical RP-HPLC elution profiles (a) of the GS wild type, and its photoswitchable analogues (b) GS-Sw^{DPro}(FP), (c) GS-Sw^{LPro}(FP), each in the open-ring (black) and closed-ring forms (red). (Conditions see in Chapter 6.).

3.4.2. Anticancer activity of GS analogues

The cytotoxic activity of the peptidomimetic GS-Sw^{LPro}(FP) was studied in order to access the potency of the new photoswitchable GS analogues in cancer therapy. To this aim, the cytotoxicity of the peptidomimetic in both photoforms was measured employing a standard MTT assay (see details in the Chapter 6.8.). Two cancer cell lines were used: cervix cancer line HeLa and hepatocellular carcinoma G2. The same way as it was in the study of antibacterial activity, the peptidomimetic forms with the open-ring and closed-ring DAET states were prepared before the tests using preparative HPLC and all the experiments were performed under dim light conditions to prevent uncontrolled photoisomerization of the peptidomimetic.

The viabilities of the cells at different concentrations of the peptidomimetic are shown in Figure 3.22. It can be seen that the open-ring form of GS-Sw^{LPro}(FP) demonstrated significant cytotoxicity against both cell lines, with calculated IC₅₀ about 12 µg/ml against cancer line HeLa and 24 µg/ml against hepatocellular carcinoma G2. Deactivated closed-ring form of the peptidomimetic showed much lower cytotoxicity against both cell lines. No cytotoxicity was observed in the experiments with hepatocellular carcinoma G2: the closed-ring form was active only at the highest tested concentration of 64 µg/ml. Since no further concentrations were employed, in both cases the IC₅₀ was assigned as > 64 µg/ml. These results clearly showed that the cytotoxic activity of the GS analogue could be controlled with light.

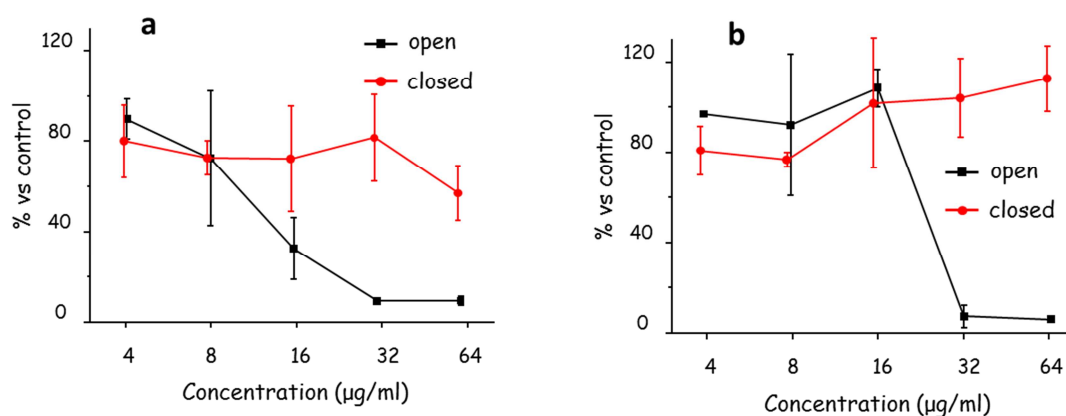


Figure 3.22. The cytotoxic activity of the photoswitchable analogue GS-Sw^{LPro}(FP) in both open-ring and closed-ring forms measured in the MTT test (a) against cervix cancer line HeLa, (b) against hepatocellular carcinoma G2 cancer line.

3.5. Photocontrolled fluorescent cell imaging with DAET containing peptides

As was discussed in Chapter 1.3., diarylethenes possess intrinsic fluorescent properties. Moreover, their fluorescence depends on the photoform. The DAET derivatives that were used in this study are dithienylcyclopentenones with two carbonyl groups at 2- and 2'-positions and produce fluorescent signal in the open-ring photoforms. In particular, the fluorescent properties of the building block **31** in water environment were studied using small peptidic derivative, as described in Chapter 3.1.1. Chapters 3.3. and 3.4. above describe photoswitchable analogues of the antimicrobial peptide gramicidin S.

In order to better understand the mechanism of action and distribution of the gramicidin S in living bacterial cells, one of the DAET-containing GS derivatives was used as a fluorescent probe. GS is a small and sensitive to modifications peptide. Its fluorescent labeling is problematic due to the fact that attachment of any large hydrophobic fluorophore will dramatically change its amphiphilic character, and, as a result, its biologically relevant interaction with the lipid bilayer. On the other hand, the DAET-modified GS analogues already have a built-in fluorescent label and thus can be used as a fluorescent probes. Showing similar spectrum of activities to the wild type peptide and comparable structural features, these analogues may have similar mode of binding to membranes and similar mechanism of action. The fluorescent properties of GS photoswitchable analogues were used in the following experiment: the bacteria cells of *Bacillus subtilis* and *Kocuria rhizophila*

strains were treated for 1 hour with GS-Sw^I(FP) at 100 µg/ml concentration in the open-ring form. Then the distribution of the fluorescent GS analogue was recorded as shown in Figure 3.23 (microscope Axioskop 40 was used). Green and weak red fluorescence of the peptidomimetic in open-ring form was observed. In experiments with both bacterial strains the peptidomimetic not only bound to the cell membrane, but also appeared translocating inside the cells. Interestingly, most intense signal inside the cells was detected in the cytoplasm which suggests that the peptidomimetic was absorbed by the inner membrane. The extracellular matrix in bacterial conglomerates appeared to be clear of the fluorescent peptidomimetic.

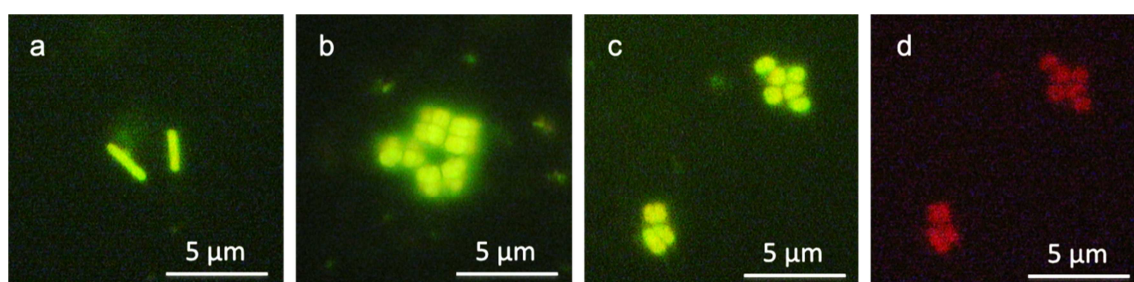


Figure 3.23. Fluorescent cell staining with peptidomimetic GS-Sw^I(FP) at 100 µg/ml in open-ring form. (a) green fluorescence of *Bacillus subtilis*, (b) and (c) green fluorescence of *Kocuria rhizophila*, (d) red fluorescence of *Kocuria rhizophila*; (a), (b) and (c) emission at 450-490 nm, (d) emission at 546 nm.

In the other set of experiments a possibility of dynamic photocontrol of the fluorescence in bacterial culture was demonstrated. The possibility to reversibly switch off and on the fluorescence in bioimaging is very useful since it allows increasing the contrast by subtracting the background fluorescence⁵⁷. This approach was demonstrated with the photoswitchable GS analogue GS-Sw^I(FP) as shown in Figure 3.24. First, a group of bacteria was identified under white light as shown in the panel (a). The same cell cluster was left under the UV light for 5 min to convert the peptidomimetic into the closed-ring form, which resulted in turning the fluorescence off (panel b). The visible light was then applied for 5 min to convert the GS analogue back to the fluorescent open-form (panel c). Finally, the fluorescence was again switched off by illumination for 5 min with UV light.

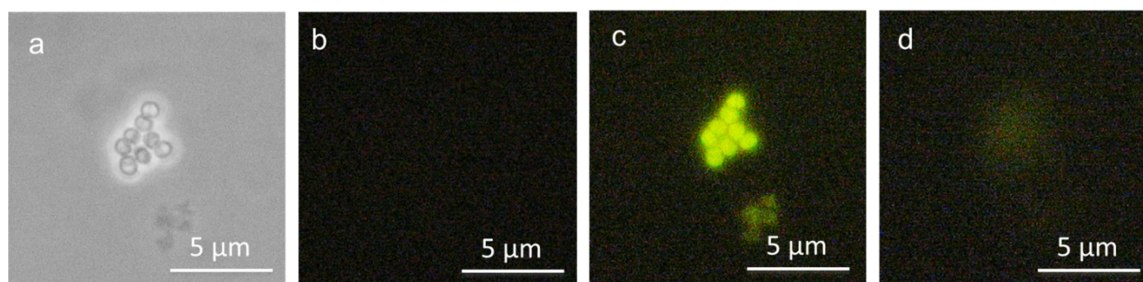


Figure 3.24. Fluorescent cell staining by GS photoswitchable analogue GS-Sw^I(FP). *Kocuria rhizophola* treated for 1 hour with 100 μg/ml of peptidomimetic GS-Sw^I(FP) in closed-ring form, emission at 450-490 nm. (a) White light microphotograph. (b), (c), (d) Illustration of the photoswitching between fluorescent and non-fluorescent states: (b) the fluorescence is absent, peptidomimetic is in the closed-ring form, (c) the fluorescence raised after photoconversion to the open-ring form by visible light, (d) the fluorescence decayed after irradiation with UV light.

3.6. Photoswitchable analogues of the anticancer peptide SVS-1 with the Sw^{II} photoswitchable building block

The photoswitching between open-ring and closed-ring forms of the DAET unit in the ideal case should provide conformational control, by either maintaining or destroying the secondary structure adjacent to the building block. In the studies with linear model peptides (Chapter 3.2.), Sw^I unit was shown being compatible with both principle secondary structure elements in peptides: the β-strand and the α-helix. The example of GS photoswitchable analogues (discussed in Chapter 3.4) illustrated the possibility to incorporate Sw^I and Sw^{II} into short cyclic peptide within the β-turn fold and to photomodulate range of peptide activities. However, gramicidin S structure is additionally stabilized via backbone macrocyclization. In the following example the degree of intrinsic isostery of a DAET-based amino acid surrogate to a β-turn fold was further explored. As well as the attempt was done to create a photoswitchable peptidic anticancer agent.

As a peptide template for incorporation of the photoswitchable building block, peptides with reported anticancer activities were considered¹⁴⁰. SVS-1 is one of them and was selected for structural reasons. This 18-residue peptide was designed to fold as a β-hairpin in the presence of negatively charged membrane surface (see Chapter 1.4.1.). This folding process was suggested to be necessary for the cytotoxicity of SVS against cancer cell lines and the critical role of the β-turn in adopting the amphiphilic β-sheet structure was

demonstrated⁸⁶. Isostery of a DAET building block to the β -turn should therefore be possible to evaluate in a functional anticancer assay or by monitoring the folding process in the presence of a negatively charged membrane.

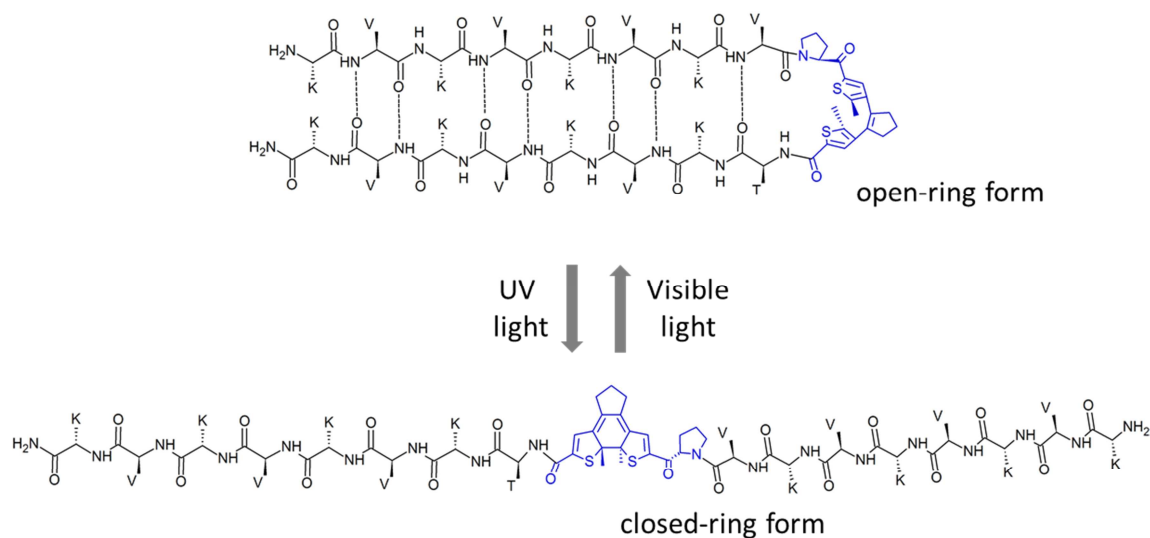


Figure 3.26. Schematic illustration of the photocontrolled β -hairpin folding of SVS- $Sw^{LPro}(PP)$ by switching between β -hairpin supporting (open-ring) and disturbing (closed-ring) forms.

The designed SVS analogues should exploit the mechanism of the structural photoswitching schematically shown in Figure 3.26. In the flexible open-ring form of the DAET unit the two peptidyl β -strands should become free to interact with each other and should be able to form a β -hairpin, stabilized by a number of intra-strand hydrogen bonds. This should happen for instance in the presence of negatively charged model membranes. At the same time, in the DAET closed-ring form the β -strands should become spatially separated through a rigid planar unit and therefore lose the ability to fold as an amphiphilic secondary structure.

Herein Sw^{II} building blocks were chosen for introduction of the photoresponsive functionality for the reasons discussed in Chapter 3.4.1 - higher chemical stability and potentially better compatibility with the β -turn geometry. The sequences were designed, as in the case of GS-analogues (Chapter 3.3.), by introduction of several substitutions around potential target place for empiric comparisons. Since molecular size approximation of a Sw^I unit in previous studies suggested rough equivalency to two to three amino acid rests, to further refine this estimate, both types of replacement - Sw^{II} for a dipeptide and Sw^{II} for a

tripeptide - were planned. The corresponding amino acid sequences are listed in Table 3.10. Substitution of three amino acid residues (-^DPPT-) with both diarylethene building blocks **39** and **40** gave peptidomimetics named SVS-Sw^{LPro}(PPT) and SVS-Sw^{DPro}(PPT), respectively. Substitution of two proline residues (-^DPP-) gave peptidomimetics named SVS-Sw^{LPro}(PP) and SVS-Sw^{DPro}(PP). And substitution of another three amino acid residues (-^VPP-) in the β-turn region gave peptidomimetics named SVS-Sw^{LPro}(VPP) and SVS-Sw^{DPro}(VPP).

Table 3.10. The list of synthesized SVS-1 photoswitchable analogues.

Peptide	Sequence*
SVS-1	KVKVKVKVPPTKVKVKVK-NH ₂
SVS-2	KVKVKVKVPPTKVKVKVK-NH ₂
SVS-Sw ^{LPro} (PPT)	KVKVKVKV-Sw ^{LRro} -KVKVKVK-NH ₂
SVS-Sw ^{DPro} (PPT)	KVKVKVKV-Sw ^{DRro} -KVKVKVK-NH ₂
SVS-Sw ^{LPro} (PP)	KVKVKVKV-Sw ^{LPro} -TKVKVKVK-NH ₂
SVS-Sw ^{DPro} (PP)	KVKVKVKV-Sw ^{DPro} -TKVKVKVK-NH ₂
SVS-Sw ^{LPro} (VPP)	KVKVKVK-Sw ^{LPro} -TKVKVKVK-NH ₂
SVS-Sw ^{DPro} (VPP)	KVKVKVK-Sw ^{DPro} -TKVKVKVK-NH ₂

* Sw^{LPro} denotes residue of building block **39**, Sw^{DPro} – **40**.

3.6.1. Synthesis and purification of SVS-1 analogues

Synthesis of the SVS-1 photoswitchable analogues was performed manually with Fmoc-based SPPS technique and described in Chapter 6.2.4. Undefined side product formation was observed at the step of Fmoc deprotection from the amino acid coupled immediately after the diarylethene building blocks **39** and **40**. Upon MALDI analysis the formed side products systematically gave masses of 18 Da less compared to the target product and these products remained throughout further synthesis. The side-products could be explained by a terminal cyclization of the N-terminus of the growing polypeptide chain that makes it inaccessible for the further coupling steps. In order to overcome this termination and complete the synthesis convergent strategy was used¹⁴¹. For construction of the SVS analogues, the couplings with the tetrapeptides were done to overcome the problematic positions in a large step. The side chain protected tetrapeptides (Fmoc-K(Boc)VK(Boc)V-COOH and Fmoc-VK(Boc)VK(Boc)-COOH) were synthesized separately and used in a single coupling cycle. In the following, syntheses were continued in accordance with the standard single-residue per cycle procedure.

As discussed in the Chapter 3.4.1. Sw^{Pro} were available as racemates. However, for the synthesis of SVS-1 photoswitchable analogues despite use of racemic mixture the final products were possible to separate chromatographically. The separation of the diastereomeric molecules was performed in two RP-HPLC steps. In each step a different ion pairing reagent was employed. During first round of purification the eluents were supplemented with 0.1% of trifluoroacetic acid (TFA). Already at this stage both peptide isomers were separated. Identification which product corresponds to which enantiomeric form of the DAET proline was not possible on this step. This way purified products were named according to their HPLC retention behaviors: peptidomimetics with smaller RTs were designated with the index 1 and their longer retaining counterparts with the index 2. The SVS analogues with the DAET unit in place of prolyl-prolyl-treonyl fragment were called SVS-A1 and SVS-A2; in place of prolyl-prolyl – SVS-B1, SVS-B2 and the remaining valyl-prolyl-prolyl substitutes – SVS-C1, SVS-C2. The second round of HPLC purification was done with eluents containing 0.1% of heptafluorobutyric acid (HFBA) – highly lipophilic ion pairing reagent. Purification of the wild type peptides SVS-1 and SVS-2 was performed in one round with the HFBA system. Notably, application of conventional eluents for peptide purification (with 5mM HCl or 0.1% TFA as ion-pairing agents) appeared to mask significant number of impurities which eluted at the same times as the target products. The SVS analogues declared as pure when being purified with conventional eluents, in HFBA purification appeared to have actual purities below 50%. This demonstrates limitations in the HPLC purity assessment when no precautions are done and in part may explain differences in the results obtained in this work and reported in the literature (see below).

3.6.2. Structural analysis of SVS-1 analogues

SVS-1 was reported not to have any structure in aqueous buffers and in presence of zwitterionic lipid vesicles (POPC) – the CD spectra at these conditions were interpreted as reflecting a random coil, unstructured, state⁸⁶. Contrastingly, when negatively charged lipid vesicles (POPC/POPS, 1:1) were applied, the CD spectra showed signals with distinct minima in the mean residue ellipticity at 218 nm, supporting the notion that the peptide adopts a β -sheet fold consistent with the hairpin formation. The other peptide SVS-2, which contains single L-proline/D-proline mutation in the β -turn and is therefore not able to fold as a β -hairpin, behaved differently⁸⁶. The CD spectra of SVS-2 resemble the “random coil” independent of the lipid charge. The ability of SVS-1 to fold into the amphiphilic hairpin in

response to the presence of negatively charged membrane was thus postulated to be responsible for selective targeting of the more negatively charged cancer cells co-present with the more neutral normal eukaryotic cells (see in Chapter 1.4.1.).

An ideal photoswitchable β -turn mimetic of SVS-1 should behave in the following way: one of the photoforms should stabilize the β -hairpin, while the other photoform should be incompatible with this structure. Therefore, if the CD spectra of peptidomimetic resemble the signal from SVS-1, the photoswitchable unit is proven of supporting a β -hairpin, at the same time similarity to SVS-2 spectra will suggest the opposite. Herein CD spectra of the wild type peptides SVS-1 and SVS-2 as well as of SVS-1 photoswitchable analogues were acquired in different media including i) aqueous buffer and ii) liposomes from zwitterionic DMPC and iii) from negatively charged DMPC/DMPS and iv) DMPC/DMPG mixtures. The peptidomimetics were studied in their both photoforms using the following procedure. The CD spectra of the closed-ring forms were measured first. Next, the samples were exposed to visible light for time periods needed to convert 100% of the peptidomimetics into the colorless open-ring forms (visual control), and the second set of the CD spectra was recorded (see details in Chapter 6.4). The obtained CD spectra are collected in Figure 3.27 and 3.28.

Figure 3.27 summarize CD study of the control peptides SVS-1 and SVS-2. According to the literature⁸⁶, both peptides should be unstructured in aqueous buffers and in presence of zwitterionic lipids. In 10 mM phosphate buffer and with DMPC vesicles, SVS-2 indeed showed a random coil CD signal (Figure 3.27a,b). SVS-1, surprisingly, appears being structured at both conditions: negative band at ca. 220 nm and a positive one at ca. 200 nm indicate that the peptide adopts a β -like fold. In the presence of negatively charged DMPC/DMPS or DMPC/DMPG liposomes, both peptides were structured (Figure 3.27c,d). Judging by the intensity of the 200 nm band, as expected, more molecules of SVS-1 appear to be folded than of SVS-2. The results directly contradict literature data for SVS-1 peptide, which should have been unstructured in water. Either peptide material in this work differ to the one used by Sinthuvanich et al. (see comment about HPLC purification in Chapter 3.6.1.) or other factors may play a role. For instance here a salt-free buffer was used, while the literature investigation was performed in presence of 150 mM NaF; here DMPC/DMPS lipid was used, while the other study have used more fluid POPC/POPS bilayers.

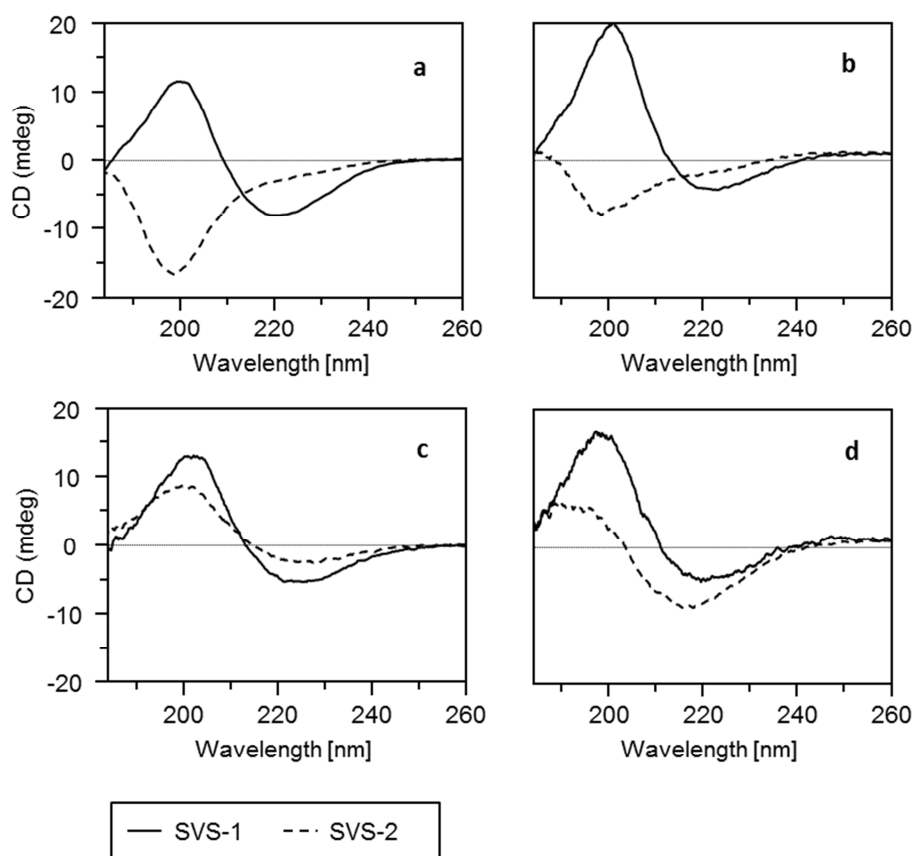


Figure 3.27. Circular dichroism spectra of SVS-1 and SVS-2 at 100 $\mu\text{g/ml}$ concentration in different conditions. (a) 10 mM PB at 25°C; (b) DMPC vesicles, P:L ratio 1:50, at 40°C; (c) DMPC/DMPS (1:1 mol) vesicles, P:L ration 1:50, at 40°C; (d) DMPC/DMPG (3:1 mol) vesicles, P:L ration 1:50, at 40°C.

Nevertheless, the photoswitchable SVS-1 analogues were measured in buffer solution and in the presence of negatively charged vesicles (DMPC/DMPG) as shown in Figure 3.28. In PB buffer solution all the peptidomimetics gave a CD spectra associated with a random coil, while in DMPC/DMPG presence appeared partially folded, resembling therefore general behavior of the SVS-2 peptide. The structures assumed by the peptidomimetics indeed correspond to expected β -folds. An interesting exception here was the SVS-C1 peptide – with membranes it shows far largest amount of the random coil signal, suggesting most of the peptide to remain non-bound. The non-bound fraction with this is even larger than for the wild type SVS-2 peptide. Difference between SVS-C1 and SVS-C2 renders the enantiomeric form of proline within DAET building block to play an important role in defining the peptide structure. This result also clearly shows that position and number of residues to be substituted by a DAET building block is indeed critical in the β -turn structures. When comparing membrane-interaction of the open-ring and closed-ring forms, both SVS-B isomers, SVS-A1

and SVS-C2 showed the differences in between, while CD spectra of SVS-A2 and SVS-C1 remained almost intact. For SVS-B1 and SVS-C2 spectral differences were the largest. Importantly, when the differences are present, all the open-ring forms spectra resemble the spectrum of SVS-1, while the closed-ring forms appear similar to CD signal of SVS-2 (Figure 3.27.d). This suggests closed-ring forms to indeed bind the membranes less and to be less structured, the same way as in the distorted SVS-2 peptide.

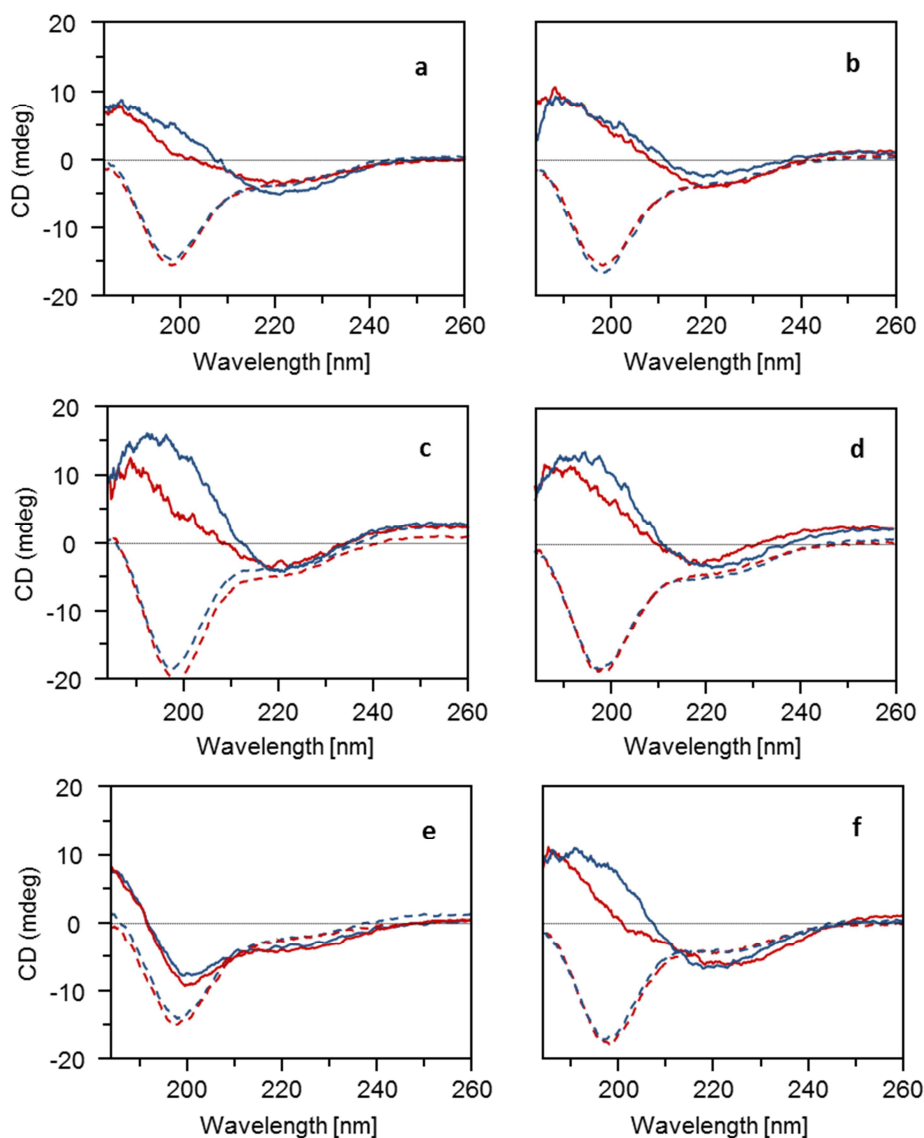


Figure 3.28. Circular dichroism spectra of the SVS-1 photoswitchable analogues at 100 $\mu\text{g/ml}$ concentration in different conditions. Blue lines correspond to peptidomimetics in the open-ring forms, red – to the closed-ring forms. Solid lines correspond to spectra recorded in DMPC/DMPG (3:1 mol) vesicles, P:L ratio 1:50, at 40°C. (a) and (b) correspond to the peptidomimetics SVS-A1 and SVS-A2, respectively; (c) and (d) to SVS-B1 and SVS-B2, (e) and (f) to SVS-C1 and SVS-C2, respectively.

Comparison of the degree of deviation between CD signals of the two photoforms (e.g. by assessing intensity at ~195 nm) across all peptide variants allows qualitative judgment about efficiency of the dipeptide- and tripeptide-Sw^{II} substitutions. The efficiency is meant here as an ability to mimic a β -turn in one photoform and to destroy the fold in the other. Substitution of three amino acids (-^DPPT-) by Sw^{II} appears to be the least effective – none of the peptidomimetics SVS-A1 or SVS-A2 showed any pronounced change of the CD lineshape during photoswitching. The same can be concluded for one of the diastereomers of the other tripeptidyl substitution (-^VDPP- in SVS-C1). In contrast to this, the substitution of two amino acids (-^DPP-, SVS-B peptides) achieved more effective photocontrol of the folding as the difference is the largest (SVS-B1) and is present in both enantiomers (compare SVS-B2). It has to be noted that dipeptidyl substitution also gave good results in GS analogues. In summary: substitution of three amino acid with DAET unit is not effective. Much better results showed substitution of two central amino acids (-^DPP-). It was also shown the enantiomeric form of the proline residue in DAET building block plays an important role. This influence was clearly seen for pair of analogues SVS-C1 and SVS-C2.

3.6.3. Antimicrobial activity of SVS analogues

The antimicrobial activity for the β -hairpin forming peptide SVS-1 and its non-foldable isomer SVS-2 was not previously reported. In the original study both peptides were only investigated for the anticancer cytotoxicity⁸⁶. However, an antimicrobial activity was expected due to close similarity to canonical antimicrobial peptides – SVS peptides possess high positive charge and acquire amphiphilic secondary structures in membranes. In this work MIC assays were used to quantitatively assess potential antimicrobial activities of the DAET-modified SVS analogues while SVS-1 and SVS-2 served control purposes. In the first round of experiments using only SVS wild type peptides (see Chapter 6.5. for details) activities against Gram-positive and Gram-negative bacteria were compared. Against Gram-negative strains SVS-1 and SVS-2 demonstrated rather weak activity: the MIC values in $\mu\text{g/ml}$ for *E. coli* were found 64, 128, and for *E. faecalis* 250, >250, respectively. However, both peptides demonstrated relatively high activity against Gram-positive bacteria strains. In the following study, which included the photoswitchable SVS analogues, the focus was set only on Gram-positive strains. Obtained MIC values are summarized in the Table 3.11.

As was expected, SVS-1 was more active comparing to SVS-2. Against *S. aureus* and *S. epidermidis* MIC values for SVS-1 were higher by one- (32 against 64 $\mu\text{g/ml}$) and two- (8

against 32 µg/ml) dilution folds, respectively. Against *S. xylosus* both peptides showed equal MIC values (8 µg/ml). Interestingly, all photoswitchable peptidomimetics generally have shown equal or stronger activities than the wild types SVS-1 and SVS-2.

The open-ring forms of peptidomimetics were designed to adopt a β-hairpin structure and in this way mimic the functions of peptide SVS-1 while the closed-ring forms should have stayed unstructured and were supposed to behave like SVS-2. This indeed was observed in the antimicrobial activity of peptidomimetics. For example, the analogue SVS-A1 in the open-ring form was more active than the closed-ring form (by two folds of dilution) against both *S. aureus* and *S. epidermidis*. At the same time against *S. xylosus* there was no difference observed in the MIC values for the two photoforms. Similar results were obtained for peptidomimetics SVS-B1, SVS-B2, SVS-C2.

Table 3.11. The antimicrobial activities of SVS-1 photoswitchable analogues in both open-ring and closed-ring forms tested against Gram-positive bacteria strains.

Peptides	MIC (µg/ml)			
	<i>S. aureus</i>	<i>S. xylosus</i>	<i>S. epidermidis</i>	
Gramicidin S	4	2	2	
SVS-1	32	8	8	
SVS-2	64	8	32	
SVS-A1	open-ring	16	8	4
	closed-ring	64	8	16
SVS-A2	open-ring	16	8	8
	closed-ring	32	8	8
SVS-B1	open-ring	16	8	8
	closed-ring	32	8	16
SVS-B2	open-ring	16	8	8
	closed-ring	32	8	16
SVS-C1	open-ring	32	4	8
	closed-ring	64	8	16
SVS-C2	open-ring	16	8	8
	closed-ring	32	4	8

3.6.4. Anticancer activity of SVS-1 analogues

The peptide SVS-1 was reported⁸⁶ to be highly active against a variety of cancer cell lines such as A549 (lung carcinoma), KB (epidermal carcinoma), MCF-7 (breast carcinoma), and MDA-MB-436 (breast carcinoma) with IC_{50} values around 10-20 $\mu\text{g/ml}$. At the same time SVS-2 was reported to be at least ten times less active with $IC_{50} > 200 \mu\text{g/ml}$.

In this work, cytotoxic activity assessments of SVS-1, SVS-2 were performed using breast cancer MCF-7 and the cervix cancer cell line HeLa (see Chapter 6.8 for details). First, the wild type peptides SVS-1 and SVS-2 were evaluated. In the Figure 3.28, viabilities of the cancer cells are expressed as a function of concentration for both of them, illustrating the study. SVS-1 showed IC_{50} values in the concentration ranges of 32-64 and of 64-128 $\mu\text{g/ml}$ against HeLa and MCF-7 cells, respectively. SVS-2 revealed IC_{50} values of 64-128 and $>256 \mu\text{g/ml}$ against two cancer cell lines, respectively. In addition, the peptides were evaluated for their influence on the apoptosis of the HeLa cells. At the concentration 128 $\mu\text{g/ml}$ both wild type peptides showed moderate proapoptotic action with slightly higher activity of the SVS-1 (Figure 3.29.).

Obtained results contradict literature data in that SVS-1 has rather moderate cytotoxicity, while SVS-2 demonstrates comparable activity levels. Opposite to the expectations, no dramatic difference between two peptides with different propensities for the β -hairpin formation was observed.

Despite rather discouraging results above, anticancer activities of the photoswitchable SVS-1 analogues were studied. Herein cytotoxicities were tested on two cancer cell lines: cervix cancer line HeLa and hepatocellular carcinoma G2. An example of concentration depended viability curves is shown in Figure 3.30. The IC_{50} values for all peptidomimetics are summarized in Table 3.12. In general the DAET modified peptidomimetics showed activities in the same concentration range as SVS-1 and SVS-2. However, neither of the analogues had shown any difference between the two photoforms (Table 3.12.).

This study had shown that the peptide SVS-1 and its analogues cannot be called promising anticancer agents in view of their low IC_{50} values. Moreover, it appears that the cell cytotoxicity of these peptides cannot be a measure to evaluate the efficiency of β -hairpin folding. The two peptides SVS-1 and SVS-2 have different potency to form an amphiphilic β -hairpin structure, but their toxicities against cancer cells are comparable.

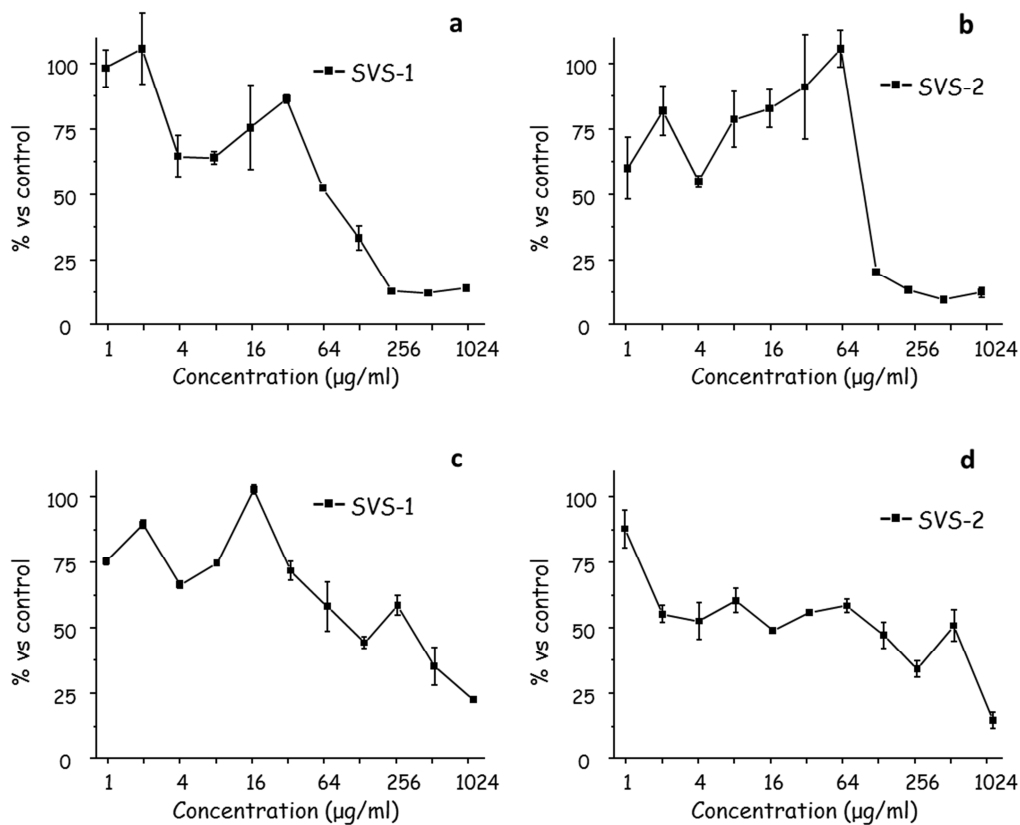


Figure 3.28. Cytotoxic activity of SVS-1 and SVS-2 measured in MTT test. (a, b) Against cervix cancer line HeLa and, (c, d) against breast cancer MCF-7.

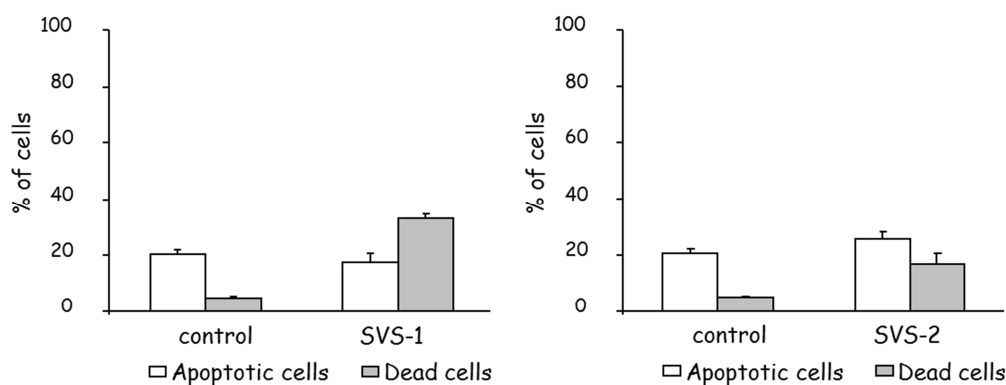


Figure 3.29. Proapoptotic action of peptides SVS-1 and SVS-2 on the cervix cancer line HeLa at concentration 128 μg/ml measured by flow cytometry.

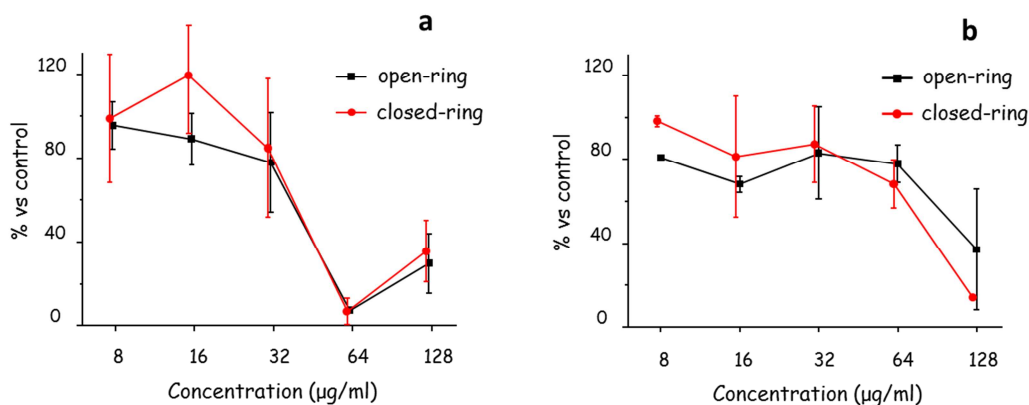


Figure 3.30. Cytotoxic activity of photoswitchable analogue SVS-B2 in both open-ring and closed-ring forms measured in MTT test. (a) Against cervix cancer line HeLa, (b) against hepatocellular carcinoma G2 cancer line.

Table 3.12. Half-lethal concentrations (IC_{50}) of photoswitchable peptidomimetics tested against cervix cancer line HeLa and hepatocellular carcinoma G2 (Hep G2).

Peptide		IC_{50} ($\mu\text{g/ml}$)	
		HeLa	Hep G2
SVS-A1	open-ring	32-64	>128
	closed-ring	32-64	>128
SVS-B1	open-ring	64	128
	closed-ring	64	128
SVS-B2	open-ring	32-64	64-128
	closed-ring	32-64	64-128
SVS-C1	open-ring	32-64	>128
	closed-ring	32-64	>128
SVS-C2	open-ring	32-64	64-128
	closed-ring	32-64	64-128

4. Summary

Incorporation of molecular photoswitches into peptides or proteins should allow reversible control of their structure and functions by means of photoisomerization. The aim of this study was to explore the practical possibilities of polypeptide modification using photoswitchable diarylethene-based building blocks, and to investigate the effects of the photoinduced isomerization on the structure and function of several biologically active peptides.

Two types of diarylethene-based building blocks suitable for incorporation into peptides with routine peptide synthesis were synthesized. In these units, which appear as amino acid surrogates, different linkers were explored to attach the amino function, including a hydrazide group and the backbone of another α -amino acid. These variations now render the photoswitchable building blocks compatible with a broad range of peptide geometries.

The suitability of the building blocks for practical incorporation in peptides was successfully demonstrated on variety of linear and cyclic peptides. The range of explored polypeptide geometries, shown to be suitable for incorporation of the building blocks, covers α -helices, β -strands, β -turns, as well as the backbone of macrocycles. Physico-chemical and biological studies on the photoswitchable peptides allowed characterization of the building blocks in the context of real polypeptides in action. In particular, the efficiencies of photoisomerization, the general hydrophobicities, and the degree of conformational flexibility were characterized, as well as the absorption and fluorescence properties of the units. The general requirements were identified for selecting a target polypeptide sequences that can be successfully modified by the building blocks. A prototype of a reversibly photocontrolled fluorescent label was demonstrated, based on the diarylethene photoswitchable moiety.

With the novel photoswitchable analogues of Gramicidin S and SVS, respectively, major and minor conformational changes of the polypeptide backbone upon photoisomerization were demonstrated. The previously reported strong anticancer activity of the SVS peptide was disproved. Gramicidin S, on the other hand, was shown to possess anticancer cytotoxicity. For the first time with a diarylethene photoswitchable unit in a peptide backbone, a functional photodynamic control was achieved for a peptide. The range of peptidomimetics allowed photoisomerization-mediated photocontrol of the antimicrobial, hemolytic and anticancer activities.

5. Zusammenfassung

Durch Einbau lichtabhängiger Schalter kann die Struktur und Funktion von Peptiden und Proteinen durch Photoumwandlung gezielt gesteuert werden. Ziel dieser Studie war es, Diarylethen-Bausteine, die sich durch Licht umwandeln lassen, zur Modifikation von Peptiden und Proteinen einzusetzen, und die Auswirkung der lichtinduzierten Umwandlung auf die Struktur und Funktion verschiedener biologisch aktiver Peptide zu untersuchen.

Hierbei wurden zwei verschiedene Diarylethen-Bausteine entwickelt, die sich für den Einbau in Polypeptide mittels Standard-Peptidsynthese eignen. Für diese Bausteine wurden verschiedene funktionelle Gruppen, wie z.B. Hydrazin oder Aminosäure-Analoga, getestet, durch die ein Einbau in Peptide anstelle von normalen Aminosäuren möglich ist. Durch Verwendung verschiedener funktioneller Gruppen wird ein Einbau dieser durch Licht umwandelbaren Bausteine in unterschiedlichste Peptidstrukturen gewährleistet. Die Eignung dieser Bausteine für verschiedene Peptidkonformationen konnte durch den Einbau in Peptide mit α -helikaler, β -Faltblatt und Schleife sowie in zyklischen Peptiden erfolgreich gezeigt werden. Durch Einbau der photoschaltbaren Module in bekannte Peptide konnten diese Bausteine unter realen Bedingungen getestet werden. Hierbei konnte die Effizienz der durch Licht induzierten Umwandlung, die Hydrophobizität, der Grad der strukturellen Flexibilität, sowie die Absorption und Fluoreszenzeigenschaften dieser Bausteine charakterisiert werden. Außerdem wurden die grundlegende Voraussetzungen für die Auswahl der Zielsequenzen identifiziert, und es wurde der Prototyp eines reversibel umwandelbaren Fluoreszenzfarbstoffes gezeigt.

Anhand neuer Analoga von Gramicidin S und SVS konnten verschiedene Licht-induzierte Strukturänderungen des Peptidrückgrats gezeigt werden. Die kürzlich postulierte anti-Krebs Wirkung des SVS Peptides konnte widerlegt werden, wohingegen für Gramicidin S eine cytotoxische Wirkung gegen Krebszellen nachgewiesen werden konnte. Mit dieser Arbeit gelang es das erste Mal, ein durch Licht kontrollierbares Peptid basierend auf Diarylethen-Bausteinen herzustellen, dessen antimikrobielle, hämolytische und anti-Krebs Aktivität beeinflusst werden konnte.

6. Experimental part

All starting materials were purchased from Merck, Acros, ABCR, Fisher, Iris Biotech, and Biosolve. Tetrahydrofuran, N,N-diisopropylethylamine, and diethyl ether were freshly distilled under a nitrogen atmosphere from sodium/benzophenone, and toluene was distilled from sodium. Analytical reversed-phase high-performance liquid chromatography (RP-HPLC) was done on Jasco system. Next columns were used: Vydac[®] C18 column (4.6 mm x 250 mm), flow rate 1.5 ml/min for analytical analysis, Vydac[®] C18 column (10 mm x 250 mm), flow rate 7 ml/min for semi-preparative purification, Vydac[®] C18 column (22 mm x 250 mm), flow rate 17 ml/min for preparative purification; solvent A: 90% water, 10% acetonitrile, solvent B: 10% water, 90% acetonitrile; 5mM hydrochloric acid, or 0.1% trifluoroacetic acid, or 0.1% heptafluorobutyric acid were used as an ion-pairing agents. For preparative HPLC individual gradients were optimized for each peptide depending on a retention time of the target peptide and type of contaminations; for analytical and semipreparative HPLC typical gradient slopes were 1% and 4% B per min, respectively. ¹H and ¹³C NMR spectra were recorded on Bruker Avance 300 spectrometer and referenced to TMS.

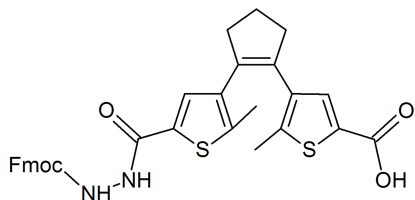
Mass spectra were recorded either on an Agilent 1100 LC/MSD SL instrument by chemical ionization (CI), or on a Bruker Autoflex III by matrix-assisted laser induced desorption/ionization (MALDI). MALDI samples were co-crystallized with a matrix of 3,5-dihydroxy-benzoic acid or α -cyano-4-hydroxycinnamic acid from acidic H₂O/MeCN solutions on a stainless steel target.

For UV illumination either standard UV lamp Spectroline[®] from Spectronics Corporation (model with the unfiltered short wave tube (UV-C, 254 nm)), or the model XX-15Fe, equipped with two integrally filtered 15-Watt tubes (BLE-1T155) were used. The latter provides peak UV intensity of 1100 μ W/cm² at 25 cm. For fluorescent microscopy in cell cultures were used Axioskop 40 with filter set 09 (λ_{ex} 450-490 nm, λ_{emm} 515 nm), Carl Zeiss, Jena, Germany.

Compound **8a** and **33** were synthesized according to ref. ²⁷. The fluorine label 3-(trifluoromethyl)bicyclopent-[1.1.1]-1-yl glycine (CF₃-Bpg) was provided by Prof. Komarov and Dr. Mykailiuk.

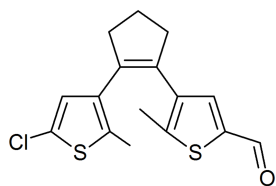
6.1. General organic synthesis

4-(2-(5-(2-(((9H-fluoren-9-yl)methoxy)carbonyl)hydrazine-1-carbonyl)-2-methylthiophen-3-yl)cyclopent-1-en-1-yl)-5-methylthiophene-2-carboxylic acid, **31**.



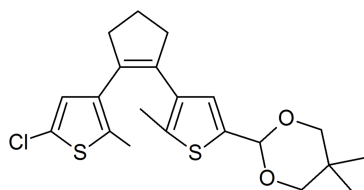
Compound **8a** (5 g, 14.3 mmol) was dissolved in dimethylformamide (25 ml). N,N-diisopropylcarbodiimide (DIC, 1.76 g, 14 mmol) and subsequently DIPEA (3.7 g, 28.6 mmol) were added to the solution. Fmoc-hydrazine (Fmoc-NH-NH₂; 3.56 g; 14 mmol) was added immediately. After stirring the reaction mixture overnight, it was poured into water (100 ml). The precipitate was filtered, dissolved in dichloromethane (200 ml) and washed twice with 0.5 M aq solution of sodium bicarbonate (100 ml), then with 0.5 M aq solution of hydrochloric acid (100 ml), in order to remove the unreacted compound **8a**. The organic phase was dried over magnesium sulfate. Evaporation of dichloromethane under reduced pressure gave the crude material which contained, along with the desirable **31**, also the by-product **32**. The by-product did not interfere with the solid-phase peptide synthesis, so the obtained material was used without additional purification. The analytically pure **31** was obtained using RP-HPLC (H₂O/MeCN mixture as the eluent). Compound **31**: ¹H-NMR (300 MHz, DMSO-d₆), δ = 1.88 (s, 3H, CH₃), 1.91 (s, 3H, CH₃), 2.02 (m, 2H, 2CH₂), 2.78 (t, 4H, 2CH₂), 4.13-4.42 (CH₂CH, two rotamers 4:1), 7.11-7.92 (m, aromatic protons, 10H), 9.01 and 9.36 (rotamers 1:4, 1H), 10.22 and 10.46 (rotamers 4:1, 1H), 12.89 (broad singlet, 1H). ¹³C-NMR (300 MHz, DMSO-d₆), δ = 14.1, 14.4, 22.2, 46.4, 66.1, 120.1, 125.2, 127.1, 127.7, 129.8, 130.4, 132.9, 133.9, 134.2, 136.2, 136.3, 140.0, 140.7, 141.7, 143.6, 156.3, 160.7, 162.6. Compound **41**: ¹H-NMR (300 MHz, DMSO-d₆), δ = 1.89 (m, 6H), 2.05 (m, 2H), 2.78 (t, 4H, 2CH₂), 4.14-4.41 (CH₂CH, 6H), 7.12-7.92 (m, aromatic protons, 18H), 9.00 and 9.36 (rotamers 1:3, 2H), 10.23 and 10.47 (rotamers 3:1, 2H). ¹³C-NMR (300 MHz, DMSO-d₆), δ = 14.2, 22.2, 38.1, 46.5, 66.1, 120.1, 125.2, 127.1, 127.7, 129.8, 132.9, 134.2, 136.2, 140.0, 140.7, 143.6, 156.3, 160.7.

4-(2-(5-chloro-2-methylthiophen-3-yl)cyclopent-1-en-1-yl)-5-methylthiophene-2-carbaldehyde, 34.



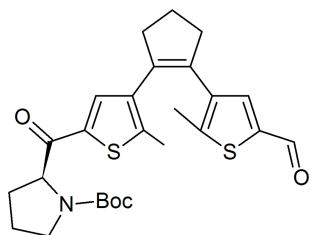
15 g of compound **33** (0.0456 mol) were dissolved in 250 ml of dried tetrahydrofuran under inert argon atmosphere. The solution was cooled to $-78\text{ }^{\circ}\text{C}$ using bath with dry ice. 20 ml (0.051 mol) of the 2.5 M butyllithium solution in hexane were added to the cooled solution. The reaction mixture was let go to the temperature $-10\text{ }^{\circ}\text{C}$ and was cooled again to $-78\text{ }^{\circ}\text{C}$. 4 g (0.0548 mol) of the dimethylformamide were added to the solution at $-78\text{ }^{\circ}\text{C}$. The solution was slowly (during half an hour) heated to $0\text{ }^{\circ}\text{C}$ and stirred at room temperature for one hour. Then the reacting mixture was poured into 200 ml of water and 55 ml (0.055 mol) of 1 M hydrochloric acid were added. The product **34** was extracted with 200 ml of diethyl ether. Separated organic phase was dried over anhydrous magnesium sulfate and volatile solvents were removed under reduced pressure. 15 g of obtained crude material were used in further synthetic steps without purification. Compound **34**: $^1\text{H-NMR}$ (300 MHz, CDCl_3), $\delta = 1.85$ (s, 3H, CH_3), 1.92 (s, 3H, CH_3), 2.00 (m, 2H, CH_2), 2.74 (t, 4H, 2CH_2), 6.59 (s, 1H, CH), 7.75 (s, 1H, CH), 9.75 (s, 1H, CHO).

2-(4-(2-(5-chloro-2-methylthiophen-3-yl)cyclopent-1-en-1-yl)-5-methylthiophen-2-yl)-5,5-dimethyl-1,3-dioxane, 35.



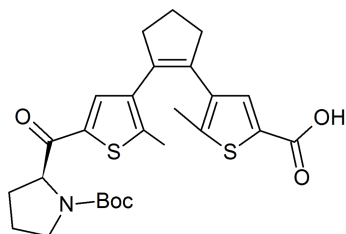
15 g of crude compound **34** (approximately 0.0456 mol) were dissolved in 250 ml of toluene. 7.1 g (0.0684 mol) of 2,2-dimethyl-1,3-propanediol and 0.1 g of p-toluenesulfonic acid were added. The solution was refluxed with Dean-Stark apparatus until all the water formed in reaction was removed (0.82 g). Toluene was removed under reduced pressure. Pure product **35** was obtained after column chromatography on silica gel with hexane/ethyl acetate 10:1 mixture used as the eluent. The yield in two steps from **33** to **35** was 14.2 g (76 % of theoretical). Compound **35**: $^1\text{H-NMR}$ (300 MHz, CDCl_3), $\delta = 1.27$ (s, 6H, 2CH_3), 1.84 (s, 3H, CH_3), 1.91 (s, 3H, CH_3), 2.00 (m, 2H, CH_2), 2.72 (t, 4H, 2CH_2), 3.66 (q, 4H, 2CH_2), 5.51 (s, 1H, CH), 6.58 (s, 1H, CH), 6.82 (s, 1H, CH).

***tert*-butyl (S)-2-(4-(2-(5-formyl-2-methylthiophen-3-yl)cyclopent-1-en-1-yl)-5-methylthiophene-2-carbonyl)pyrrolidine-1-carboxylate, 37.**



3 g (0.00733 mol) of compound **35** were dissolved in 50 ml of dried tetrahydrofuran under inert argon atmosphere. The solution was cooled to $-78\text{ }^{\circ}\text{C}$ by cooling bath with dry ice. To the cooled solution were added 3.52 ml (0.0088 mol) of the 2.5 M butyllithium solution in hexane. The reaction mixture was let go to the temperature $-10\text{ }^{\circ}\text{C}$ and then again was cooled to $-78\text{ }^{\circ}\text{C}$. 2.27 g (0.0088 mol) of the compound **36** (*tert*-butyl (S)-2-(methoxy(methyl)carbamoyl)pyrrolidine-1-carboxylate) were dissolved in 10 ml of dried tetrahydrofuran and added to the cooled solution. The solution was slowly (during half an hour) heated to $0\text{ }^{\circ}\text{C}$ and stirred at room temperature for one hour. The reaction mixture was poured into 100 ml of water and 9 ml (0.009 mol) of 1 M hydrochloric acid were added. The product **37** was extracted with 100 ml of diethyl ether. The separated organic phase was dried over anhydrous magnesium sulfate and volatile solvents were removed under reduced pressure. Pure product **37** was obtained after column chromatography on silica gel with hexane/ethyl acetate 5:1 mixture used as the eluent. The obtained yield was 3.1 g (73 % of theoretical). Compound **37**: $^1\text{H-NMR}$ (300 MHz, CDCl_3), δ = 1.27 (s, 9H, 3 CH_3), 1.89 (m, 3H), 2.01-2.08 (rotamer, m, 6H, 2 CH_3), 2.12 (m, 2H, CH_2), 2.23 (m, 1H, CH), 2.84 (t, 4H, 2 CH_2), 3.45-3.56 (rotamer, m, 2H), 4.70-4.94 (rotamer, m, 1H), 7.40-7.47 (rotamer, two singlets, 2H, 2CH), 9.73-9.75 (rotamer, s, 1H, CHO).

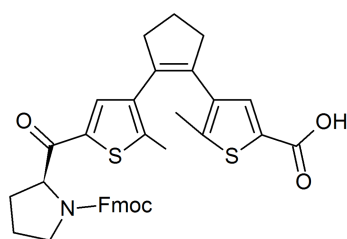
4-(2-(5-((*tert*-butoxycarbonyl)-L-prolyl)-2-methylthiophen-3-yl)cyclopent-1-en-1-yl)-5-methylthiophene-2-carboxylic acid, 38.



3.1 g (0.0064 mol) of compound **37** were dissolved in 40 ml of ethanol. 7.42 g (0.032 mol) of freshly prepared silver oxide and 0.5 g (0.0128 mol) sodium hydroxide were added and vigorously stirred for two hours. 20 ml (0.02 mol) of 1 M hydrochloric acid and 40 ml of ethanol were added. Formed precipitate was filtered through a paper filter and the product **38** was extracted twice with 100 ml of diethyl ether from the obtained filtrate. Separated organic phases were combined and dried over anhydrous magnesium sulfate. Volatile solvents were removed under reduced pressure. The yield was 3.2 g (100% of theoretical) of pure compound **38**. Compound **38**: $^1\text{H-NMR}$

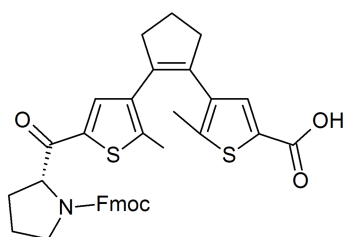
NMR (300 MHz, CDCl₃), δ = 1.28 (s, 9H, 3CH₃), 1.89 (m, 3H), 1.96-2.01 (rotamer, s, 3H, CH₃), 2.06-2.07 (rotamer, s, 3H, CH₃), 2.10 (m, 2H, CH₂), 2.23 (m, 1H, CH), 2.81 (m, 4H, 2CH₂), 3.46-3.56 (rotamer, m, 2H), 4.71-4.95 (rotamer, m, 1H), 7.39-7.45 (rotamer, s, 1H, CH), 7.59-7.60 (rotamer, s, 1H, CH).

4-(2-(5-(((9H-fluoren-9-yl)methoxy)carbonyl)-L-prolyl)-2-methylthiophen-3-yl)cyclopent-1-en-1-yl)-5-methylthiophene-2-carboxylic acid, 39.



3.2 g (0.0064 mol) of compound **38** were dissolved in 20 ml of dichloromethane. 2 ml of trifluoroacetic acid were added to the solution and it was kept afterwards for 2 hours at room temperature. The volatile solvents were removed under reduced pressure. The obtained yellow oil was dissolved in 50 ml of water/acetone 1:1 mixture and 1,075 g (0.0128 mol) of sodium bicarbonate and 3.3 g (0.0128 mol) of fluorenylmethoxycarbonyl chloride (FmocCl) were added. The solution was actively stirred for 4 hours at room temperature. 12.8 ml (0.0128) of 1 M hydrochloric acid were slowly added and the product **39** was extracted twice with 100 ml of diethyl ether. Separated organic phases were combined and dried over anhydrous magnesium sulfate and volatile solvents were removed under reduced pressure. Pure compound **39** was obtained after column chromatography on silica gel with hexane/ethyl acetate 5:1 mixture used as the eluent. The obtained yield was 4 g (91 % of theoretical). Compound **39**: ¹H-NMR (300 MHz, CDCl₃), δ = 1.92 (m, 3H), 1.97-2.03 (rotamer, s, 3H, CH₃), 2.10 (s, 3H, CH₃), 2.12 (m, 2H, CH₂), 2.25 (m, 1H, CH), 2.82 (m, 4H, 2CH₂), 3.61-3.74 (rotamer, m, 2H), 4.08-4.43 (rotamer, m, 3H, CH₂CH) 4.86-5.05 (rotamer, m, 1H), 7.14-7.79 (m, aromatic protons, 10H).

4-(2-(5-(((9H-fluoren-9-yl)methoxy)carbonyl)-D-prolyl)-2-methylthiophen-3-yl)cyclopent-1-en-1-yl)-5-methylthiophene-2-carboxylic acid, 40.



Compound **40** was synthesized likewise compound **39** with the difference that precursor **35** was treated with D-proline N-Boc protected Weinreb amide (*tert*-butyl (R)-2-(methoxy(methyl)carbamoyl)pyrrolidine-1-carboxylate) instead of compound **36**. Compound **40**: ¹H-NMR (300 MHz, CDCl₃), δ = 1.92 (m, 3H), 1.97-2.03 (rotamer, s, 3H, CH₃), 2.10 (s, 3H, CH₃), 2.12 (m, 2H, CH₂), 2.25

(m, 1H, CH), 2.82 (m, 4H, 2CH₂), 3.61-3.74 (rotamer, m, 2H), 4.08-4.43 (rotamer, m, 3H, CH₂CH) 4.86-5.05 (rotamer, m, 1H), 7.14-7.79 (m, aromatic protons, 10H).

6.2. Synthesis of peptides containing Sw^I and Sw^{II}

6.2.1. Synthesis of β/α -model peptide and its ¹⁹F-labeled analogues

Standard Fmoc-based solid-phase peptide synthesis (SPPS) and commercially available reagents were used for the peptide synthesis. Leucine pre-loaded Rink amide MBHA resin with loading 0.67 mmol/g (150 mg, 1 equiv) was used. Coupling of the amino acids was performed using the following molar ratios of the reagents: Fmoc-amino acid (4 equiv), HOBt (4 equiv), HBTU (3.9 equiv), DIPEA (8 equiv). Incorporation of the diarylethene building block Sw^I was performed by coupling with **31** (in the crude mixture; the amount was taken to provide 1.5 equiv), HOBt (1.5 equiv), PyBOP (1.5 equiv), DIPEA (3 equiv). The coupling time in all cases was 40 min. N-Fmoc deprotection was carried out by treating the resin with 20% piperidine in DMF for 20 min. After completing the synthesis, the resin was washed with dichloromethane and dried under vacuum for 24 h. The peptides were cleaved from the resin with cleavage cocktail (trifluoroacetic acid, triisopropylsilane and water, 92.5:2.5:5 v/v mixture, 10 ml, 30 min). The volatile products from the filtered solution were blown off by a flow of argon. The residual material was dissolved in an acetonitrile-water (1:1) mixture and lyophilized. The crude peptidomimetics in open-ring form were purified on a preparative C18 column with a linear A:B gradient of 5% B/min. The purity of the peptidomimetics was checked on the analytical C18 column with a linear A:B gradient of 1% B/min. The identity of each peptidomimetic was confirmed by MALDI-TOF mass spectrometry; m/z = 2618.5 [β/α -model peptide], 2696.5 [β 2I/ α -, β 4I/ α -, β 8I/ α -, β/α 3L-, β/α 7I-, β/α 8L-, β/α 11L-model peptides], 2738.5 [β 6A/ α -model peptide], 2662.5 [β/α 4F-model peptide], 2646.5 [β/α 10Y-model peptide].

6.2.2. Synthesis of α/α -model peptide and its ¹⁹F-labeled analogues

Labeled fragments of peptide BP100 was synthesized as describe in Chapter 6.2.1 to the point of Fmoc deprotection after coupling of the 12th amino acid. Further, the resin was treated for two hours with the mixture of next reagents: building block **8a** (0.5 equiv), HOBt (0.5 equiv), PyBOP (0.5 equiv), DIPEA (1 equiv). After the reaction was completed, the resin

was washed with dichloromethane and dried under vacuum for 24 h. The peptidomimetics were cleaved and purified as describe in Chapter 6.2.1. The identity of each peptidomimetic was confirmed by MALDI-TOF mass spectrometry; $m/z = 3151$ [α/α -model peptide], 3311 [α/α -3L-, α/α -7I-, α/α -8L-model peptides], 3242 [α/α -4F-model peptide], 3210 [α/α -10Y-model peptide].

6.2.3. Syntheses of GS analogues containing Sw^I

Standard SPPS was used for the peptide synthesis. D-phenylalanine pre-loaded 2-chlorotrityl resin with loading 0.70 mmol/g (143 mg, 1 equiv) was used. Coupling of the amino acids and incorporation of the building block Sw^I was performed as describe in Chapter 6.2.1. After completing the synthesis, the resin was washed with dichloromethane and dried under vacuum for 24 h. The linear precursors were cleaved from the resin with maintaining side chain protecting groups with a mixture of hexafluoroisopropanol and dichloromethane (1:3, 10 ml, 5 min). The volatile products from the filtered solution were blown off by a flow of argon. After dissolving the residual material in an acetonitrile-water (1:1) mixture, and subsequent lyophilization, the crude linear precursors were obtained and used for the cyclization without further purification. The conversion of the linear precursors into the targeted cyclic peptidomimetics was done in dichloromethane (1 L, the precursors did not dissolve completely) with the solution of PyBOP (3 equiv) and HOBt (3 equiv) in DMF (2 ml), followed by adding DIPEA (6 equiv) to the suspension of the corresponding precursor. The reaction mixture was stirred for 8 h, and additional amount (the same as above) of the coupling reagents (PyBOP, HOBt, DIPEA) was added. After 16 h, the solvent was evaporated under reduced pressure and the residual material was lyophilized. The deprotection cocktail (trifluoroacetic acid, triisopropylsilane and water, 92.5:2.5:5 v/v, 10 ml) was added. After 15 min, the volatiles were blown off by flow of argon and the residual oil was lyophilized. The crude cyclic peptides in the open-ring form were purified in two steps using RP-HPLC: on a first step with a preparative column with a linear A:B gradient of 8% B/min followed by a second step on a semi-preparative column with a linear A:B gradient of 4% B/min. The purity of the peptides was checked on the analytical column with a linear A:B gradient of 1% B/min. The identity of each peptidomimetic was confirmed by MALDI mass spectrometry; $m/z = 1225.4$ [GS-Sw^I(LF)], 1241.5 [GS-Sw^I(FP)], 1289.5 [GS-Sw^I(PV)].

6.2.4. Syntheses of GS analogues containing Sw^{II}

Synthesis of GS analogues containing building blocks **39** and **40** was performed as describe in Chapter 3.4.1. The crude cyclic peptides in the open-ring form were purified using RP-HPLC on a preparative column with a linear A:B gradient of 2% B/min. The purity of the peptides was checked on the analytical column with a linear A:B gradient of 1% B/min. The identity of each peptidomimetic was confirmed by MALDI mass spectrometry; $m/z = 1280,5$ [GS-Sw^{LPro}(FP), GS-Sw^{DPro}(FP)].

6.2.5. Syntheses of SVS-1 analogues containing Sw^{II}

Standard SPPS was used for the peptide synthesis. Lysine pre-loaded 2-chlorotrityl resin with loading 0.70 mmol/g (143 mg, 1 equiv) was used. The synthesis was carried out manually. The coupling of the amino acids was performed using the same mixture as describe in Chapter 6.2.1. In cases of lysine and threonine introduction, double coupling was performed since not completed reaction was observed after single coupling. The amino acid sequences were grown to the place of the diarylethene building block incorporation, which then was introduced following the procedure describe in Chapter 6.2.1. To overcome the side-product formation on the step of Fmoc deprotection of the next amino acid after building blocks Sw^{II} was coupled a tetrapeptide fragment with protected side chains and N-terminus. For SVS-1 A- and B-type analogues were used tetrapeptide Fmoc-K(Boc)VK(Boc)V-COOH. For C-type was used Fmoc-VK(Boc)VK(Boc)-COOH tetrapeptide. The corresponding tetrapeptides were synthesized on chlorotrityl resin and then cleaved with hexafluoroisopropanol and lyophilized. Couplings of the tetrapeptides were performed using the following molar ratios of the reagents: Fmoc-tetrapeptide (2 equiv), HOBt (2 equiv), PyBOP (2 equiv), DIPEA (4 equiv). The coupling process was monitored with RP-HPLC and normally was completed after 24 hours. After attaching of the tetrapeptide fragments, the sequences were completed with standard protocol (Chapter 6.2.1). Separation (in case of racemic mixture of building blocks **39** and **40**) and purification of the peptides was done on preparative column in two steps: first, with the eluent containing 0.1% of trifluoroacetic acid as ion pairing reagent, second, with the eluent containing 0.1% of heptafluorobutyric acid. In both cases a linear A:B gradient of 4% B/min was used. The purity of the peptides was checked with the analytical C18 column with a linear A:B gradient of 1% B/min. The identity of each peptide was confirmed by MALDI-TOF mass spectrometry; $m/z = 2031.7$ [SVS-1,

SVS-2], 2119.7 [SVS-Sw^{LPro}(PPT), SVS-Sw^{DPro}(PPT)], 2220.7 [SVS-Sw^{LPro}(PP), SVS-Sw^{DPro}(PP)], 2121.7 [SVS-Sw^{LPro}(VPP), SVS-Sw^{DPro}(VPP)].

6.3. Solid-state ¹⁹F-NMR measurements

All oriented samples were prepared at peptide to lipid ration 1:100 in 1,2-dimyristoyl-sn-glycero-3-phosphocholine (DMPC). 0.206 μ mol of peptide (0.54 mg – 0.68 mg) and 20.6 μ mol of lipid (14 mg) were dissolved in methanol and spread over 14 glass plates (18 x 7.5 mm, Marienfeld Laboratory Glassware). For the samples with the peptides in closed-ring form method was modified: first, the peptides was dissolved in methanol and the solutions was exposed to UV light for 15 min. Then the needed amount of lipid was added and the mixture was spread over the glass plates. The spread solvent was allowed to dry out for 40 min and after that the glass plates were dried in vacuum for 8 hours. The plates were stacked and hydrated in chambers with saturated potassium sulfate (96% relative humidity) for 12 hours and wrapped in Nescofilm[®] and Sarogold[®] films. Between the measurements the samples were stored at -20°C.

In order to check the sample quality and degree of lipid orientation ³¹P NMR measurements were done at 202.5 MHz on an Avance III Bruker NMR spectrometer (Bruker Biospin, Karlsruhe, Germany) with a wide bore 500 MHz magnet. Standard flat-coil double-resonance ¹H/X probe from Bruker was used. As a pulse sequence were used a Hahn echo with a 90° pulse of 5 μ s and a 30 μ s echo time with ¹H SPINAL64 decoupling during acquisition^{142,143}. The acquisition time was 10 ms and the recycle time 1 s. Typically 128 scans were acquired.

Solid-state ¹⁹F-NMR experiments were performed using double-tuned goniometer-equipped ¹⁹F/¹H probes from Doty Scientific (Columbia, USA) at a frequency of 470.6 MHz using an anti-ringing sequence with a 90° pulse of 3.25 μ s, a sweep width of 500 kHz, 4096 data points, and proton decoupling using TPPM^{144,145}. The ¹⁹F chemical shift was referenced using the fluorine signal of a 100 mM solution of NaF, of which the chemical shift was set to -119.5 ppm. Typically 8,000 scans were accumulated.

6.4. Circular dichroism measurements

CD spectra were recorded on Jasco J-815 Spectrophotometer between 400 and 180 nm at 0.1 nm intervals, using 1 mm Suprasil[®] quartz glass cuvettes (Hellma) at 25°C. Three consecutive scans at a scan-rate of 10 nm/min, 8 s response time and 1 nm bandwidth were averaged each for the sample and for the background spectra. After subtraction of the appropriate background spectra, the corrected CD data were processed using Jasco Spectra Analysis software.

The phosphate buffer (PB) was of 20 mM concentration and pH 7.2 (at 30°C). For all measured peptides were prepared their stock solutions in 50% ethanol (1000 µg/ml) with RP-HPLC concentration correction. The needed amounts of material were sampled into 2 ml glass vials and the solvent was dried in vacuum. The stock solutions and all samples of peptides in closed-ring form were kept in dark.

The lipid vesicles were prepared accordingly to following protocol: the lipids (DMPC and DMPG) stock solution was prepared at concentration 10 mg/ml in methanol/chloroform 1:1 mixture, and aliquoted in 2 ml glass vials to supply with 0.4 mg of either pure DMPC or mixture of DMPC/DMPG 3:1. The solvents were removed by a flow of argon and the vials were dried under vacuum for 8 hours. 300 µl of the PB was added to vials and the mixture was vortexed for 10 min. Then 10 times freeze-thaw cycle was repeated. The resulting mixture was sonicated for 30 min at 40°C. To the glass vials with sample peptides were added 100 µl of the PB, sonicated for 5 min, followed by adding the suspension of vesicles (300 µl) prepared as describe above to yield 400 µl volume in each case. The resulting samples have lipid concentration 1 mg/ml and peptide to lipid ratio 1:50.

6.5. Antimicrobial activity assays

The antimicrobial activities of peptides were measured using a stepwise microdilution assay according to standard protocols with some modifications^{146,147}. Wild type peptides and their analogues in open-ring and closed-ring forms were dissolved in 50% ethanol to give stock solutions with concentrations 512 µg/ml. Sterile flat-bottom polystyrene, non-tissue culture-treated, 96-well microtiter plates (Nunc[™]) were used for the assay. First, 50 µl of the double concentrated Mueller-Hinton (MH) medium (Mast Diagnostika, Reinfeld, Germany) were filled to the initial row. Next, 50 µl of the non-concentrated MH medium were applied to the remaining test wells, for the positive (without peptides), and the negative (sterility)

controls. Addition of the peptide stock solutions (50 μ l) to the wells of the initial row provided the starting peptide concentration for the gradient. For construction of the gradient all subsequent rows were filled by transfer of 50 μ l aliquots from the preceding rows. From the last row of wells 50 μ l aliquots were discarded. Bacterial suspensions were prepared from the culture in the exponential growth phase, which was diluted first to the OD550 = 0.2 and then 1:100 in order to inoculate each well with 5×10^5 CFU/ml, excluding the negative control. To examine bacterial growth, the plates were incubated for 22 hours at 37°C without agitation. Then, 20 μ l of an aqueous 0.2 mg/ml solution of the redox indicator resazurin (7-hydroxy-3H-phenoxazin-3-one-10-oxide) were added to each well. The plates were incubated for another 2 hours at 37°C, and the redox status of resazurin was determined spectrophotometrically using a microplate reader FLASHScan 550 (Jena Analytic, Germany). The difference in absorbance of resorufin at 570 nm and resazurin at 600 nm was used to assess bacterial growth and thereby to determine the lowest concentrations that inhibit bacterial growth (Minimum Inhibitory Concentration, MIC). Both Gram-positive and Gram-negative bacteria strains were used (*E.coli* DSM 1103, *S. typhimurium*, *B. Subtilis*, *aureus* DSM 1104, *Staphylococcus epidermidis* DSM 1798 and *Staphylococcus xylosum* DSM 20267).

6.6. Visualization of antimicrobial activity

The plate-pouring technique was used to find out the optimal light exposition length and concentration of the inactive peptidomimetic GS-Sw^I(FP) that would show a distinct photoswitching effect. The desired amount of peptidomimetic was added to a 17 ml aliquot of melted LB-Miller agar that had been cooled to 60°C. To obtain a uniform bacterial lawn, the medium was at the same time inoculated with 100 μ l exponentially growing bacterial culture diluted to a suspension with an OD550 of 0.2. This mixture was poured into a Petri dish. Once the medium was solidified, each of these prepared plates was exposed to visible light through holes in a cardboard mask for a discrete period of time. The geometrical shapes were cut out from black paper covering the entire Petri dish, such that the photoswitchable compound was converted into the open-ring form only in the areas exposed to light. The plates were incubated at 37°C overnight and then photographed.

6.7. Hemolytic activity assays

To test the hemolytic activities of peptides and their analogues, human erythrocytes (RBC) were used. RBC concentrates in 10 % citrate-phosphate-dextrose medium were obtained from Karlsruhe municipal hospital. The cells were washed twice in Tris-HCl buffer (HB, 310 mOs/ml, pH 7.6) by centrifugation at $300\times g$, $4^{\circ}C$. The final pellet was diluted 200-fold in HB and incubated for 5 min at $37^{\circ}C$ before it was added to the solutions of the peptides. These solutions were prepared as a two-fold dilution series of 200 μl aliquots in the same buffer in 1.5 ml Eppendorf™ tubes. The hemolysis reaction was initiated by the addition of 200 μl RBC suspension. The samples were incubated under periodic agitation for 30 min at $37^{\circ}C$, after which their content was centrifuged for 10 min at $13000\times g$. The absorption of the supernatant at 540 nm gives the extent of hemolysis, with 0% taken from the peptide-free control, and 100% after treatment with 0.1% Triton X-100. To make sure that this step did not interfere with the analysis, the samples with GS analogous in the closed-ring forms were back-converted to their open-ring colorless forms by 30 min exposure to visible light before absorption measurements.

6.8. Anticancer assays

Experiments were carried out at the Institute of Biology of Taras Shevchenko National University of Kyiv. The following cell lines were used in the study: the cervix cancer line HeLa, the breast cancer line MCF-7, hepatocellular carcinoma G2 cancer line.

The cytotoxic effect of peptides was evaluated in MTT-colorimetric test as percent of live cells related to control and characterized by IC_{50} index^{148,149}. For the MTT assay performing 96 well plates were used. As a culture media, DMEM («Sigma», USA) with 10 % FBS («Sigma»), 2 mM L-glutamine, and 40 $\mu g/ml$ gentamicin were used. Cells were plated with starting concentration about 5×10^4 cells/ml in the sample volume of 100 μl in each of 96 well. After a 24 hours period of plated cells adaptation in normal conditions (5 % CO_2 , 100 humidity, $37^{\circ}C$), the peptides were added (in 100 μl of media). For each tested peptide at least two rows of repetition and 5 or 11 two-fold diluted concentrations were used. After the 24 hours period of incubation, to the medium in each well 10 μl of MTT solution was added and the plates were left for 4 hours preincubation. The medium from each well was removed and 100 μl of DMSO were added instead. 30 min later amount of reduced MTT were calorimetrically assayed.

The number of living cells was determined using MTT-colorimetric test, cell counts were performed using a tripan blue dye after 24 h incubation with peptides.

The cell distribution in different phases of the cell cycle was assessed by a flow cytometry¹⁵⁰. Cells were plated in 6-well plates at the density 5×10^4 cells/ml in total volume 5 ml of the complete culture medium. The cells were then incubated with a peptide for 48 h under normal conditions. The proportions of cells in different phases of the cell cycle were measured by flow cytometry with argon laser ($\lambda_{\text{ex}} = 488$ nm, $\lambda_{\text{em}} = 585/40$ nm) («Becton Dickinson», USA) following standard staining. The samples were analyzed with the help of the Mod Fit LT 3.0 («BDIS», USA) software¹⁵¹.

7. References

- ¹ I. R. Edwards, J. K. Aronson. Adverse drug reactions: definitions, diagnosis, and management. *Lancet*, **2000**, 356, 1255.
- ² E. Raschi, V. Vasina, M.G. Ursino, G. Boriani, A. Martoni, F. De Ponti. Anticancer drugs and cardiotoxicity: Insights and perspectives in the era of targeted therapy. *Pharmacol. Ther.*, **2010**, 125, 196.
- ³ D. E. Mager. Quantitative structure–pharmacokinetic/pharmacodynamic relationships. *Adv. Drug Delivery Rev.*, **2006**, 58, 1326.
- ⁴ V. Malhotra, M. C. Perry. Classical chemotherapy: mechanisms, toxicities and the therapeutic window. *Cancer Biol. Ther.*, **2003**, 2, S2.
- ⁵ S. Sonis et al. Perspectives on cancer therapy-induced mucosal injury. *Cancer*, **2004**, 100, 1995.
- ⁶ J. Carlet, et al. Society's failure to protect a precious resource: antibiotics. *Lancet*, **2011**, 378, 369.
- ⁷ S. Sortino. Photoactivated nanomaterials for biomedical release applications. *J. Mater. Chem.*, **2012**, 22, 301.
- ⁸ W. A. Velema, W. Szymanski, B. L. Feringa. Photopharmacology: Beyond proof of principle. *J. Am. Chem. Soc.*, **2014**, 136, 2178.
- ⁹ C. Alvarez-Lorenzo, L. Bromberg, A. Concheiro. Light-sensitive intelligent drug delivery systems. *Photochem. Photobiol.*, **2009**, 85, 848.
- ¹⁰ M. Ferrari, Cancer nanotechnology: opportunities and challenges. *Nat. Rev. Cancer*, **2005**, 5, 161.
- ¹¹ C. Brieke, F. Rohrbach, A. Gottschalk, G. Mayer, A. Heckel. Light-controlled tools. *Angew. Chem. Int. Ed.*, **2012**, 51, 8446.
- ¹² W. Szymanski, J. M. Beierle, H. A. V. Kistemaker, W. A. Velema, B. L. Feringa. Reversible photocontrol of biological systems by the incorporation of molecular photoswitches. *Chem. Rev.*, **2013**, 113, 6114.
- ¹³ M. Triesscheijn, P. Baas, J. H. M. Schellens, F. A. Stewart, Photodynamic therapy in oncology. *Oncologist*, **2006**, 11, 1034.
- ¹⁴ P. C. Ford. Polychromophoric metal complexes for generating the bioregulatory agent nitric oxide by single- and two-photon excitation. *Acc. Chem. Res.*, **2008**, 41, 190.
- ¹⁵ L. O. Svaasand, C. J. Gomer and E. Morinelli, On the physical rationale of laser induced hyperthermia. *Lasers Med. Sci.*, **1990**, 5, 121.
- ¹⁶ G. C. R. Ellis-Davies, Caged compounds: photorelease technology for control of cellular chemistry and physiology. *Nat. Methods*, **2007**, 4, 619.
- ¹⁷ A. P. Pelliccioli, J. Wirz. Photoremovable protecting groups: reaction mechanisms and applications. *Photochem. Photobiol. Sci.*, **2002**, 1, 441.
- ¹⁸ M. Mahmoudi, K. Azadmanesh, M. A. Shokrgozar, W. S. Journey and S. Laurent. Effect of nanoparticles on the cell life cycle. *Chem. Rev.*, **2011**, 111, 3407.
- ¹⁹ F. Puntoriero, P. Ceroni, V. Balzani, G. Bergamini and F. Vögtle, Photoswitchable dendritic hosts: A dendrimer with peripheral azobenzene groups. *J. Am. Chem. Soc.*, **2007**, 129, 10714.
- ²⁰ H. Sakai, Y. Orihara, H. Kodashima, A. Matsumura, T. Ohkubo, K. Tsuchiya and M. Abe. Photoinduced reversible change of fluid viscosity. *J. Am. Chem. Soc.*, **2005**, 127, 13454.
- ²¹ Y. Zhu, M. Fujiwara, Installing dynamic molecular photomechanics in mesopores: a multifunctional controlled-release nanosystem. *Angew. Chem., Int. Ed.*, **2007**, 46, 2241.
- ²² J. P. Overington, B. Al-Lazikani, A. L. Hopkins. How many drug targets are there? *Nat. Rev. Drug Discov.*, **2006**, 5, 993.
- ²³ H. K. Cammenga, V. N. Emel'yanenko, S. P. Verevkin. Re-investigation and data assessment of the isomerization and 2,2'-cyclization of stilbenes and azobenzenes. *Ind. Eng. Chem. Res.*, **2009**, 48, 10120.
- ²⁴ A. Kaneko, A. Tomoda, M. Ishizuka, H. Suzuki, R. Matsushima. Photochemical fatigue resistances and thermal stabilities of heterocyclic fulgides in PMMA film. *Bull. Chem. Soc. Jpn.* **1988**, 61, 3569.
- ²⁵ M. Hanazawa, R. Sumiya, Y. Horikawa, M. Irie. Thermally irreversible photochromic systems. *J. Chem. Soc., Chem. Commun.*, **1992**, 206.
- ²⁶ L. N. Lucas, J. Van Esch, R. M. Kellogg, B. L. Feringa. A new synthetic route to symmetrical photochromic diarylperfluorocyclopentenes. *Tetrahedron Letters*, **1999**, 40, 1775.
- ²⁷ L. N. Lucas, J. J. D. Jong, J. H. Esch, R. M. Kellogg, B. L. Feringa. Syntheses of dithienylcyclopentene optical molecular switches. *Eur. J. Org. Chem.*, **2003**, 155.
- ²⁸ J. E. McMurry. Titanium-induced dicarbonyl-coupling reactions. *Acc. Chem. Res.*, **1983**, 16, 405.
- ²⁹ S. Nakamura, M. Irie. Thermally irreversible photochromic systems. A theoretical study. *J. Org. Chem.* **1988**, 53, 6136.
- ³⁰ F. Siebert in photochromic molecules and systems (Eds.: H. Duerr, H. Bouas-Laurent), Elsevir, Amsterdam, **1990**, p. 756.
- ³¹ C. Dugave, L. Demange. Cis-trans isomerization of organic molecules and biomolecules: implications and applications. *Chem. Rev.*, **2003**, 103, 2475.

- ³² D. Chen, Z. Wang, H. Zhang. Theoretical study on thermal stability and absorption wavelengths of closed-ring isomers of diarylethene derivatives. *Journal of Molecular Structure: Theochem*, **2008**, 859, 11.
- ³³ I. Willner, S. Rubin. Control of the structure and functions of biomaterials by light. *Angew. Chem. Int. Ed. Engl.*, **1996**, 35, 367.
- ³⁴ M. Irie, M. Mohri. Thermally irreversible photochromic systems. Reversible photocyclization of diarylethene derivatives. *J. Org. Chem.*, **1988**, 53, 803.
- ³⁵ K. Uchida, Y. Nakayama, M. Irie. Thermally Irreversible Photochromic Systems. Reversible photocyclization of 1,2-bis(benzo[b]thiophen-3-yl)ethene derivatives. *Bulletin of the Chemical Society of Japan*, **1990**, 63, 1311.
- ³⁶ M. Irie, T. Lifka, K. Uchida, S. Kobatake, Y. Shindo. Fatigue resistant properties of photochromic dithienylethenes: by-product formation. *Chem. Commun.*, **1999**, 747.
- ³⁷ J. Massaad, J.-C. Micheau, C. Coudret, R. Sanchez, G. Guirado, S. Delbaere. Gated photochromism and acidity photomodulation of a diacid dithienylethene dye. *Chem. Eur. J.*, **2012**, 18, 6568.
- ³⁸ G. Feher, J. P. Allen, M. Okamura, D. C. Rees. Structure and function of bacterial photosynthetic reaction centres. *Nature*, **1989**, 339, 111.
- ³⁹ L. Stryer. Cyclic GMP cascade of vision. *Annu. Rev. Neurosci.*, **1986**, 9, 87.
- ⁴⁰ E. Pontecorvo, C. Ferrante, C. G. Elles, T. Scopigno. Structural rearrangement accompanying the ultrafast electrocyclization reaction of a photochromic molecular switch. *J. Phys. Chem. B*, **2014**, 118, 6915.
- ⁴¹ H. Nishi, T. Namari, S. Kobatake. Photochromic polymers bearing various diarylethene chromophores as the pendant: synthesis, optical properties, and multicolor photochromism. *J. Mater. Chem.*, **2011**, 17249.
- ⁴² M. Irie, K. Sakemura, M. Okinaka, K. Uchida. Photochromism of dithienylethenes with electron-donating substituents. *J. Org. Chem.*, **1995**, 60, 8305.
- ⁴³ S. L. Gilat, S. H. Kawai, J. M. Lehn. Light-triggered molecular devices: photochemical switching of optical and electrochemical properties in molecular wire type diarylethene species. *Chem. Eur. J.* **1995**, 1, 275.
- ⁴⁴ Y. Nakayama, K. Hayashi, M. Irie. Thermally irreversible photochromic systems. Reversible photocyclization of non-symmetric diarylethene derivatives. *Bulletin of the Chemical Society of Japan*. **1991**, 64, 789.
- ⁴⁵ S. L. Gilat, S. H. Kawai, J.M. Lehn. Light-triggered electrical and optical switching devices. *J. Chem. Soc., Chem. Commun.*, **1993**, 1439.
- ⁴⁶ K. Uchida, M. Irie. A photochromic dithienylethene that turns yellow by UV irradiation. *Chemistry Letters*. **1995**, 24, 969.
- ⁴⁷ K. Uchida, S. Nakamura, M. Irie. Thermally irreversible photochromic systems. substituent effect on the absorption wavelength of 11,12-dicyano-5a,5b-dihydro-5a,5b-dimethylbenzo[1,2-b:6,5-b']bis[1]benzothiophene. *Bull. Chem. Soc. Jpn.*, **1992**, 65, 430.
- ⁴⁸ M. Irie, T. Eriguchi, T. Takada, K. Uchida. Photochromism of diarylethenes having thiophene oligomers as the aryl groups. *Tetrahedron*, **1997**, 53, 214.
- ⁴⁹ A. T. Bens, D. Frewert, K. Kodatis, C. Kryschi, H. D. Martin, H. P. Trommsdorf. Coupling of chromophores: carotenoids and photoactive diarylethenes – photoreactivity versus radiationless deactivation. *Eur. J. Org. Chem.*, **1998**, 2333.
- ⁵⁰ K. Uchida, E. Tsuchida, Y. Aoi, S. Nakamura, M. Irie. Substitution effect on the coloration quantum yield of a photochromic bisbenzothienylethene. *Chem. Lett.*, **1999**, 63.
- ⁵¹ M. Takeshita, C. N. Choi, M. Irie. Enhancement of the photocyclization quantum yield of 2,2'-dimethyl-3,3'-(perfluorocyclopentene-1,2-diyl)bis(benzo[b]-thiophene-6-sulfonate) by inclusion in a cyclodextrin cavity. *Chem. Commun.*, **1997**, 2265.
- ⁵² M. Takeshita, N. Kato, S. Kawachi, T. Imase, J. Watanabe, M. Irie. *J. Org. Chem.*, Photochromism of dithienylethenes included in cyclodextrins. **1998**, 63, 9306.
- ⁵³ M. Takeshita, M. Irie. Photoreversible circular dichroism change of 1,2-bis(1-benzothiophen-3-yl)perfluorocyclopentene modified cyclodextrins. *Tetrahedron Lett.*, **1999**, 40, 1345.
- ⁵⁴ M. Irie. Diarylethenes for memories and switches. *Chem. Rev.*, **2000**, 100, 1685.
- ⁵⁵ Z. H. Chen, S. M. Zhao, Z. Y. Li, Z. Zhang, F. S. Zhang. Acid/alkali gated photochromism of two diarylperfluorocyclopentenes. *Sci. China Ser. B*, **2007**, 50, 581.
- ⁵⁶ M. Irie, O. Miyatake, K. Uchida. Blocked photochromism of diarylethenes. *J. Am. Chem. Soc.*, **1992**, 114, 8715.
- ⁵⁷ C. Yun, J. You, J. Kim, J. Huh, E. Kim. Photochromic fluorescence switching from diarylethenes and its applications. *Journal of Photochemistry and Photobiology C: Photochemistry Reviews*, **2009**, 111.
- ⁵⁸ M. Takeshita, M. Irie. Reversible fluorescence intensity change of a diarylethene. *Chem. Lett.*, **1998**, 1123.
- ⁵⁹ A. Fernandez-Acebes, J.M. Lehn. Optical switching and fluorescence modulation properties of photochromic metal complexes derived from dithienylethene ligands. *Chem. Eur. J.*, **1999**, 3285.
- ⁶⁰ J. Ern, A.T. Benz, H.D. Martin, S. Mukamel, S. Tretiak, K. Tsyganenko, K. Kuldova, H.P. Trommsdorff, C. Kryschi. Reaction dynamics of a photochromic fluorescing dithienylethene. *J. Phys. Chem. A.*, **2001**, 1741.
- ⁶¹ K. Yagi, C. F. Soong, M. Irie. Synthesis of fluorescent diarylethenes having a 2,4,5-triphenylimidazole chromophore. *J. Org. Chem.*, **2001**, 5419.

- ⁶² H. Cho, E. Kim. Highly fluorescent and photochromic diarylethene oligomer bridged by p-phenylenevinylene. *Macromolecules*, **2002**, 8684.
- ⁶³ S. F. Yan, V. N. Belov, M. L. Bossi, S. W. Hell. Switchable fluorescent and solvatochromic molecular probes based on 4-amino-N-methylphthalimide and a photochromic diarylethene. *Eur. J. Org. Chem.*, **2008** 2531.
- ⁶⁴ Y. Jeong, S. Yang, E. Kim, K. Ahn. Development of highly fluorescent photochromic material with high fatigue resistance. *Tetrahedron*, **2006**, 5855.
- ⁶⁵ Y. Jeong, S. Yang, K. Ahn, E. Kim. Highly fluorescent photochromic diarylethene in the closed-ring form. *Chem. Commun.*, **2005**, 2503.
- ⁶⁶ H. Hu, M. Zhu, X. Meng, Z. Zhang, K. Wei, Q. Guo. Optical switching and fluorescence modulation properties of photochromic dithienylethene derivatives. *J. Photochem Photobiol. A: Chem.*, **2007**, 307.
- ⁶⁷ Y. Chen, D.X. Zeng. A Selective, fluorescent sensor for Zn²⁺. *Chem Phys Chem*, **2004**, 564.
- ⁶⁸ N. Soh, K. Yoshida, H. Nakajima, K. Nakano, T. Imato, T. Fukaminato, M. Irie. A fluorescent photochromic compound for labeling biomolecules. *Chem. Commun.*, **2007**, 5206.
- ⁶⁹ Y. Zou, T. Yi, S. Xiao, F. Li, C. Li, X. Gao, J. Wu, M. Yu, C. Huang. Amphiphilic diarylethene as a photoswitchable probe for imaging living cells. *J. Am. Chem. Soc.*, **2008**, 15750.
- ⁷⁰ Y. Kim et al. High-contrast reversible fluorescence photoswitching of dye-crosslinked dendritic nanoclusters in living vertebrates. *Angew. Chem. Int. Ed.*, **2012**, 1.
- ⁷¹ R.E.W. Hancock, R. Lehrer. Cationic peptides: a new source of antibiotics. *Trends Biotechnol.*, **1998**, 16, 82.
- ⁷² M. Zasloff. Antimicrobial peptides of multicellular organisms. *Nature*, **2002**, 415, 389.
- ⁷³ H. G. Boman, Peptide antibiotics and their role in innate immunity. *Annu. Rev. Immunol.*, **1995**, 13, 61.
- ⁷⁴ A. Tossi, L. Sandri, A. Giangaspero. Amphipathic, α -helical antimicrobial peptides. *Biopolymers*, **2000**, 55, 4.
- ⁷⁵ B. Christensen, J. Fink, R. B. Merrifield, D. Mauzerall. Channel-forming properties of cecropins and related model compounds incorporated into planar lipid membranes. *Proc Natl Acad Sci USA.*, **1988**, 85, 5072.
- ⁷⁶ Y. Shai. Mode of action of membrane active antimicrobial peptides. *Peptide Science.*, **2002**, 66, 236.
- ⁷⁷ K. A. Brogden. Antimicrobial peptides: pore formers or metabolic inhibitors in bacteria? *Nature Reviews Microbiology*. **2005**, 3, 238.
- ⁷⁸ M. Hong, Y. Su. Structure and dynamics of cationic membrane peptides and proteins: Insights from solid-state NMR. *Protein Science*, **2011**, 20, 641.
- ⁷⁹ F. Harris, S. R. Dennison, J. Singh, D. A. Phoenix. On the selectivity and efficacy of defense peptides with respect to cancer cells. *Medicinal Research Reviews*, **2013**, 33, 190.
- ⁸⁰ R. G. Dubos, C. Cattaneo. Studies of a bactericidal agent extracted from a soil bacillus. *J. Exp. Med.*, **1939**, 70, 249.
- ⁸¹ M. Waki, N. Izumiya, H. Kleinkaug, H. van Doren. Biochemistry of peptide antibiotics: recent advances in the biotechnology of L-lactams and microbial bioactive peptides. *Walter de Gruyter, Berlin*, **1990**, 205.
- ⁸² L. H. Kondejewski, S. W. Farmer, D. Wishart, C. M. Kay, R. E. W. Hancock, R. S. Hodges. Gramicidin S is active against both gram-positive and gram-negative bacteria. *Int. J. Pept. Protein Res.*, **1996**, 47, 460.
- ⁸³ J. Blazyk, R. Wiegand, J. Klein, J. Hammer, R. M. Epand, R. F. Epand, W. L. Maloy, U. P. Kari. A novel linear amphipathic β -sheet cationic antimicrobial peptide with enhanced selectivity for bacterial lipids. *Journal of Biological Chemistry*, **2001**, 276, 27899.
- ⁸⁴ E. Badosa, R. Ferre, M. Planas, L. Feliu, E. Besalú, J. Cabrefiga, E. Bardají, E. Montesinos. A library of linear undecapeptides with bactericidal activity against phytopathogenic bacteria. *Peptides*, **2007**, 28, 2276.
- ⁸⁵ K. Eggenberger, C. Mink, P. Wadhvani, A. S. Ulrich, P. Nick. Using the peptide Bp100 as a cell-penetrating tool for the chemical engineering of actin filaments within living plant cells. *ChemBioChem*, **2011**, 12, 132.
- ⁸⁶ C. Sinthuvanich, A. S. Veiga, K. Gupta, D. Gaspar, R. Blumenthal, J. P. Schneider. Anticancer β -hairpin peptides: membrane-induced folding triggers activity. *J. Am. Chem. Soc.*, **2012**, 6210.
- ⁸⁷ K. Fujimoto, T. Maruyama, Y. Okada, T. Itou, M. Inouye. Development of a new class of photochromic peptides by using diarylethene-based non-natural amino acids. *Tetrahedron*, **2013**, 6170.
- ⁸⁸ K. Fujimoto, M. Kajino, I. Sakaguchi, M. Inouye. Photoswitchable, DNA-Binding helical peptides assembled with two independently designed sequences for photoregulation and DNA recognition. *Chem. Eur. J.*, **2012**, 9834.
- ⁸⁹ M. Goodman, A. Kossoy. Conformational aspects of polypeptide structure. Azoaromatic side-chain effects. *J. Am. Chem. Soc.*, **1966**, 5010.
- ⁹⁰ O. Pieroni, J. L. Houben, A. Fissi, P. Costantino. Reversible conformational changes induced by light in poly(L-glutamic acid) with photochromic side chains. *J. Am. Chem. Soc.*, **1980**, 5913.
- ⁹¹ O. Pieroni, A. Fissi. Synthetic photochromic polypeptides: possible models for photoregulation in biology. *Journal of Photochemistry and Photobiology, B: Biology*, **1992**, 125.
- ⁹² O. Pieroni, A. Fissi, A. Viegi, D. Fabbri, F. Ciardelli. Modulation of chain conformation of spiropyran-containing poly(L-lysine) by combined action of visible light and solvent. *J. Am. Chem. Soc.*, **1992**, 2734.
- ⁹³ A. Ueno, K. Takahashi, J. Anzai, T. Osa. Photocontrol of polypeptide helix sense by cis-trans isomerism of side-chain azobenzene moieties. *J. Am. Chem. Soc.*, **1981**, 6410.

- ⁹⁴ M. Schutt, S. S. Krupka, A. G. Milbradt, S. Deindl, E. K. Sinner, D. Oesterhelt, C. Renner, L. Moroder. Photocontrol of cell adhesion processes: model studies with cyclic azobenzene-RGD peptides. *Chem. Biol.*, **2003**, 487.
- ⁹⁵ E. Ruoslahti. RGD and other recognition sequences for integrins. *Annu. Rev. Cell Dev. Biol.*, **1996**, 697.
- ⁹⁶ A. G. Milbradt, M. Loweneck, S. S. Krupka, M. Reif, E. K. Sinner, L. Moroder, C. Renner. Photomodulation of conformational states. IV. Integrin-binding RGD-peptides with (4-aminomethyl)phenylazobenzoic acid as backbone constituent. *Biopolymers*, **2005**, 304.
- ⁹⁷ R. Behrendt, C. Renner, M. Schenk, F. Q. Wang, J. Wachtveitl, D. Oesterhelt, L. Moroder. Photomodulation of the conformation of cyclic peptides with azobenzene moieties in the peptide backbone. *Angew. Chem., Int. Ed.*, **1999**, 2771.
- ⁹⁸ Wadhvani et al, unpublished results.
- ⁹⁹ M. Loweneck, A. Milbradt, C. Root, H. Satzger, W. Zinth, L. Moroder, C. Renner. A conformational two-state peptide model system containing an ultrafast but soft light switch. *Biophysical Journal*, **2006**, 2099.
- ¹⁰⁰ L. G. Ulysse, J. Chmielewski. A light-activated β -turn scaffold within a somatostatin analog: NMR structure and biological activity. *Chem. Biol. Drug Des.*, **2006**, 127.
- ¹⁰¹ C. Hoppmann, S. Seedorff, A. Richter, H. Fabian, P. Schmieder, K. Rück-Braun, M. Beyermann. Light-directed protein binding of a biologically relevant β -sheet. *Angew. Chem., Int. Ed.*, **2009**, 6636.
- ¹⁰² J. Robinson. β -hairpin peptidomimetics: Design, structures and biological activities. *A. Acc. Chem. Res.*, **2008**, 1278.
- ¹⁰³ A. Aemissegger, V. Krautler, W. F. van Gunsteren, D. Hilvert. A photoinducible β -hairpin. *J. Am. Chem. Soc.*, **2005**, 2929.
- ¹⁰⁴ J. F. Espinosa, S. H. Gellman. A designed β -hairpin containing a natural hydrophobic cluster. *Angew. Chem., Int. Ed.*, **2000**, 2330.
- ¹⁰⁵ M. S. Vollmer, T. D. Clark, C. Steinem, M. R. Ghadiri. Photoswitchable hydrogen-bonding in self-organized cylindrical peptide systems. *Angew. Chem., Int. Ed.*, **1999**, 1598.
- ¹⁰⁶ A. G. Cochran, N. J. Skelton, M. A. Starovasnik. Tryptophan zippers: Stable, monomeric β -hairpins. *Proc. Natl. Acad. Sci. U.S.A.*, **2001**, 5578.
- ¹⁰⁷ S. L. Dong, M. Loweneck, T. E. Schrader, W. J. Schreier, W. Zinth, L. Moroder, C. Renner. A photocontrolled β -hairpin peptide. *Chem. Eur. J.*, **2006**, 1114.
- ¹⁰⁸ M. Varedian, M. Erdelyi, A. Persson, A. Gogoll. Interplaying factors for the formation of photoswitchable β -hairpins: the advantage of a flexible switch. *J. Pept. Sci.*, **2009**, 107.
- ¹⁰⁹ M. Erdelyi, A. Karlen, A. Gogoll. A new tool in peptide engineering: A photoswitchable stilbene-type β -hairpin mimetic. *Chem. Eur. J.*, **2006**, 403.
- ¹¹⁰ J. R. Kumita, O. S. Smart, G. A. Woolley. Photo-control of helix content in a short peptide. *PNAS*, **2000**, 3803.
- ¹¹¹ J. R. Kumita, D. G. Flint, O. S. Smart, G. A. Woolley. Photo-control of peptide helix content by an azobenzene cross-linker: steric interactions with underlying residues are not critical. *Protein Eng.*, **2002**, 561.
- ¹¹² V. Borisenko, G. A. Woolley. Reversibility of conformational switching in light-sensitive peptides. *J. Photochem. Photobiol. A.*, **2005**, 21.
- ¹¹³ C. Renner, L. Moroder. Azobenzene as conformational switch in model peptides. *ChemBioChem*, **2006**, 7, 869.
- ¹¹⁴ B. He, O. S. Wenger. Photoswitchable organic mixed valence in dithienylcyclopentene systems with tertiary amine redox centers. *J. Am. Chem. Soc.*, **2011**, 133, 17027.
- ¹¹⁵ Z. H. Zhou et al., Synthesis of optically active N-protected α -aminoketones and α -amino alcohols. *Heteroatom Chemistry*, **2003**, 7, 603.
- ¹¹⁶ P. Wadhvani, E. Strandberg, N. Heidenreich, J. Buerck, S. Fanghaene, A. S. Ulrich. Self-assembly of flexible β -strands into immobile amyloid-like β -sheets in membranes as revealed by solid-state ^{19}F NMR. *J. Am. Chem. Soc.*, **2012**, 134, 6512.
- ¹¹⁷ P. Wadhvani, E. Strandberg, J. Berg, C. Mink, J. Buerck, R. A.M. Ciriello, A. S. Ulrich. Dynamical structure of the short multifunctional peptide BP100 in membranes. *Biochimica et Biophysica Acta*, **2014**, 940.
- ¹¹⁸ P. K. Mykhailiuk, S. Afonin, A. N. Chernega, E. B. Rusanov, M. Platonov, G. Dubinina, M. Berditsch, A. S. Ulrich, I.V. Komarov. Conformationally rigid trifluoromethyl-substituted α -amino acid designed for peptide structure analysis by solid state ^{19}F -NMR spectroscopy. *Angew. Chem. Int. Ed.*, **2006**, 45, 5659.
- ¹¹⁹ V. S. Kubyshkin, I. V. Komarov, S. Afonin, P. K. Mykhailiuk, S. L. Grage, A. S. Ulring "Trifluoromethyl-substituted α -amino acids as solid-state ^{19}F NMR labels for structural studies of membrane-bound peptides" in *Fluorine in pharmaceutical and medicinal chemistry* (Ed.: V. Gouverneur, K. Müller), Imperial College Press, **2012**, 91.
- ¹²⁰ A. S. Ulrich. Solid state ^{19}F NMR methods for studying biomembranes. *Prog Nuc Mag Res Spec.*, **2005**, 46, 1.

- ¹²¹ A. S. Ulrich, P. Wadhvani, U.H.N. Dürr, S. Afonin, R.W. Glaser, E. Strandberg, P. Tremouilhac, C. Sachse, M. Berditchevskaia, S.L. Grage “Solid-state 19F-Nuclear magnetic resonance analysis of membrane-active peptides” in *NMR spectroscopy of biological solids* (Ed.: A. Ramamoorthy), CRC Press, **2006**, 215.
- ¹²² P. Wadhvani, J. Reichert, E. Strandberg, J. Bürck, J. Misiewicz, S. Afonin, N. Heidenreich, S. Fanghänel, P. K. Mykhailiuk, I. V. Komarov, A. S. Ulrich. Stereochemical effects on the aggregation and biological properties of the fibril-forming peptide [KIGAKI]₃ in membranes. *Phys. Chem. Chem. Phys.*, **2013**, 15, 8962.
- ¹²³ Wadhvani et al., in preparation.
- ¹²⁴ Misiewicz et al., in preparation.
- ¹²⁵ D. L. Lee, R. S. Hodges. Structure-activity relationships of de novo designed cyclic antimicrobial peptides based on Gramicidin S. *Peptide Science*, **2003**, 71, 28.
- ¹²⁶ T. Kato, N. Izumiya, Conformations of di-N-Methylleucine gramicidin S and N-Methylleucine gramicidin S compatible with the sidedness hypothesis. *Biochim. Biophys. Acta*, **1977**, 493, 235.
- ¹²⁷ V. V. Kapoerchan, E. Spalburg, A. J. Neeling, R. H. Mars-Groenendijk, D. Noort, J. M. Otero, P. Ferraces-Casais, A. L. Llamas-Saiz, M. J. Raaij, J. Doorn, G. A. Marel, H. S. Overkleef, M. Overhand. Gramicidin S derivatives containing cis- and trans-morpholine amino acids (MAAs) as turn mimetics. *Chem. Eur. J.*, **2010**, 16, 14, 4259.
- ¹²⁸ B. Legrand, L. Mathieu, A. Lebrun, S. Andriamanarivo, V. Lisowski, N. Masurier, S. Zirah, Y. K. Kang, J. Martinez, L. T. Maillard. Thiazole-based γ -building blocks as reverse-turn mimetic to design a Gramicidin S analogue: conformational and biological evaluation. *Chem. Eur. J.*, **2014**, 20, 6713.
- ¹²⁹ S. Reisser Computational studies of membrane-active antimicrobial peptides and comparison with NMR data. **2014** Dissertation. Karlsruhe Institute of Technology.
- ¹³⁰ P. Wadhvani, S. Afonin, M. Ieronimo, J. Buerck, A. S. Ulrich. Optimized protocol for synthesis of cyclic gramicidin S: starting amino acid is a key to high yield. *J. Org. Chem.*, **2006**, 55.
- ¹³¹ J. J. D. Jong, P. Rijn, T. D. Tiemersma-Wegeman, L. N. Lucas, W. R. Browne, R. M. Kellogg, K. Uchida, J. H. Esch, B. L. Feringa. Dynamic chirality, chirality transfer and aggregation behaviour of dithienylethene switches. *Tetrahedron*, **2008**, 64, 8324.
- ¹³² O. V. Krokhin. Sequence-specific retention calculator. Algorithm for peptide retention prediction in ion-pair RP-HPLC: Application to 300- and 100-Å pore size C18 sorbents. *Anal. Chem.*, **2006**, 78, 7785.
- ¹³³ M. Jelokhani-Niaraki, L. H. Kondejewski, S. W. Farmer, C. M. Kay, R. S. Hodges. Diastereoisomeric analogues of gramicidin S: Structure, biological activity and interaction with lipid bilayers. *Biochemical Journal*, **2000**, 349, 747.
- ¹³⁴ L. H. Kondejewski, M. Jelokhani-Niaraki, S. W. Farmer, B. Lix, C. M. Kay, B. D. Sykes, R. E. W. Hancock, R. S. Hodges. Dissociation of antimicrobial and hemolytic activities in cyclic peptide diastereomers by systematic alterations in amphipathicity. *Journal of Biological Chemistry*. **1999**, 274, 13181.
- ¹³⁵ J. J. D. Jong, P. Rijn, T. D. Tiemersma-Wegeman, L. N. Lucas, W. R. Browne, R. M. Kellogg, K. Uchida, J. H. Esch, B. L. Feringa. Dynamic chirality, chirality transfer and aggregation behaviour of dithienylethene switches. *Tetrahedron*, **2008**, 64, 8324.
- ¹³⁶ S. Rotem, A. Mor. Antimicrobial peptide mimics for improved therapeutic properties. *Biochimica et Biophysica Acta - Biomembranes*, **2009**, 8, 1582.
- ¹³⁷ H. P. Lambert, F. W. O’Grady. Antibiotic and Chemotherapy. *Churchill Livingstone*, Edinburgh, U.K., **1992**.
- ¹³⁸ K. Okamoto, Y. Tomita, H. Yonezawa, T. Hirohata, R. Ogura, N. Izumiya. Inhibitory effect of gramicidin S on the growth of murine tumor cells in vitro and in vivo. *Oncology*, **1984**, 41, 43.
- ¹³⁹ N. Izumiya, T. Kato, H. Aoyaga, M. Waki, M. Kondo. Synthetic aspects of biologically active cyclic peptides: Gramicidin S and Tyrocidines. *Halsted Press, New York*, **1979**.
- ¹⁴⁰ D. Gaspar, A. S. Veiga, M. A. R. B. Castanho. From antimicrobial to anticancer peptides. A review. *Front. Microbiol.*, **2013**, 4, 1.
- ¹⁴¹ P. Lloyd-Williams, F. Albericio, E. Giralt. Chemical approaches to the synthesis of peptides and proteins. *CRC Press, Boca Raton*, New York, **1997**.
- ¹⁴² M. Rance, R. A. Byrd, Obtaining high-fidelity spin-1/2 powder spectra in anisotropic media - phase-cycled Hahn echo spectroscopy. *J. Magn. Reson.*, **1983**, 52, 221.
- ¹⁴³ B. M. Fung, A. K. Khitrin, K. Ermolaev. An improved broadband decoupling sequence for liquid crystals and solids. *J. Magn. Reson.*, **2000**, 142, 97.
- ¹⁴⁴ S. Zhang, X. L. Wu, M. Mehring, Elimination of ringing effects in multiple-pulse sequences. *Chem. Phys. Lett.*, **1990**, 173, 481.
- ¹⁴⁵ A. E. Bennett, C. M. Rienstra, M. Auger, K. V. Lakshmi, R. G. Griffin. Heteronuclear decoupling in rotating solids. *J. Chem. Phys.*, **1995**, 103, 6951.
- ¹⁴⁶ D. Amsterdam, in *Antibiotics in laboratory medicine* (Ed.: V. Loman), Williams and Wilkins, Baltimore, MD, **1996**, pp. 52-111.
- ¹⁴⁷ I. Wiegand, K. Hilpert, R. E. W. Hancock, *Nat. Protoc.*, **2008**, 3, 163.

- ¹⁴⁸ T. Mosmann. Rapid colorimetric assay for cellular growth and survival: application to proliferation and cytotoxicity assays. *J. Immunol. Methods*. **1983**, 65, 55.
- ¹⁴⁹ M. C. Alley, D. A. Scudiero, A. Monks, M. L. Hursey, M. J. Czerwinski, D. L. Fine, B. J. Abbott, J. G. Mayo, R. H. Shoemaker, M. R. Boyd. Feasibility of drug screening with panels of human tumor cell lines using a microculture tetrazolium assay. *Cancer Res.*, **1988**, 48, 589.
- ¹⁵⁰ I. Nicoletti, G. Migliorati, M. C. Pagliacci, F. Grignani, C. Riccardi. A rapid and simple method for measuring thymocyte apoptosis by propidium iodide staining and flow cytometry. *J. Immunol. Methods*, **1991**, 139, 271.
- ¹⁵¹ L. V. Garmanchuk, E. O. Denis, V. V. Nikulina, O. I. Dzhus, O. V. Skachkova¹, V. K. Ribalchenko, L. I. Ostapchenko. MI1 – derivative of maleimide inhibits cell cycle progression in tumor cells of epithelial origin. *Biopolymers and Cell*. **2013**, 29, 70.

List of publications:

1. O. Babii, S. Afonin, M. Berditsch, S. Reißer, P. K. Mykhailiuk, V. S. Kubyshkin, T. Steinbrecher, A. S. Ulrich, I. V. Komarov. Controlling biological activity with light: diarylethene-containing cyclic peptidomimetics. *Angewandte Chemie International Edition*, 2014 (53): 3392–3395.
2. A. N. Tkachenko, P. K. Mykhailiuk, D. S. Radchenko, O. Babii, S. Afonin, A. S. Ulrich, I. V. Komarov. Design and synthesis of a monofluoro-substituted aromatic amino acid as a conformationally restricted ^{19}F NMR label for membrane-bound peptides. *European Journal of Organic Chemistry*, 2014 (2014): 3584-3591.
3. Preparation of diarylethene-containing peptidomimetics possessing photo-controlled biological activity. Babii, Oleg; Afonin, Sergiy; Komarov, Igor; Mykhailiuk, Pavlo; Ulrich, Anne. *Eur. Pat. Appl.* (2014), EP 2769983 A1 20140827; *PCT Int. Appl.* (2014), WO 2014127919 A1 20140828

Conference contributions:

1. Probing local dynamics of antimicrobial peptides in lipid bilayers by using solid-state ^{19}F -NMR relaxometry. *EBSA Biophysics Course*, Bordeaux, France, June 24-29, 2012. [Oral presentation]
2. Switching the antimicrobial activity of Gramicidin S by light. *58th Annual Meeting of the Biophysical Society*. San Francisco, California, USA, February 15-19, 2014. [Oral presentation]
3. Switching the antimicrobial activity of Gramicidin S by light. *Drug Discovery & Therapy World Congress 2014*. Boston, MA, USA, June 16th-19th, 2014. [Oral presentation]